Simulation of present and future discharges at the Nile River upstream Lake Nasser

Daniel Tollenaar

University of Twente
Enschede - The Netherlands

Deltares
Enabling Delta Life

Simulation of present and future discharges at the Nile River upstream Lake Nasser

Enschede, September 2009

Master Thesis of:

D. Tollenaar
Water Engineering & Management
University of Twente

Supervisors

Prof. ir. E. van Beek
Water Engineering & Management
University of Twente

Verkenning en Beleidsanalyse
DELTARES

Dr. ir. M.J. Booij
Water Engineering & Management
University of Twente

Dr. J.C.J. Kwadijk
Zoetwatersystemen
DELTARES

University of Twente
Enschede - The Netherlands

Deltares
Enabling Delta Life

Front cover: polygon overlay of the Nile Basin in Goolge Earth

Summary

The objective of this study is to simulate present and future discharges at the Nile River upstream Lake Nasser. For this purpose a rainfall-runoff model is integrated in an existing model which describes the water distribution in the upper Nile; RIBASIM-NILE. The latter is a result of the Lake Nasser Flood and Drought Control / Integration of Climate Change uncertainty and flood risk (LNFDC/ICC) project and described in (MWRI/Deltares, 2009a). In the LNFDC/ICC project, RIBASIM-NILE is used to describe effects of developments upstream the High Aswan Dam on Nile discharges, with the focus on Lake Nasser inflows.

For the purpose of this study the HBV rainfall-runoff model (Bergström & Forsman, 1973) is used Where RIBASIM-NILE is forced by sub-catchment runoff. The combination of the two models is referred to as the Nile Hydrological Simulation Model (NHSM). To assess the performance of the NHSM in simulating discharges under the current climate it is forced by observed rainfall and potential evapotranspiration for the years 1961 till 2000. The first 20 years are used for model calibration and the second 20 years for model validation.

To simulate future discharges, NHSM meteorological forcing is derived from simulated series by three Global Circulation Models (GCMs) under two SRES climate emission scenarios (see Nakicenovic & Swart (2000)). Bias from GCM simulations is removed by a correction of derived rainfall and evapotranspiration to the observed 1961-1990 mean monthly climatology. Thereafter, the performance of NHSM-GCM combinations in simulating the current climate is assessed by comparison of simulated and observed mean monthly discharges and interannual variability. Finally, NHSM-GCM simulations under the two SRES scenarios are used to describe the 2065 and 2100 hydro-climates.

Results of NHSM calibration and validation are satisfying on the scale of main tributaries; The White Nile, draining the Great Lakes district and the Blue Nile and Atbara River draining the Ethiopian Highlands. The hydrographs of observed and simulated discharges show a good overall agreement and long term volume errors fall between acceptable limits. However, especially on sub-catchments belonging to the White Nile performance is considerably lower ranging from a poor representation of discharge peaks to a structural underestimation of discharges. Although some poor results are related to errors in model forcing others are related to the NHSM. It is presumed that performance will increase when improvements are made in the description of rainfall-runoff processes in HBV and the representation of lakes and swamps in RIBASIM-NILE.

The performance of NHSM-GCM in simulating 1961-1990 discharges is low. Uncorrected meteorological forcing derived from GCM simulations shows a high bias compared to the observed climatology. After the bias correction the spatio-temporal representation of observed meteorological forcing is insufficient, especially for rainfall. This is revealed when actual evapotranspiration simulations by NHSM with observed and simulated meteorological forcing are compared. Actual evapotranspiration is a function of bias corrected potential evapotranspiration and the state of the NHSM (soil moisture storage, lake levels, etc.). Differences in states of the NHSM forced by observed and simulated forcing are caused by remaining differences in the spatio-temporal domain of bias corrected rainfall. Where actual evapotranspiration differs, so will the amount of rainfall being available as runoff and river discharge.

NHSM-GCM simulations for the 2065 and 2100 hydro-climates result in a high degree of randomness. Therefore, uncertainty in trends regarding the future climate and discharges is high. Though, literature agrees on the high uncertainty in predicting the future Nile climate, some peculiar results cannot be explained. More detailed studies to the performance of the used GCMs in representing the local climate are required to give conclusive answers. For now, uncertainty in the simulated future hydro-climates is too high for being useful in water resources management.

In conclusion on the objective to this research it is found that NHSM performance with observed meteorological forcing at the scale of main tributaries is satisfactory. For sufficient performance on sub-catchment scale, improvements on NHSM simulations of White Nile basin have to be made. Regarding the simulation of future discharges, an attempt is made to provide representative future meteorological forcing series for the NHSM. Discharges simulated by NHSM-GCM combinations show to much randomness and uncertainty in trends to have sufficient predictive value. The methods by which representative future meteorological forcing is derived are to be improved to increase predictive value within satisfactory limits.

Further research is recommended to improve the NHSM performance on sub-catchment scale. NHSM performance on sub-catchment scale can be improved. This can be achieved by (1) improving the quality of meteorological forcing, (2) changing the distribution of HBV, (3) improving the representation of river-lake dynamics in RIBASIM-NILE and (4) an integrated calibration of HBV and RIBASIM-NILE. Future meteorological forcing series with a lower level of uncertainty can be derived by improving the method by which GCM simulations are directly used as meteorological. When results are still unsatisfying, statistics of observed forcing can be manipulated with trends derived from GCM simulations to achieve forcing representing a future period.

Beyond the scope of this research a recommendation is made to use the NHSM in assessing climate change in combination with other socio-economic and river developments in the Nile basin. Furthermore RIBASIM-NILE can be used to assess the impacts of climate change in relation to mitigating river basin management strategies.

Table of Contents

Summary III
Preface VII

1. Introduction 1
1.1 Background 1
1.1.1 Modeling the future climate and river discharges 1
1.1.2 Overview of previous research to Nile water resources and climate change 2
1.1.3 Lake Nasser Flood and Drought Control Project 4
1.2 Problem description 4
1.3 Objective and Research questions 5
1.4 Scope and outline 5

2. The Nile River basin 6
2.1 Basin Topography 6
2.1.1 The Great Lakes district 6
2.1.2 The Sudd 6
2.1.3 The Ethiopian Plateau 6
2.2 Climate and hydrology 8

3. Methodology 10
3.1 Nile Hydrologic Simulation Model 10
3.1.1 Meteorological forcing 10
3.1.2 HBV rainfall-runoff model 11
3.1.3 RIBASIM Nile Model 15
3.1.4 Integration of HBV and RIBASIM-NILE to NHSM 18
3.1.5 NHSM calibration and validation 18
3.2 NHSM simulations with forcing derived from GCM simulations 22
3.2.1 Global Circulation Models 23
3.2.2 Combining GCM data with the NHSM 24
3.2.3 Assessing NHSM-GCM simulations 26

4. NHSM optimization and performance 29
4.1 Model calibration 29
4.1.1 White Nile 31
4.1.2 Blue Nile 33
4.1.3 Main Nile 34
4.2 Validation over 1981-2000 data series 35
4.2.1 White Nile Validation 35
4.2.2 Blue Nile Validation 37
4.2.3 Main Nile Validation 37
4.3 Discussion 38

5. NHSM-GCM simulations of present and future discharges....39
5.1 Discharge sensitivity on changed meteorological forcing....39
5.2 Simulating the reference hydro-climate using NHSM-GCM combinations....40
5.2.1 Bias correction on meteorological forcing....40
5.2.2 Reference climate NHSM-GCM simulations....41
5.3 NHSM-GCM simulations for 2065 and 2100 hydro-climates....44
5.3.1 Meteorological projections....44
5.3.2 Discharge projections....46
5.3.3 Water resources projections....48
5.4 Discussion....49
6. Conclusions and Recommendations....51
6.1 Conclusions....51
6.2 Recommendations....53
6.2.1 On further development of the NSHM....53
6.2.2 On the simulation of the future hydro-climate....53
6.2.3 On further research....53

References....54
Abbreviations....57
Symbols....58

Appendices
A Derivation of meteorological forcing....60
B Issues related to RIBASIM-NILE areal representation....62
C Golden ratio parameter optimization....64
D Calibration and validation hydrographs....65
E Bias correction results....67
F Bias issues in NHSM-GISS reference hydro-climate....69

Preface

'If we can recognize that change and uncertainty are basic principles, we can greet the future and the transformation we are undergoing with the understanding that we do not know enough to be pessimistic.'

Hazel Henderson (1933 - present)

In September 2008, I got the opportunity to finish my master Water Engineering and Management at the University of Twente with a study to assess climate change impacts on river discharges at the Nile River upstream Lake Nasser. For this study I stayed from November that year till May 2009 at Deltares in Delft. Thereafter I returned to Enschede to finish my thesis to this final product.

I would like to thank the employees at Deltares for their willingness to help me with my thesis. The open door policy made it much easier solving issues related to my project. When RIBASIM got nasty, Wil van de Krogt was always willing to help me finding a solution. Ronald Vernimmen gave relevant input every time I shared issues regarding my project. Most time was probably invested by Frederiek Sperna Weiland for providing me with gigabytes of rainfall and evapotranspiration data. Many thanks for the given support to all of you!

Back in Enschede, I got kindly adopted by the inhabitants of the famous graduation room. I would like to thank all roommates for helping me seeing some light at the end of the tunnel the difficult months halfway my project. Some simple coffee and lunch breaks proved to be sufficient for blowing of steam and recharging my batteries. By all the passion you guys show in your own projects, I am confident there will be brilliant futures ahead!

Special thanks to three of my best friends and study mates, Erwin Sterrenburg, Wiebe de Boer and Stephan van der Horst. Though it is moved to one of the annexes, using the golden ratio optimization method in model calibration was Erwin's idea. With help from his side, I managed to implement it into my model, which didn't only look cool, but also saved heaps of time. Besides listening to all my complaints of various kinds, Wiebe was helpful in reviewing my report in his well known thorough way. Stephan shined his light on my conclusions and recommendation the long night before the final deadline, which lead to allot of improvements. Thanks a lot guys!

I thank my committee, Eelco van Beek, Martijn Booij and Jaap Kwadijk, for providing the right combination of skills in my supervision. Eelco reminded me more than once not to forget the objective of my study when I was getting lost in details. For the same reason, Jaap reminded me it was important to take a pragmatic approach. Martijn, there are many reasons to thank you. I am very grateful for the precise critics on my work, the input you provided and the time you invested to improve the quality of my research!

To my mother: bedankt voor je begrip bij het verwaarlozen van wekelijkse telefoontjes in de tijd dat mijn gedachten bij mijn onderzoek zaten.

And finally to Karin, how can somebody be so understanding, sweet and beautiful as you are?

Daniël Tollenaar

Enschede, 6 September 2009

1. Introduction

This chapter serves as an introduction to the study. A background, giving the model framework and an overview of previous research, is found in the first paragraph. In the second paragraph, the problem is defined, followed by the formulation of the objective and research questions in the third paragraph. The scope and outline of the study are given in the last paragraph.

1.1 Background

The study background is divided into three parts. The first section describes the theoretical framework of climate change impact modeling. In the second section, an overview of previous research related to the Nile Basin water resources will be given. In the third section, results of the Lake Nasser Flood and Drought / Integration of Climate Change Uncertainty and Flood Risk (LNFD/ICC) project (MWRI/Deltares, 2009b) will be discussed.

1.1.1 Modeling the future climate and river discharges

To compare outcomes of different studies on climate change a framework is proposed by the IPCC (Nakicenovic & Swart, 2000). This framework is the standard in which predictions of future demographic, social/economic, and technological developments are used to develop climate change scenarios. These scenarios can be used to analyze impacts of climate change on the water resources in a river basin.

Climate Change impact assessment

Figure 1.1 shows the framework by which hydrological impacts are related to greenhouse gas (GHG) emission scenarios (Kwadijk et al., 2008). The methodology behind the development of such scenarios is standardized and described in the IPCC Special Report on Emission Scenarios (SRES) by Nakicenovic and Swart (2000). With chemical models these GHG emission scenarios are transferred to atmospheric GHG concentrations which are the driving forces of Global Circulation Models (GCMs). GCMs construct climate change projections based on GHG emission scenarios, which can be used for environmental studies. Impact assessment on river basin hydrology is one field in which these impacts are studied. For these purposes, climate change scenarios are used as input for hydrological models to assess the effect of these scenarios on hydrological quantities such as soil moisture and discharges.

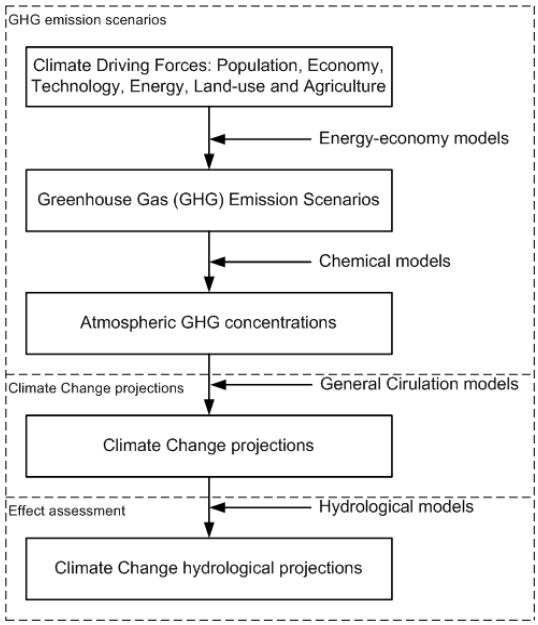

Figure 1.1 – Framework for climate change impact assessment (Kwadijk et al., 2008)

Global Circulation Models

GCMs are used to simulate climate change, forced by GHG concentrations, which are confined by the SRES emission scenarios (see Figure 1.1). The most advanced of these models couple atmospheric-oceanic GCMs with a three dimensional terrestrial biosphere model into one GCM, relating atmospheric, oceanic and land surface processes all together (Viner, 2000). If models are to predict the seasonal variability of rainfall accurately, a number of processes, such as evapotranspiration, condensation and transport have to be modeled correctly (Nakicenovic & Swart, 2000).

Until now, performance in simulating the current climate highly varies for different GCMs and for different parts of the world. In comparison with observations, temperature is considered to be simulated reasonably well, with rainfall problems emerge. The spatio-temporal variability of rainfall is strongly influenced by vertical movements of air due to atmospheric instabilities of various kinds and by the flow of air over orographic features, such as mountain ridges. The model resolution of GCMs is not sufficient to cover the spatio-temporal variability of these features and therefore the spatio-temporal variability of rainfall. With respect to future predictions of climate change GCM-SRES combinations show a wild variation in future projections. The high level of disagreement limits the certainty in which conclusions can be drawn (Randall et al., 2007).

Using GCM results in climate change impact studies

Climate projections from GCMs are used to assess impacts on ecosystems and/or socio-economic systems. These systems usually have smaller characteristic scales than the relatively course resolution of 250 to 600 km in which meteorological data is provided by GCMs. Generating information below the resolution of GCMs is referred to as downscaling. In Christensen et al. (2007), two methods of downscaling are discussed; dynamic and statistical downscaling.

In dynamic downscaling, high-resolution Regional Climate Models (RCMs) are used to represent regional sub-domains. Observed and/or GCM data is used at RCM boundaries. Dynamic downscaling has the potential for capturing meso-scale non-linear effects and providing coherent information among multiple meteorological variables. The models are formulated using physical principles and can credibly reproduce a broad range of climates around the world, which increases confidence in their ability to downscale future climates. The main drawback of RCMs is their computational cost (Christensen et al., 2007).

Statistical Downscaling methods use relations between climate data and other geospatial characteristics, such as elevation (see e.g. Conway, 1997), to downscale meteorological variables to a desired scale. Statistical downscaling is computationally inexpensive, can cover finer scales than dynamical methods and is applicable to parameters that cannot be directly obtained from the RCM outputs. Due to their empirical basis, statistical models have to be calibrated and validated, requiring sufficient meteorological data. The main drawback of statistical downscaling methods is the assumption that derived cross-scale relationships remain stable. When the climate is perturbed, they cannot effectively accommodate regional feedbacks and sometimes can lack coherency among multiple meteorological variables (Christensen et al., 2007).

1.1.2 Overview of previous research to Nile water resources and climate change

The spatial division of water supply and demand in the Nile River is high. While the majority of supply is accounted for by rainfall upstream in the Blue and White Nile tributaries, demands are highest downstream, in Sudan and Egypt. The latter two countries experience high water stress, whereby Sudan and Egypt use more than 50% and 90% of their long term renewable water resources (Arnell, 1999). At high water stress, only small changes in water supply have enormous consequences for the socio-economic system in the demanding countries. Basin sensitivity studies indicate the degree of perturbation of water resources in changing climatic conditions. Studies in climate simulation and projections of climate change, give insight to which extend the future climate can be modeled. In this section a brief overview of studies related to these topics will be given.

Hydrological sensitivity studies

In Gleick (1991), the high sensitivity of the Blue Nile to changed meteorological conditions is quantified. He found that 20% decrease in rainfall caused 50% reduction in discharge. Conway and Hulme (1993) studied the relation between rainfall and runoff in the Equatorial Lakes (White Nile) and the Blue Nile. In this study, 40 Years of discharges and rainfall (1945-84) are compared. The ten-year mean flows of this period varied +/- 20%. They concluded that significant fluctuations in discharges of the Nile River where largely caused by fluctuations in rainfall, primarily over the Blue Nile basin and secondly over the Equatorial Lakes.

GCM regionalization studies

In Mohammed et al. (2005) progress has been made in the downscaling of meteorological variables. They applied the Regional Atmospheric Climate Model (RAMCO), to describe the basins hydro-climatology. The model covers the entire Nile Basin and uses a resolution of ±50km to simulate the climate between 1995 and 2000. More recently the Africa@Home project started developing statistical regional models for specific regions in Africa (Africa@Home, 2009), which can be used in combination with GCM simulations.

When regional climate simulations are compared with observations, systematic errors are reported by the SRES (Nakicenovic & Swart, 2000). For instance, the Atlantic Inter-Tropical Convergence Zone, an important factor in rainfall regimes is displaced to the south. Also, interannual variability caused by the El Niño Southern Oscillation is not well represented in GCMs. In regional downscaling, the natural climatic variability of the semi-arid tropical savanna eco-region Sahel is highly under-represented. Overall, it is not known how well output from GCMs can be downscaled into regional projections and the limitations of empirical downscaling results are not fully understood.

Climate change projections

In the study of Hulme et al. (2001), past and future climates for the African continents are analyzed. Trends in the past climate are analyzed by observational data. The future climate is predicted in a combination of four GHG emission scenarios with seven GCMs. The study confirmed temperatures have risen during the previous century and that this is expected to continue in the 21st century. With respect to rainfall a slight increase was observed over the equatorial lakes. Future rainfall could only be predicted with a high level of uncertainty. Especially for the Ethiopian Plateau uncertainty was high. For the year 2050, rainfall predictions ranged between -10% to +25% during the whole season and +/- 100% for the flooding season alone.

In a later study Conway and Hulme (1996) drew conclusions about impacts of climate change on water resources. They used multiple hydrological models and three GCMs to highlight inter-model differences in future climate change scenarios. They found Lake Victoria outflows ranging from -9.2% to +11.8% in 2025. For the Blue Nile, outflow varied from -8.6% to +15.3% in the same period. Based on these scenarios, they estimated a mean annual flow for the Egyptian Nile varying between -10 and +18%. From both studies it can be concluded that fluctuations in the Main Nile, are mainly caused by changing rainfall patterns within the Blue Nile basin. Both tributaries are however highly sensitive to changes in meteorological variables, especially rainfall.

With regard to the high level of uncertainty, the third assessment report if the Intergovernmental Panel on Climate Change (IPCC) gives mostly quantitative prognoses for climate change (Boko et al., 2007). With respect to temperature rises it is concluded that it is likely to be larger for Africa than for the rest of the world throughout the entire continent and in all seasons. Dryer subtropics (e.g. the

Ethiopian Plateau) warm more than wetter tropics. Mean annual rainfall is likely to decrease along the Mediterranean coast extending into the northern Sahara up to -20%. In tropics and east Africa it is expected to increase with about 7%. Boko et al. (2007) draws only limited conclusions about extreme events, but the number of extremely dry and wet years are expected to increase during the present century.

1.1.3 Lake Nasser Flood and Drought Control Project

In 2009, MWI/Deltares completed the Lake Nasser Flood and Drought Control / Integration of Climate Change Uncertainty and Flood Risk (LNFDC/ICC) project (MWRI/Deltares, 2009b). One of the objectives was to assess the effects of upstream developments upstream the High Aswan Dam to Lake Nasser inflows. For this purpose, the water distribution of the upstream river basin is described in the River Basin Simulation Model (RIBASIM) developed by Deltares (Deltares, 2004). Henceforward, the RIBASIM model applied for the upper Nile Basin will be referred to as RIBASIM-NILE. The model describes routing between the main components of the river system, consisting of the river itself, lakes, reservoirs and swamps. The model is forced by rainfall and evaporation over the main components and sub-catchment runoff derived from observed discharges (MWRI/Deltares, 2009e).

Since RIBASIM-NILE uses sub-catchment runoff as its boundary, the possibility to study climate change impacts on Nile water resources is limited. Therefore, Deltares used the Nile Forecasting System (NFS) (MWRI/Deltares, 2009c), the hydrological forecast system for the Nile Basin upstream of Dongola, installed at the Nile Forecasting Centre (NFC) within the Egyptian Ministry of Water Resources and Irrigation (MWRI). Results of the study showed large differences in Nile discharges based on different GCM-SRES climate change projections. Predictive uncertainty with different GCM simulations was higher than scenario uncertainty under different SRES scenarios. On average, annual Lake Nasser inflows were expected to increase up to 10% in 2100, but with a high level of uncertainty. Predictions compared with the current inflow ranged from a decrease of 90% to an increase of 100%.

1.2 Problem description

In the Nile Basin two interrelated problems are observed in relation to water resources. First of all, most Nile countries are under severe water stress, using most of their long term renewable water resources. These stresses urge the need for improved efficiency under current water availability. Since the socio-economic system highly depends on the current amount of inflow, minor changes on this water budget will have great consequences. The RIBASIM-NILE model provides a tool to assess impacts of upstream developments on available water resources along the Nile River.

The second problem is to cope with the effects of climate change on water resources. Many studies quantify the sensitivity of parts of the Nile Basin to climate change (e.g. Conway & Hulme, 1993, 1996; Gleick, 1989, 1991). However, as acknowledged in the LNFDC/ICC project (MWRI/Deltares, 2009d), these impacts should be assessed for the entire basin in combination with other developments, such as land use change or population growth. A model which can be used to describe impacts of upstream developments and climate change is therefore to be developed.

1.3 Objective and Research questions

In this study, an integrated model is developed which enables impact assessment of upstream developments and climate change in an integrative manner. The objective of this study is formulated as follows:

To simulate present and future discharges at the Nile River upstream Lake Nasser by integrating a rainfall-runoff model in RIBASIM-NILE.

Though the use of RIBASIM-NILE would allow simulating discharges under many upstream development scenarios, this study is limited to 'Scenario A', describing the natural-state of the Nile River (see: MWRI/Deltares, 2009a). However, the final model design will allow simulating other scenarios defined by LNFDC/ICC in combination with climate change. For the purpose of this study, the integration of a rainfall-runoff model with RIBASIM-NILE will henceforward be referred to as the Nile Hydrological Simulation Model (NHSM)

To meet the objective, the following research questions are formulated:

1. What is the performance of the NHSM in simulating discharges forced by observed meteorological variables?
2. How well is the current climate represented by meteorological variables derived from GCM output and what is the performance of the NHSM when it is forced by these variables?
3. What is the predictive value of the future climate and discharges, when meteorological projections are derived from GCM output and used as forcing for the NHSM?

1.4 Scope and outline

Scope

The scope of this study is confined in time and space. Regarding the temporal component, the study covers simulations of the present climate (a period of 30 years) and simulations of future climates until 2100. The present climate period, the observed meteorological variables and discharges are used for model calibration and validation. It also serves as a reference period which can be compared with projections of future climates and discharges. In space, the study is confined by the part of the Nile basin upstream Dongola, the most downstream gauging station ±700km upstream Lake Nasser. This covers an area of about $2.8*10^6$ km^2. Hydrological sub-catchments are confined by the RIBASIM-NILE model.

Outline

In chapter 0, the topography, climate and hydrology of Nile Basin will be described in further detail. The methodology followed to answer the research questions is expounded in chapter 3. Results are found in the next chapters. In chapter 4, the performance of the NHSM after model calibration and validation is described and discussed. In chapter 5 NHSM model simulations with simulated meteorological forcing is discussed. In chapter 6 the conclusions and recommendations of this study are discussed.

2. The Nile River basin

Around 500 BC Herodotus, a Greek historian, wrote "The Nile is Egypt and Egypt is the Nile". Already by that time, the Nile River water resources where vital to the Egyptian socio-economic system as it is today. However, in total the river basin crosses the boundaries of ten countries. In this chapter, the basin topography and hydro-climatology are given in paragraph 2.1 and 2.2.

2.1 Basin Topography

The position of the Nile River on the world ranking of longest rivers is much under debate, whereby it is competing with the Amazone River for the first place. Due to the re-discovery of its source, the river now holds a marginal leading position, with a length of around 6400 km covering a range of latitudes from 4° south to 32° north. Relative to its length, the river catchment is modest with an area of $3.3*10^6$ km^2. As shown in Figure 2.1, the Nile River has two main tributaries; the White Nile and Blue Nile River with their confluence at Khartoum. Downstream the Main Nile is also fed by the Atbara River which is dry most of the year and drains the northern part of the Ethiopian Plateau during the rainy season. After it passes the famous Great Bend the river enters Lake Nasser, which is formed after the construction of the High Aswan Dam, completed in 1902. In this paragraph, a short description is given of the main regions of Nile Basin. For a more detailed description is referred to Sutcliffe and Parks (1999) and Dumont (2009).

2.1.1 The Great Lakes district

The most upstream reach of the White Nile is the Kagera River (see Figure 2.1). It drains the Nygungwe Forest in Rwanda and flows in northeast direction, where it enters Lake Victoria at an altitude of about 1200 m relative to mean sea level. Lake Victoria, one of the world's largest lakes with an average size of 68,800 km^2, feeds the Victoria Nile from its outlet at Jinja, located at the north side of the Lake. From here, the Nile runs northwest, where it enters Lake Kyoga, in fact a grass filled rift valley with an average surface elevation of about 920 m. Here, the Lake is joined by the Semliki. The Semliki drains Lake Edward, located in Uganda, close to the Congolese border. It flows into Lake Albert from where it confluences with the Victoria Nile entering the Albert Nile.

2.1.2 The Sudd

North of the Sudan Border at Mongalla, the Albert Nile enters the Sudd, one of the world's largest freshwater wetlands with an area varying from 30,000 to 130,000 km^2, depending on its inflow (see Figure 2.1). Besides the Albert Nile, the Sudd is fed by outflow from Lake No, which is fed by the Bahr el Ghazal from the west. Due to the semi-arid local conditions, more than half of Sudd inflow is lost to evapotranspiration. Therefore, the construction of the Jonglei diversion canal began in 1978, with the aim to increase White Nile flow. However, due to the political controversy of the project and regional instability, constructions where brought to a halt in 1984, when 240 km of the total 360 km long canal was excavated. Downstream the outlet of the Sudd, the river is called the White Nile as is flows north towards Khartoum.

2.1.3 The Ethiopian Plateau

Rainfall over the Ethiopian Plateau feeds three rivers, the Sobat River, Blue Nile and Atbara River, draining the southern, central and northern part of the plateau respectively. The Sobat River is the last tributary of the White Nile and has two main tributaries, the Baro and Pibor Rivers (see Figure 2.1). Part of the flow is diverted to the Mashar Swamps, where it is lost to evapotranspiration. The remainder drains to the White Nile downstream the Sudd Swamps.

The Blue Nile has its source near Lake Tana at an elevation of about 2,750 m. The lake is with a surface area of 2,150 km^2 considerably smaller than Lake Victoria. From the Blue Nile Falls at the outlet of the lake, the Blue Nile flows southeast, where after it makes a turn in western and later southwestern direction to its mouth at Khartoum, where it confluences with the White Nile to the Main Nile. In its course, the river is fed by two small tributaries, the Dinder and Rahad Rivers.

The last tributary of the Main Nile is the Atbara River. This river drains the part of the plateau north of Lake Victoria. Close to its source, the river basin contains of steep mountain ridges with steep slopes. When it crosses the Ethiopian-Sudanese border, slopes decrease considerably. Though, the river contributes a considerable of Main Nile flow during the flooding season, it is dry during the rest of the year. Downstream the Atbara, the Main Nile flows through the Great Bend where after it enters Lake Nasser ±700km downstream Dongola.

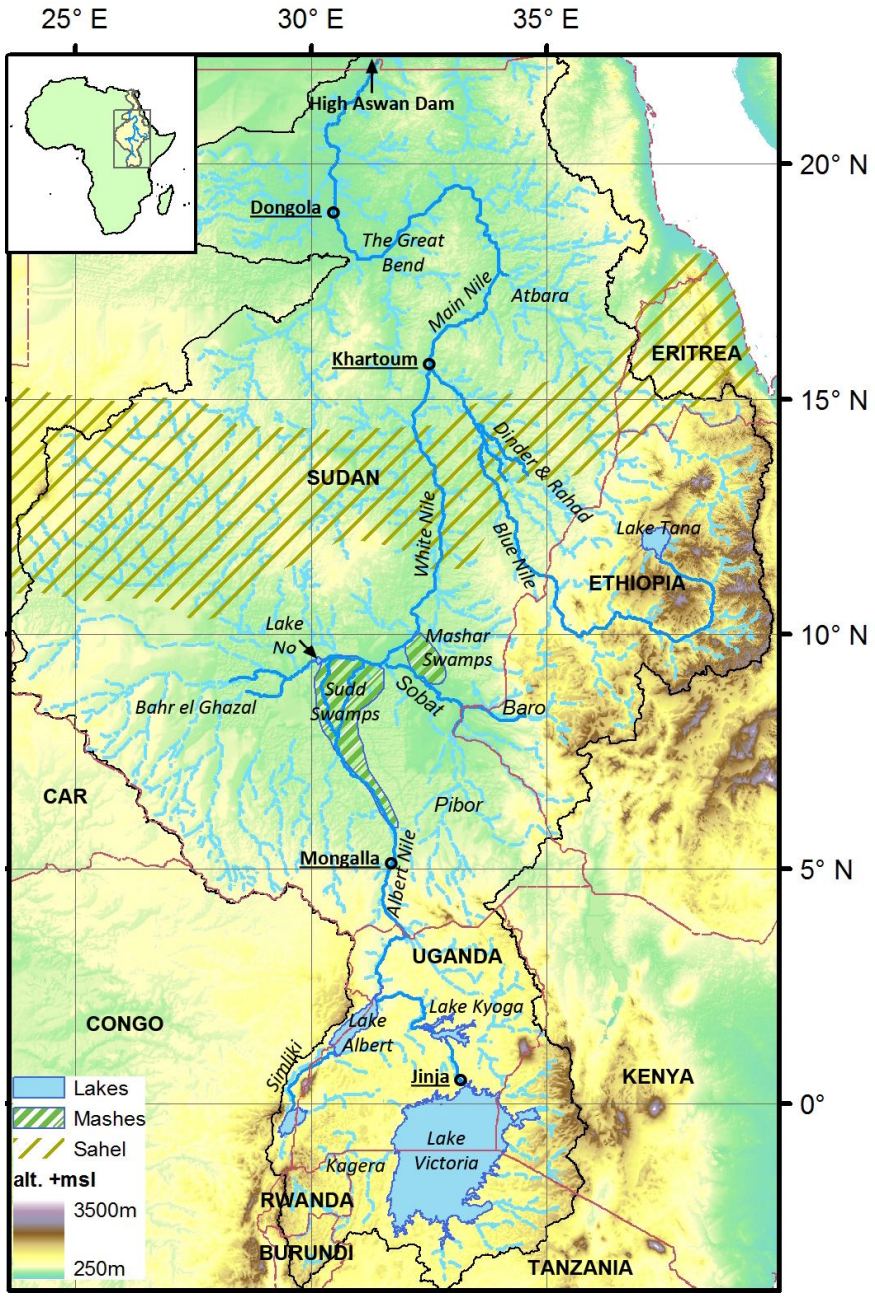

Figure 2.1 - The Nile River Basin (elevation according to GTOPO30 (USGS, 2009b))

2.2 Climate and hydrology

Climates across the Nile Basin have to be classified in more than one type. As shown in Figure 2.2, the annual amount of rainfall is highest in the tropical regions at the Great Lakes and the Ethiopian Plateau with annual maxima up to 2,100mm and 1,900mm respectively. Where the climate at the Great Lakes is characterized by a bimodal distribution with two rainy seasons, at the Ethiopian Plateau a clear wet and dry season is distinguished, as shown in Figure 2.4. In a transition zone downstream the Great Lakes, rainfall is gradually concentrated to a single rainy season. Between 6° and 13° north the climate is characterized as semi-arid with less than 500mm rainfall per year. North of 13th latitude, the climate is considered arid, with annual rainfall less than 100mm.

In Figure 2.3, the annual variation of reference evapotranspiration is given. It must be noted that these amounts do not exactly represent potential evapotranspiration, as vegetation influences are neglected. The figure shows the lowest values for reference evapotranspiration at the Great Lakes region and the Ethiopian Plateau, due to the high humidity and surface elevation of these regions. Values increase further north as the temperature rises and humidity decreases. At Dongola, reference evapotranspiration is around 2,500 mm/year, indicating high open water evaporation over the river, lakes and reservoirs.

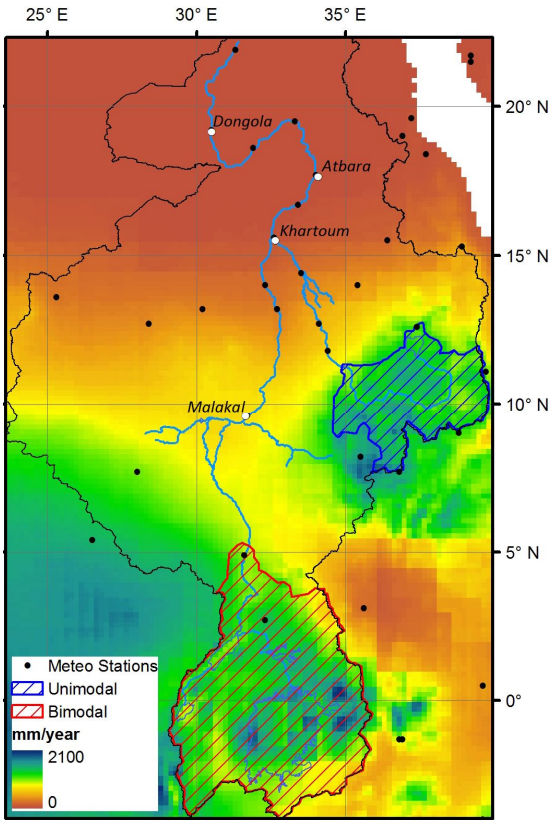

Figure 2.2 - Rainfall (New, Lister, Hulme, & Makin, 2002)

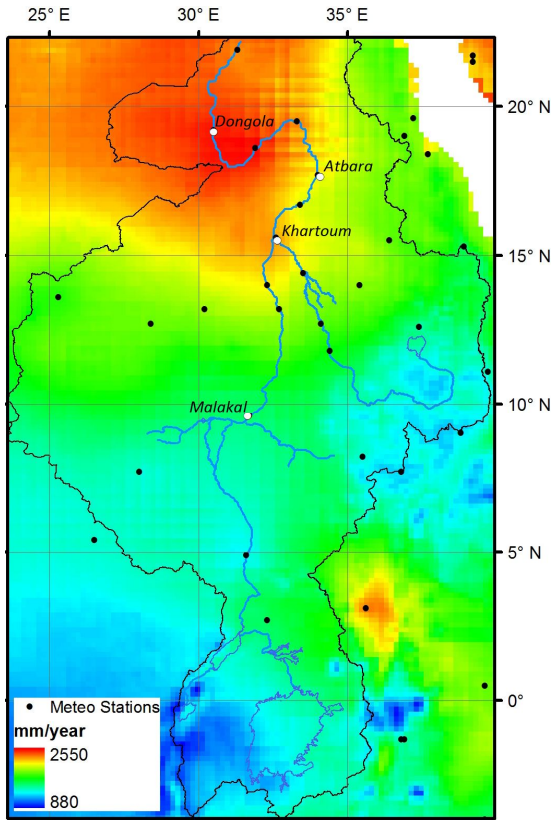

Figure 2.3 - Reference evapotranspiration (van Beek, 2008)

Though annual rainfall is high at the Great Lakes region, only a small proportion contributes to Main Nile discharge, as shown in Figure 2.5. In Lake Victoria a big portion of annual rainfall is lost to evaporation. As mentioned in the previous section more than half of the runoff from the Great Lakes district is on its turn lost to evapotranspiration in the Sudd swamps. As discharge from the Bahr el Ghazal River totally evapotranspirates it has nil contribution to the discharge at Malakal. Where the Malakal hydrograph (see Figure 2.5) shows a slight peak, floods from the Sobat River contribute to White Nile flow.

As the hydrographs of Khartoum and Atbara in Figure 2.5 show, the majority of Main Nile discharge at Dongola is contributed by inflow from the Equatorial Plateau. The unimodal climate concentrates annual rainfall to one season (see Figure 2.4), where it highly exceeds evapotranspiration. As a result, the majority of rainfall is available as runoff. In the river itself, retention is much lower than in the White Nile. Combined with a lower aridity of the local climate, the amount of open water evaporation is considerably lower. Therefore, over 70% of the annual discharge at Dongola is accounted for by runoff from the Blue Nile and Atbara River.

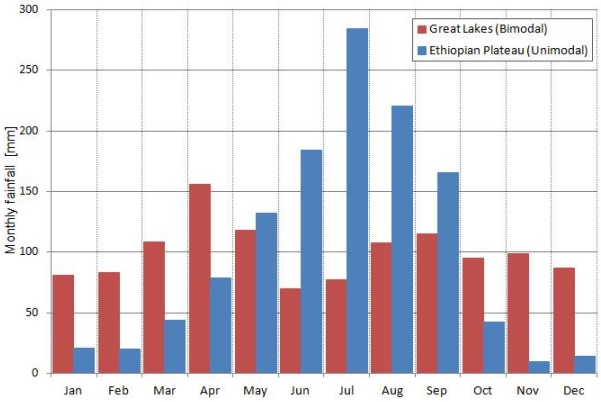

Figure 2.4 - Mean monthly rainfall at Great Lakes and Ethiopian plateau (New et al., 2002)

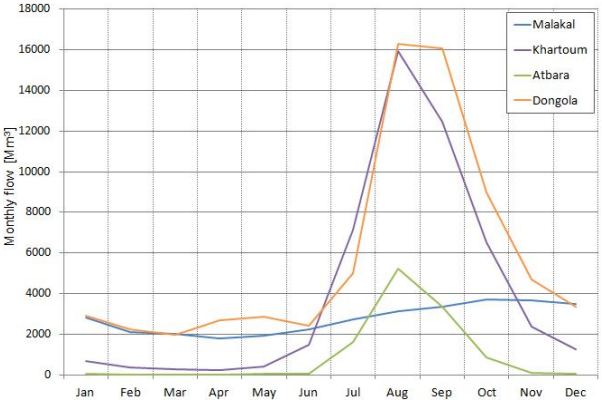

Figure 2.5 - Mean monthly hydrographs (MWRI/Deltares, 2009e)

3. Methodology

This chapter unfolds the methods used to answer the research questions formulated in paragraph 1.3. A major part of this study is devoted to the integration of a rainfall-runoff model with RIBASIM-NILE. This is explained in the first paragraph. The second paragraph describes how present future hydro-climates simulated and assessed by NHSM-GCM combinations.

3.1 Nile Hydrologic Simulation Model

Part of the objective is to integrate a rainfall runoff model with RIBASIM-NILE and develop the Nile Hydrological Simulation Model. Where RIBASIM-NILE uses sub-catchment runoff as forcing a rainfall runoff model is developed to determine its value based on meteorological forcing. The Meteorological forcing used in NHSM is described in the first section. Thereafter, the applied rainfall-runoff model, RIBASIM-NILE and the model integration are described in section two, three and four respectively. The final section of this paragraph is devoted to the calibration and validation of the NHSM.

3.1.1 Meteorological forcing

Observational data series are provided by the Climatic Research Unit (CRU) and the European Centre for Medium-Range Weather Forecasts (ECMWF). From these data sources, meteorological forcing grids with a spatial resolution of ΔXY 10' (≈ 20km) and a temporal resolution of 1 day over the period 1961-2000 are generated. Characteristics of the used data sources are summarized in Table 3.1.

Table 3.1 – Data sources with meteorological variables used to derive forcing series

Source	*Forcing variable*	*Series length*	*ΔXY*	*ΔT*
CRU-TS2.1	P, ET_0	1901-2002	30' (≈ 55 km)	Monthly
CRU-CL1.0		1961-1990 Climatology	10' (≈ 20 km)	
ERA40	P	1958-2001	30' (≈ 55 km)	Daily

The CRU provides two datasets of meteorological variables describing earth's terrestrial surface climate. The CRU-TS2.1 time series (New et al., 2002), provides 95 years of monthly mean values on a resolution of 30'. By the CRU-CL1.0, a 1961-1990 mean monthly climatology is provided (New, Hulme, & Jones, 2000) with a spatial resolution of 10'. Both CRU series are interpolations of ground observed data. Observed meteorological series have been subjected to extensive quality control throughout the years (Eischeid, Diaz, Bradley, & Jones, 1991). Meteo stations are automatically tested on internal consistency (e.g. ensuring that monthly means follow consistent seasonal cycle) and between-variable consistency (e.g. ensuring that months with zero wet days have no rainfall). During interpolation, station months with large residuals where defined as potentially in error and in some cases removed (New et al., 2002). Despite extensive quality control, rainfall data have not been corrected for gauge biases (related to used gauge types), since sufficient meta-information of stations isn't available. Meteorological variables have been interpolated using statistical interpolation methods, assuming relations between the variables latitude, longitude and surface elevation.

The ERA40 data series is a product of weather forecast models used by the ECMWF. The observational dataset used in this study is the ERA40 reanalysis, providing a global analysis of the atmospheric conditions over the 1958-2001 period (Uppala et al., 2005). These are a composition of observations, previous forecast results and model assumptions about the evolution of different meteorological variables (Hagemann, Arpe, & Bengtsson, 2005). As far as observational input is

considered, data series can be classified in a pre-satellite period (1961-1972), where no satellite data were available, a transition period (1973-1988) where the amount of satellite data assimilated increases with time and a satellite period (1988-1990), where a large amount of satellite data has been assimilated into the ERA40 data series. In validation of the hydrological cycle presented by ERA40 data, it is concluded the data provides a poor representation of rainfall volumes (Hagemann et al., 2005). Especially in the tropics rainfall seems to be highly overestimated (Troccoli & Källberg, 2004). Therefore the dataset is used for temporal interpolation of the CRU-TS2.1 dataset to obtain daily values and not for direct application as rainfall forcing.

Derivation of observed rainfall and evaporation series

Van Beek (2008) used the datasets described in Table 3.1 to derive daily rainfall and evapotranspiration grids, which are used in this study. The ERA40 dataset is corrected to the amount of wet days and rainfall of the CRU-TS2.1 dataset. To correct for the amount of wet days, a monthly threshold is applied on the ERA40 dataset. The threshold is set to a value for which the amount of days where rainfall exceeds this value corresponds with the wet days given by the CRU-TS2.1 dataset. The cumulative monthly volume of ERA40 rainfall days above this threshold is corrected to meet the rainfall amount of CRU-TS2.1.

The dataset of Van Beek (2008)has a grid cell size of 30'. To increase the resolution of the rainfall grid to grid cells of 10', it is spatially interpolated by rainfall of the CRU-CL1.0, according to equation 3.1. Twelve interpolation grids are created by dividing mean monthly grid cell values by the sum of the cells under the 30' grids defined by Van Beek. The Van Beek data series are resampled to 10' and thereafter multiplied with the interpolation grids to arrive at daily rainfall grids with a cell size of 10'.

$$INT_P(x,y)_t = \frac{P(x,y)_t}{\sum P(x,y)_t} \tag{3.1}$$

Where:

$INT_p(x,y)_t$ = interpolation factor of grid cell x,y at month t [-]

$P(x,y)_t$ = rainfall in grid cell x,y at month t [mm]

Van Beek also derived gridded monthly potential evapotranspiration from the CRU-CL1.0 and CRU-TS2.1 dataset (van Beek, 2008), in line with to the FAO guidelines for the prediction of crop water requirements (Allen, Pereira, Raes, & Smith, 1998; Doorenbos & Pruitt, 1977). Besides the CRU datasets, the GTOPO30 digital elevation model (USGS, 2009b) is used in calculating pressure and head flux capacities at respective cell heights. Grids are available at a 10' mean monthly climatology and a 30' 1961-1990 climate series with mean monthly values, corresponding with the two CRU datasets. A brief description of the calculations used by Van Beek (2008) is given in Annex A. For the purpose of this study, the monthly values for evapotranspiration are divided by the amount of days in the respective month, to obtain daily evapotranspiration values.

3.1.2 HBV rainfall-runoff model

To simulate rainfall-runoff the conceptual HBV model is used. This model is developed in the 1970s at the Swedisch Meteorological and Hydrological Institute (SMHI) and first published by Bergström and Forsman (1973). Though initially developed for runoff simulation and hydrological forecasting, its scope of applications increased rapidly, requiring modifications to its structure. In 1993 the old HBV model was revised to overcome drawbacks concerning areal representation and physical inconsistencies. The objective was to re-evaluate the existing model and develop a new version with a stronger physical basis. Results led to the publication of HBV-96 by Lindström et al. (1997).

Though the HBV model applied in this research generally follows the structure of HBV-96, some modifications have been made. The snowfall routine is omitted, making the final structure comparable with the version used by Lidén and Harlin (2000). Also a different choice is made with respect to its spatial distribution. Where HBV-96 is usually applied on a lumped basis, considering sub-catchments as homogeneous areas, with average values for forcing, storages and model parameters, in this study a semi-distributed version is used. In this respect, the model version can be compared with the previous application of HBV-96 by De Kort and Booij (2007) at the Song Hong, northern Vietnam. Although some processes are still described on a lumped basis, the primary hydrological unit of the HBV version applied in this research is a grid with cell sizes of 10', confined by the model forcing.

A schematization of the applied HBV version is given in Figure 3.2. The model discriminates four routines:

- A *Soil Moisture Routine*, accounting for actual evapotranspiration (ET_a,), recharge (*RC*) capillary flux (*CF*) and percolation (*PC*) all in [mm·day^{-1}].
- A *Fast Runoff Routine,* accounting for overland flow and rapid through flow combined in quick runoff (R_{uz}, [mm·day^{-1}]).
- A *Slow Runoff Routine,* accounting for base flow (R_{lz}, [mm·day^{-1}]).
- *Routing Routine,* representing routing over the sub basin. Where the upper three routines operate on the cell basis, this routine operates on the scale of sub-catchments. A simple Unit Hydrograph (UH) redistributes the area totals of quick runoff and base flow over time and determines the total runoff (R_{sub},[mm·day^{-1}]) at the outlet of the sub-catchment.

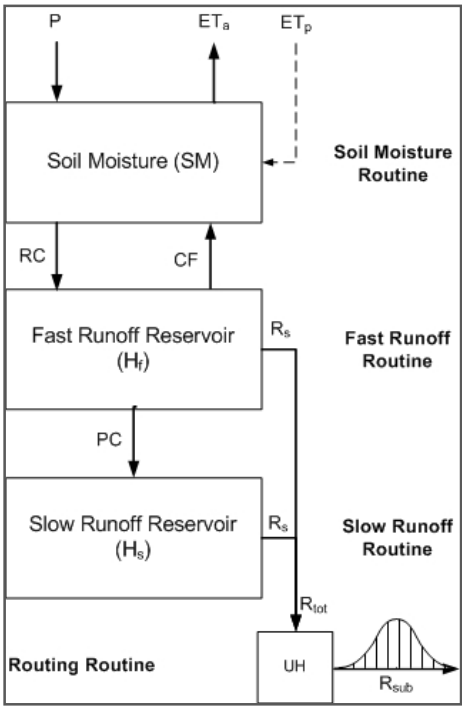

Figure 3.1 - HBV model schematization

The soil moisture routine

The soil moisture routine is responsible for internal routing between soil moisture (*SM,* [mm]), the quick runoff reservoir (H_f, [mm]) and the slow runoff reservoir (H_s, [mm]). Actual evapotranspiration is calculated by equation 3.2. In case the soil moisture exceeds the limit for evapotranspiration *(LP,* [mm]), it equals potential evapotranspiration. Below this threshold, actual evapotranspiration reduces in a linearly relation to soil moisture storage.

$$ET_a = \left(\frac{SM}{LP}\right) \times ET_p \quad \text{if} \quad SM < LP$$
$$ET_a = ET_p \quad \text{if} \quad SM \geq LP \qquad (3.2)$$

Where:

ET_a = Actual evapotranspiration [mm·day^{-1}]
ET_p = Potential evapotranspiration [mm·day^{-1}]
SM = Soil moisture storage [mm]
LP = Limit for potential evapotranspiration [mm]

From soil moisture, water flows to the response reservoirs by recharge, described by equation 3.3. Recharge depends on the maximum soil moisture content (*FC,* [mm]), a soil routing parameter *β* [-] and rainfall. Recharge is distributed over the upper and lower response reservoirs by percolation (*PC* [mm·day^{-1}]) described in equation 3.4. When rainfall is lower than percolation parameter *PERC* [mm·day^{-1}], all recharge is distributed to the lower response reservoir. When rainfall exceeds *PERC*, the remainder is available for the fast runoff reservoir.

$$RC = \left(\frac{SM}{FC} \right)^{\beta} P \tag{3.3}$$

Where besides *SM,* given in eq. 3.2:

RC = Recharge [mm·day^{-1}]
FC = Maximum soil moisture storage [mm]
β = Soil routing parameter [-]
P = Rainfall [mm·day^{-1}]

$$PC = \min\left(PERC, RC \right) \tag{3.4}$$

Where besides *RC,* given by eq. 3.3:

PC = Percolation [mm·day^{-1}]
$PERC$ = Percolation parameter [mm·day^{-1}]

Depending on the soil moisture content, capillary flux (*CF,* [mm·day^{-1}]) may occur from the fast runoff reservoir to the soil moisture storage. The flux is null when soil moisture is fully saturated. Capillary flux is at its maximum when the soil moisture storage is empty and in this case equal to parameter *CFLUX* [mm] as shown in equation 3.5.

$$CF = CFLUX \left(\frac{FC - SM}{FC} \right) \tag{3.5}$$

Where besides the quantities given in eq. 3.3:

CF = Capillary flux [mm·day^{-1}]
$CFLUX$ = Capillary flux parameter [mm·day^{-1}]

The water balance for soil moisture is described by equation 3.6. Soil moisture content is influenced by fluxes from outside the model boundary, meteorological forcing and fluxes to response reservoirs. Rainfall and capillary flux increase soil moisture storage and evapotranspiration and recharge drain the soil moisture content. The initial value for *SM* is set on 100mm (being an arbitrary, but realistic value).

$$\Delta SM = P - ET_a + CF - RC \tag{3.6}$$

Where besides the quantities given in eq. 3.3 t/m 3.5:

ΔSM = Change in soil moisture storage [mm]

The fast and slow runoff routines

From every cell runoff is generated via the quick runoff and base flow routines. Quick runoff flows from the fast runoff reservoir and is calculated by means of equation 3.7. Runoff from this reservoir shows non-linear behavior defined by the parameters k_f [day^{-1}] and α [-]. The recession parameter k_f is defined by equation 3.8, whereby *hq* [mm] is half of the mean annual flood and k_{hq} [-] a recession parameter at *hq*. For simplification, the value of parameter k_f is later directly optimized directly

rather than using equation 3.7 to determine its value. This more simplified approach has been previously used by Booij (2005) and Deckers (2006).

Slow runoff occurs from the lower response reservoir and is calculated by equation 3.9. It relies on lower reservoir storage and linear recession coefficient k_s [day^{-1}]. Quick runoff and base flow are calculated based on reservoir levels after soil routing is determined and are always limited by reservoir storages shown in equation 3.7 and 3.9. Total runoff R_{tot} is the sum of quick runoff and base flow given by equation 3.10.

$$R_f = \min(k_f \times H_f^{(1+\alpha)}, H_f) \tag{3.7}$$

Where:

R_f = Fast runoff [mm·day^{-1}]
k_f = Recession parameter in fast runoff [day^{-1}]
H_f = Quick runoff reservoir storage [mm]
α = Non-linearity parameter to fast runoff [-]

$$k_f = \frac{k_{hq}^{1+\alpha}}{hq^{\alpha}} \tag{3.8}$$

Where (besides k_f and α given in eq. 3.7):

hq = Half of mean annual flood [mm]
k_{hq} = Recession parameter to hq [-]

$$R_s = k_s \times H_s \tag{3.9}$$

Where:

R_s = Slow runoff [mm·day^{-1}]
k_s = Recession parameter to slow flow [day^{-1}]
H_s = Slow runoff storage [mm]

$$R_{tot} = R_f + R_s \tag{3.10}$$

Where (besides R_f and R_s, given by eq. 3.7 and 3.9):

R_{tot} = Total runoff [mm·day^{-1}]

The water balance of the fast response reservoir is given by equation 3.11. Reservoir storage changes due to capillary flux and loss to the lower response reservoir through percolation. The remaining storage partially lost by quick runoff. Influx from to the lower reservoir is provided by percolation as to be seen in equation 3.12. The remaining storage partially lost by base flow. The initial value for, H_{uz} and H_{lz} are set on 0mm for the entire basin. With the interpretation simulation results for the first period of days, effects of the chosen initial conditions (SM, H_f and H_s) should be taken into account.

$$\Delta H_f = RC - PC - CF - R_f \tag{3.11}$$

$$\Delta H_s = PC - R_s \tag{3.12}$$

Where (besides the quantities given by the equations above):

Δh_f = Change in quick runoff storage
Δh_s = Change in slow runoff storage

The routing routine

After runoff is calculated on cell basis, total runoff is accumulated per sub-catchment. Thereafter a routing routine is applied to redistribute the sub-catchment runoff R_{sub} [mm·day^{-1}] over time. A simple Unit Hydrograph, *UH,* based on an isosceles triangle, describes the distribution of runoff over time (See Figure 3.2). The base of this triangle is the sub-catchment's time of concentration, which is equal to the parameter *MAXBAS* [day]. It equals the travel time of the last water particle before it reaches the outlet of the sub-catchment. Over the length of MAXBAS, for every day *i*, following the current time step *t* a discharge release factor $F_R(i)$ [-] is calculated according to the triangular unit hydrograph, as illustrated by Figure 3.2. The contribution sub-catchment runoff R_{tot} to future sub-catchment runoff $\Delta R_{sub}(i)$ is given by equation 3.13, being a multiplication of the total runoff today R_{tot} and the future discharge release factors $F_R(i)$ untill $t+MAXBAS$ is reached. The sub-catchment runoff at the outlet of the catchment at time step *t* is the summation of sub-catchment runoff of past days *i* allocated to *t*, as described by equation 3.14. As the unit hydrograph can be seen as water storage, its water balance is given by equation 3.15.

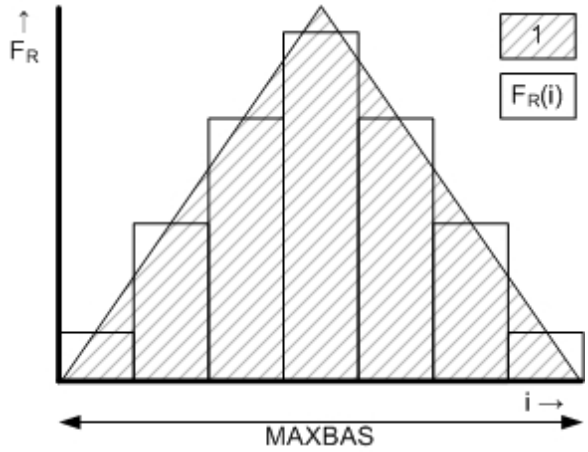

Figure 3.2 - Triangular UH for Runoff Routing

$$for \quad t \le i \le t + MAXBAS$$
$$\Delta R_{sub}(i) = F_R(i) \cdot R_{tot} \tag{3.13}$$

$$R_{sub}(t) = \sum_{i-MAXBAS}^{i} \left(\Delta R_{sub}(i)\right) \tag{3.14}$$

$$\Delta UH = R_{tot} - R_{sub} \tag{3.15}$$

Where, besides R_{tot} given in eq. 3.10:

R_{sub}	= Sub-catchment runoff [mm·day^{-1}]
F_R	= Discharge release factor
t	= Indicator of the current time step
i	= Indicator of future (eq. 3.13) or past (eq. 3.14) days

3.1.3 RIBASIM Nile Model

The RIBASIM Nile Application used in this project is developed for the LNFDC/ICC project as mentioned in section 1.1.3. In this section only a brief description, relevant for understanding the schematization of the Nile River in the NHSM is given. A full description, including water distribution equations, is given in original RIBASIM-NILE documentation (MWRI/Deltares, 2009a).

A flow diagram of the Nile River implementation in RIBASIM is given in Figure 3.3. The schematization discriminates the three tributaries of the Main Nile: the White Nile, Blue Nile and Atbara River. Where the HBV model simulates runoff with a time step of one day, RIBASIM-NILE relocates water in the tributaries at a monthly scale. Therefore, routing within river sections is only present in cases the response time of that section is more than the calculation time step of the model. In other cases, all upstream water is allocated to the downstream point at the end of the time step. Several methods of river routing have been chosen for different river sections (see: MWRI/Deltares (2009a)). Furthermore, the model simulates the behavior of Lakes, Reservoirs, Swamps and irrigation schemes, for which the equations are given in the same annex. The model is forced by sub-catchment runoff and rainfall and evaporation over water bodies as shown in Figure 3.3.

The White Nile

As shown in Figure 3.3, the upstream boundary of the White Nile is the sub-catchment draining in Lake Victoria. From Lake Victoria water is directed towards Lake Kyoga, together with the runoff contribution of the catchment between both lakes. Outflow from Lake Kyoga is accumulated with outflow from Lake Albert. The lakes Edward and George, upstream Lake Albert are not incorporated in the model schematization. Accumulated flow from Lake Albert and Lake Kyoga is aggregated with sub-catchment runoff between Pakwach and Mongalla, where after it drains in the Sudd swamps. Since the geophysics and hydrology of the Sudd swamps is not accurately known, it is simplified by two fixed storage reservoirs neglecting a major part of the systems dynamic behavior. Sudd outflow is accumulated with water from Lake No, also simplified with a fixed storage reservoir. The interaction between Lake No and the Sudd system is ignored. From the east, the Sobat River with its two tributaries, the Pibor and Baro Rivers, enters the system. In the upstream part of the Baro River a part is lost from the system and a part is diverted towards the Machar Swamps simplified by a fixed storage reservoir with a possible release to the White Nile. The sum of Pibor and Baro flows enter a Sobat routing reservoir from which it is released to the White Nile. There it is accumulated with outflow from the Sudd and Lake No. Release from this reservoir enters the Ghabal Aulia reservoir which drains in the Main Nile.

The Blue Nile

The Blue Nile is essentially schematized as a sequence of storage reservoirs starting with Lake Tana (see Figure 3.3). From Lake Tana, water is partly diverted to an irrigation scheme and downstream towards the Deim. In this reach, it accumulates outflow from the Ficha reservoir, and flows subsequently through the Roseires and Sennar reservoirs each with a flow division, to allow for reservoir overtopping. Downstream, inflow from the Dinder and Rahad Rivers is accumulated to Blue Nile flow. The latter two rivers are schematized as one reach with and sub-catchment. Downstream, water enters a Blue Nile routing reservoir, releasing water to the Main Nile.

The Main Nile

From Khartoum, the Main Nile flows downstream towards a routing storage reservoir. This reservoir is also fed by water from the Atbara River, entering the system from the east. Upstream, the Atbara is fed by the outflow of two reservoirs. From there, it passes small irrigation schemes, and enters the Kashm el Girba Dam. Outflow from the Kashm el Girba Dam is partly diverted towards the New Halfa Irrigation scheme. Remaining flow is added to the Main Nile routing storage. Outflow from the storage reservoir is accounted to Dongola, which is used as a downstream boundary in this study.

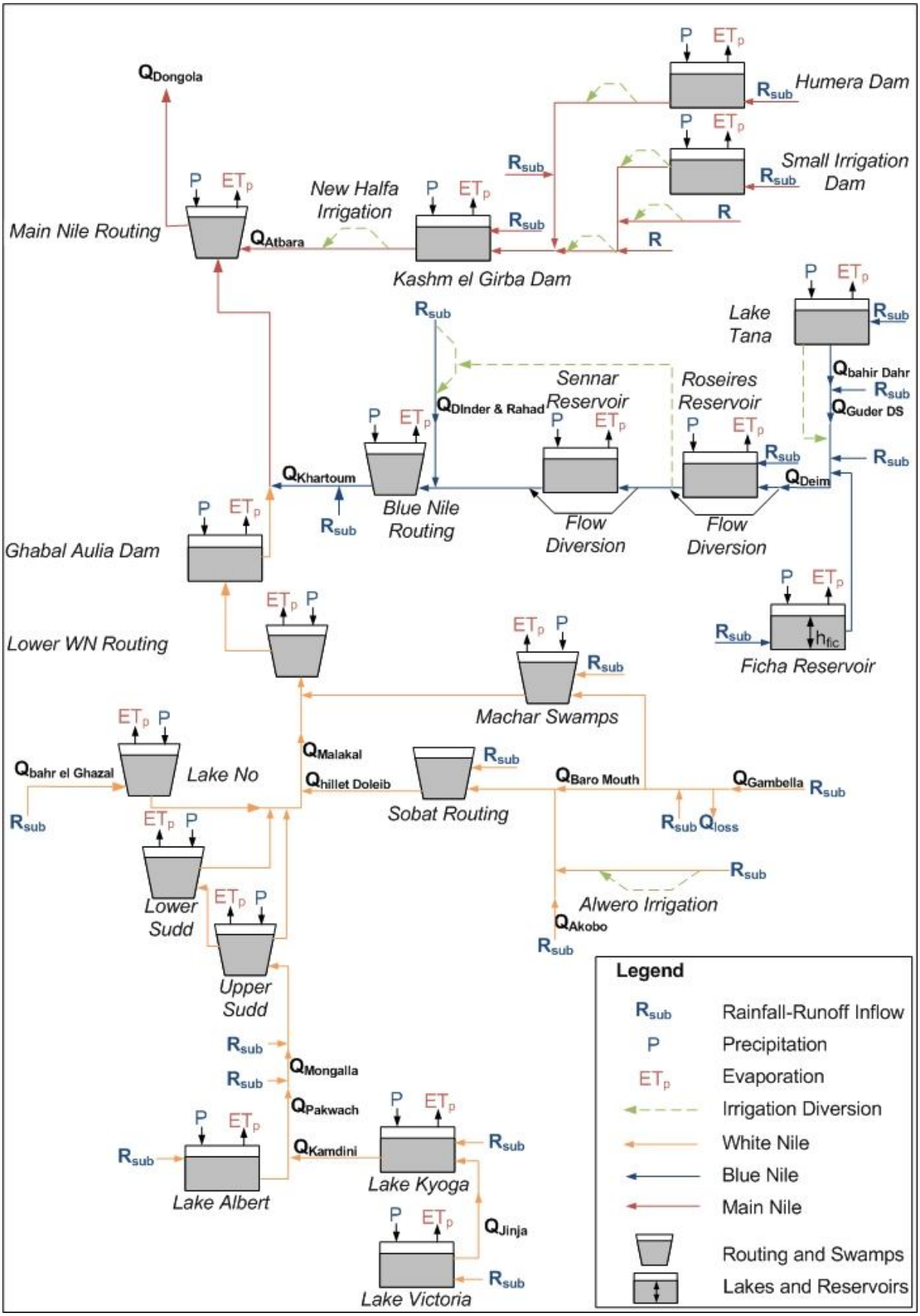

Figure 3.3 – Flow diagram of RIBASIM Nile model. Included are the White Nile, Blue Nile and Atbara tributaries. For the downstream boundary Dongola town is taken 700 km upstream of the HAD. The diagram only describes the layout of Scenario A, describing the Natural State (See MWRI/Deltares (2009a) for further details).

3.1.4 Integration of HBV and RIBASIM-NILE to NHSM

Model integration implies sub-catchment runoff R_{sub} [mm·month^{-1}], one of the forcing variables of RIBASIM-NILE, is supplied by the HBV rainfall-runoff model, using rainfall and potential evapotranspiration as its forcing variables. Since the latter runs on a daily time step, HBV output is aggregated over the respective month, before it is used as input for RIBASIM-NILE.

As shown in Figure 3.3, RIBASIM is forced by meteorological forcing and sub-catchment runoff. The used meteorological forcing is required on locations (reservoirs, small lakes, etc). For sub-catchments, besides runoff, area average rainfall and evapotranspiration are required to simulate effects of irrigation schemes on river discharge. Since the model does not consider geographical space, area average forcing values are multiplied with representative areas of the sites of interest (being lakes, reservoirs or sub-catchments). Therefore, documentation of the LNFDC/ICC project solely shows sub-catchment areas rather than its geographical locations (MWRI/Deltares, 2009e). To redefine RIBASIM-NILE and HBV forcing, the map shown Figure 3.4, discriminating 32 hydrological sub-catchments, is reconstructed from the areas specified in LNFDC/ICC data. A full discussion on the issues involved in the derivation of the map presented in Figure 3.4 is found in Annex B. Though, the map shows some clear errors, a proper reanalysis of sub-catchments would require an adjustment of sub-catchment areas in RIBASIM-NILE and a recalibration of the model, which is considered beyond the scope of this research. For this reason, the map is accepted. However, in future studies a revision of the areal representation of RIBASIM-NILE, and therefore the NHSM is recommended.

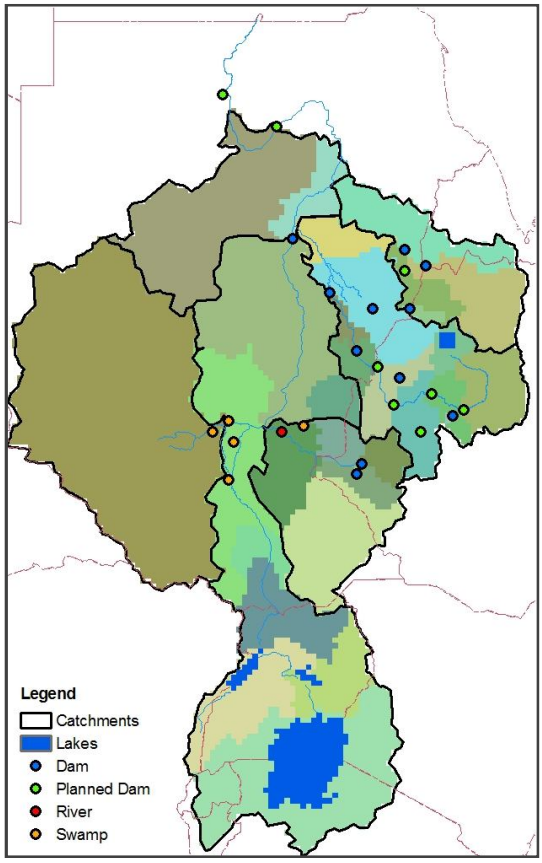

Figure 3.4 - Spatial distribution of model input (colored areas represent hydrological sub-catchments)

Figure 3.4 shows besides the hydrological sub-catchments described above other geographical features:

- Area average values for potential evapotranspiration and rainfall are to be specified over *lakes*, as far as incorporated in the model schematization
- Location values for *dams, swamps* and *rivers* are required to force de model with potential evaporation and rainfall.
- Location values for *planned dams* are incorporated to allow for simulations with other scenarios than the one representing the natural state of the Nile River.

3.1.5 NHSM calibration and validation

The NHSM is calibrated by comparing simulated and observed discharges (Q_{sim} and Q_{obs}) at seventeen locations along the river for which observational series are available (see: MWRI/Deltares (2009e)). The locations and corresponding upstream catchments are given in Figure 3.5. Since, hydrological catchments outnumber calibration catchments, some upstream areas (referred to as calibration sub-catchments) consist of multiple hydrological sub-catchments.

Model calibration and parameter selection

All model simulations are subject to uncertainty. This uncertainty arises in that no rainfall-runoff model is a true reflection of the processes involved, that it is impossible to specify the initial and boundary conditions required by the model with complete accuracy and that the observational data available for model calibration are not error-free (Beven, 2004). Uncertainty in model predictions can be reduced by the optimization of model parameters.

Optimization of all nine adjustable parameters in the applied version of HBV would lead to similar model performance for different sets of parameters suggesting different geophysics. This problem arises due to other sources of uncertainty mentioned above and is referred to as the *equifinality* problem (extensively described by Beven (2004)). One way in diminishing equifinality is to only adjust parameters clearly identifiable to hydrological processes. Based on these considerations and previous experience with the identifiability of HBV model parameters (Booij, 2002), the following parameters are optimized:

- Parameters related to the soil moisture routine: *FC*, *LP* and *β*.
- Parameters related to quick runoff and base flow routine: *PERC*, k_s and k_f.

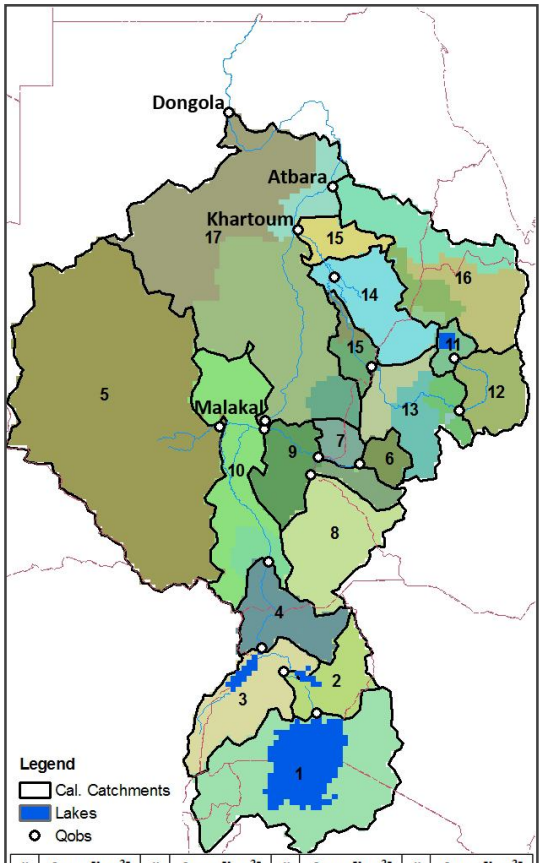

#	Area [km²]	#	Area [km²]	#	Area [km²]	#	Area [km²]
1	189,000	6	21,000	11	15,000	16	174,000
2	54,000	7	22,000	12	57,000	17	470,000
3	85,000	8	112,000	13	100,000		
4	74,000	9	60,000	14	85,000		
5	572,000	10	135,000	15	63,000		

Figure 3.5 - Calibration and hydrological (colored) sub-catchments

Parameters are optimized within their possible domains. Default parameter values are given by the SMHI (1999). An overview of domain choices made in previous HBV applications given by Booij (2005) and considerations of Deckers (2006) motivate the choice of the parameter ranges given in Table 3.2.

Table 3.2 – Calibration parameters with their domains and default values

Parameter	*FC [mm]*	*LP [mm]*	*β [-]*	K_f [day^{-1}]	K_s [day^{-1}]	*PERC [mm·day^{-1}]*
Min. Value	100	0.1	1	0.005	0.0005	0.5
Max. Value	800	1	6	0.10	0.15	6
Def. Value	200	0.9	2	0.01[1]	0.05	1

[1] Value based on equation 3.8 with default values for kHq=0.17 and Hq=3.0 (SMHI, 1999)

Parameters excluded from calibration are given in Table 3.3. *MAXBAS* and *α* are related to the description of peak floods, a phenomenon with a characteristic scale of hours to days, which is smaller than the scale of the available monthly discharges. *Alpha* is kept on its default value (SMHI, 1999). *MAXBAS*, the time of concentration, is proportional to the sub-catchment area A_{sub} [km^2]. With an assumed average flow velocity of 1 m/s, *MAXBAS* is calculated as in Table 3.3. The sensitivity of *CFLUX* to model performance is considered to be limited (Booij, 2002) and is therefore kept constant on 1 mm/day.

Table 3.3 - Default values of unchanged parameters

Parameter	*A [-]*	*CFLUX [mm·day^{-1}]*	*MAXBAS [days]*
Value	1	1	$\frac{1000}{60^2 \times 24} \times \sqrt{A_{sub}}$

Parameter optimization

Methods used for the optimization of model parameters can be divided to qualitative and quantitative methods. Although with qualitative optimization good results can be achieved the method is subject to bias, since a 'good fit' between simulated and observed hydrographs vary with the hydrologist's perception. Therefore a quantitative method is used.

In quantitative model optimization single objective functions (SOFs), explicitly state the level of agreement between certain aspects of the observed versus simulated hydrograph. Many SOFs have been developed (Green & Stephenson, 1986) emphasizing certain aspects of agreement. Selecting only one SOF, would mean some aspects of hydrograph agreement would be neglected increasing the chance of equifinality as described by (Beven, 2004). Therefore, according to Madsen (2000) multiple SOFs should be selected based on the following aspects.

1. The overall water balance between observations and simulations.
2. The overall shape of the observed and simulated hydrograph.
3. The agreement between observation and simulation on timing, rate and volume of peak flows.
4. The agreement between observed and simulated low flows.

With respect to the first aspect, the representation of long term discharged volumes, the commonly used relative volume error *RVE* is selected, given by equation 3.16. *RVE* is either given as a percentage or a fraction of observed discharge. A *RVE* of zero indicates total simulated discharge equals observed discharge. Negative and positive *RVEs* indicate under- and overestimation of simulated discharges respectively.

$$RVE = \sum_{i=1}^{n} \frac{Q_{sim;i} - Q_{obs;i}}{Q_{obs;i}} \tag{3.16}$$

Where:

RVE = Relative Volume Error [-]
Q_{sim} = Simulated discharge [m3·s^{-1}]
Q_{obs} = Observed discharge [m3·s^{-1}]
i = Subscript indicating a respective month

With respect to the other aspects of agreement, the Nash and Sutcliffe coefficient *NS* is selected, given by equation 3.17 (Nash & Sutcliffe, 1970). *NS* is most commonly used in the optimization of HBV (e.g. Booij, 2005; Lidén & Harlin, 2000; G. Lindström, 1997; Göran Lindström et al., 1997) and has also been applied when results are compared for average monthly discharges (Guo, Wang, Xiong, Ying, & Li, 2002). An optimal simulation is achieved when *NS* equals one. A *NS* lower than zero indicates the simulation is a worse predictor than mean observed discharge.

$$NS = 1 - \frac{\sum_{i=1}^{n}\left(Q_{sim;i} - Q_{obs;i}\right)^2}{\sum_{i=1}^{n}\left(Q_{obs;i} - \overline{Q}_{obs}\right)^2} \quad (3.17)$$

Where, besides the quantities mentioned in equation 3.16:

NS = Nash and Sutcliffe Coefficient [-]

$\overline{Q}_{obs}$ = Average monthly observed discharge [m3·s^{-1}]

To give one explicit statement about model performance, a combined objective function *COF* is introduced. Here, *RVE* and *NS* are combined as in equation 3.18, dividing the Nash and Sutcliffe Coefficient by one plus the absolute relative volume error. In an optimal model performance *COF* = 1, whereby the relative volume error is zero and the agreement between the two hydrographs is perfect. *COF* departures from zero indicate worse *NS* and/or *RVE* values. An earlier successful application of the *COF* function is found in (Akhtar, Ahmad, & Booij, 2008).

$$COF = \frac{NS}{1 + |RVE|} \quad (3.18)$$

Where, besides NS and RVE given in equation 3.16 and 3.17:

COF = Combined Objective Function [-]

Optimization routine

Since in this study the equifinality problem is acknowledged and effort has been made, a logical step would be to optimize NHSM using a Monte Carlo optimization method (see: Beven (2004)). A disadvantage of this method is the large amount of simulations required for a sufficient examination of the parameter space (Harlin & Kung, 1992). Therefore the NHSM will be optimized by automatic calibration. Examples of automatic calibration of HBV can be found in Lindström (1997). The latter applied a simple calibration routine for the HBV model based on *NS* and *RVE*, similar to the method applied in this study. However, as Lindström optimized all parameters on the original version of HBV96, here a choice is made for specific parameters, given in Table 3.2.

In the calibration routine, first the length of the calibration series is determined by finding the first and last low flow period narrowing the calibration series length to entire hydrological years (see Figure 3.6). Thereby effects of initial conditions on model performance are negligible. Thereafter, soil moisture parameters *FC*, *LP* and *β* are optimized by repetitive single parameter optimizations, determined by a smart search routine similar to Lindström (1997), explained in Annex C. Optimization stops when the ΔCOF changes less than 1% over the last optimization sequence. Thereafter routing parameters *PERC*, k_s and k_f are optimized identical to the optimization of soil moisture routing. This yields the optimal parameter set.

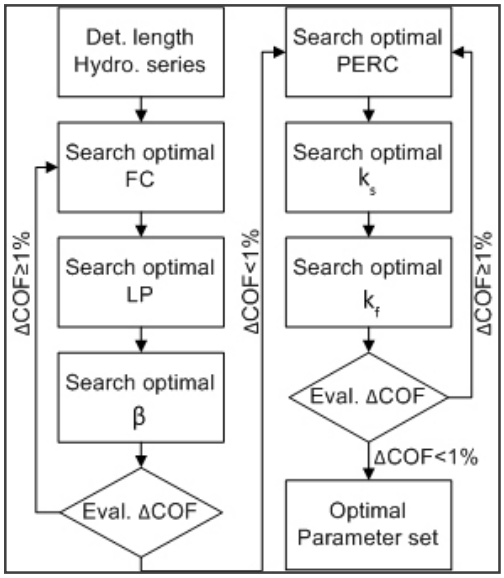

Figure 3.6 – Parameter optimization routine

3.2 NHSM simulations with forcing derived from GCM simulations

The second step of this study is to generate meteorological forcing for the NHSM based on simulations with GCMs. Thereafter, NHSM-GCM simulations are assessed under (1) the current climate and (2) the future climate. The first type of assessment allows for a comparison of GCM and NHSM-GCM simulations with observed climate and discharges. For the second type of assessment, predictive uncertainty can be tested by using multiple GCMs and see whether there is any agreement in future trends of climate and discharges.

Since the majority of rainfall over the Nile Basin falls over the Great Lakes district and the Ethiopian Plateau (see Figure 2.2), these areas are of principal interest when changes in climate are to be assessed. The sub-catchments belonging to these areas are hatched in Figure 3.7. The Great Lakes area covers an area of 481.000 km^2, the Blue Nile upstream Deim an area of 175.000 km^2, and the Atbara catchment an area of 174.000 km^2. Analyses of GCM simulations for the current and future climates primarily focus on these areas.

Principal locations for assessment of discharges simulated with NHSM-GCM combinations are the outlets of the areas where climate simulations are analyzed (see Figure 3.7). Since changes in evapotranspiration also has an effect on water flowing through the Sudd swamps, another location is Malakal, the most downstream gauging station in the White Nile. Effects on river discharges reaching Lake Nasser can be compared at Dongola, the downstream boundary of the NHSM.

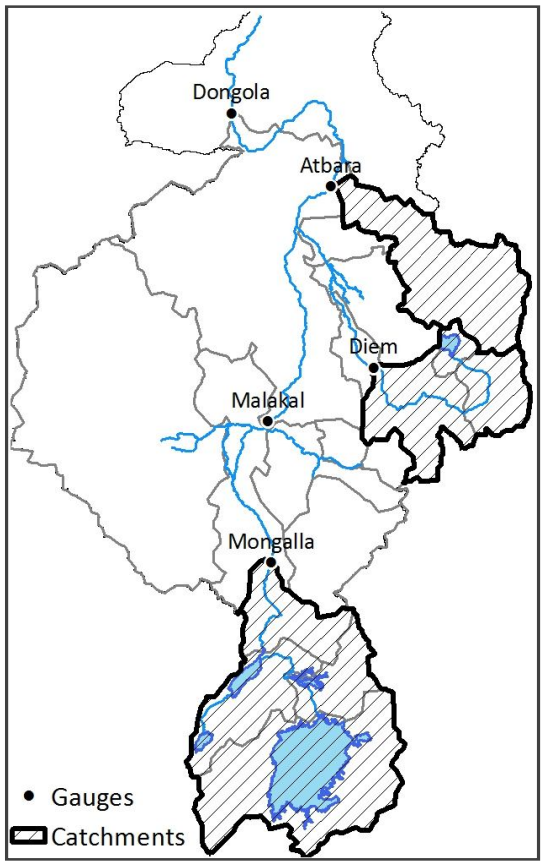

Figure 3.7 – Geographical layout for climate change analysis

In analysis, the following steps are taken:

1. Assessment of river sensitivity to a changing climate by adjusting meteorological forcing for the NHSM and assessing effects on river discharge.
2. The construction meteorological forcing series from outputs of GCM simulations
3. Assessment of the performance of NHSM-GCM in representing the current hydro-climate by comparison of simulations with observations
4. Assessing the predictive power of NHSM-GCM combinations for the future climate by Intercomparison of discharges for different GCMs

The first step is a necessary for understanding the NHSM sensitivity for changed inputs. Whether these changes are a good reflectance of the real system can be justified in the comparison of results with literature. The rest of the steps involved will be expounded in the remainder of this paragraph. In section 3.2.1 and 3.2.2, the used GCMs and the derivation of meteorological forcing from their output is described. In section 0, the methodology for assessing NHSM-GCM combinations under the current climate is expounded. In section 0, the method for assessing future climate and discharge simulations is described.

3.2.1 Global Circulation Models

Gridded GCM data used in this study contain daily values for temperature (*T* [K]) and rainfall (*P* [kg/m^2/s]), retrieved from the Program for Climate Model Diagnosis and Intercomparison (PCMDI, 2009). At Deltares, resampled grids to NHSM spatio-temporal resolution are available for three GCMs; ECHAM5 (Roeckner et al., 2003), GISS-ER (Schmidt et al., 2006) and CSIRO-mk3.0 (Gordon et al., 2002). For all models, datasets are supplied for period 1961-1990, 2046-2065 and 2081-2100. Simulations for the latter two periods are based on the SRES B1 and A2 scenarios (Nakicenovic & Swart, 2000). A brief description of the models is given in the sections below.

ECHAM5

ECHAM5 is the newest version of the ECHAM model family, developed at the German Max Planck Institute for Meteorology (MPI) and described by Roeckner et al (2003). The model supplies output for vorticity, divergence, temperature, surface pressure, water vapor, cloud liquid water and cloud ice (PCMDI, 2009). It uses the T63/L31 grid, equal to a spatial resolution of ±200km and discriminates 31 vertical layers (see Figure 3.8). Henceforward the model will be referred to as ECHAM.

GISS-ER

The GISS-ER model is developed by the NASA Goddard Institute for Space Studies (GISS) and will henceforward be referred to as GISS. The model is extensively described by Schmidt et al (2006). GISS supplies output for temperature, specific humidity and total condensated water. It uses a grid size of 5' x 4' (Lon. x Lat.)and discriminates 20 vertical layers (see Figure 3.8). The developers did not try to uniquely pursue higher model resolutions. In their philosophy it might improve some aspects of simulations, but is also likely to raise issues in model parameterization. Besides, higher resolutions severely limit the extent to which experiments are possible due to high computation times.

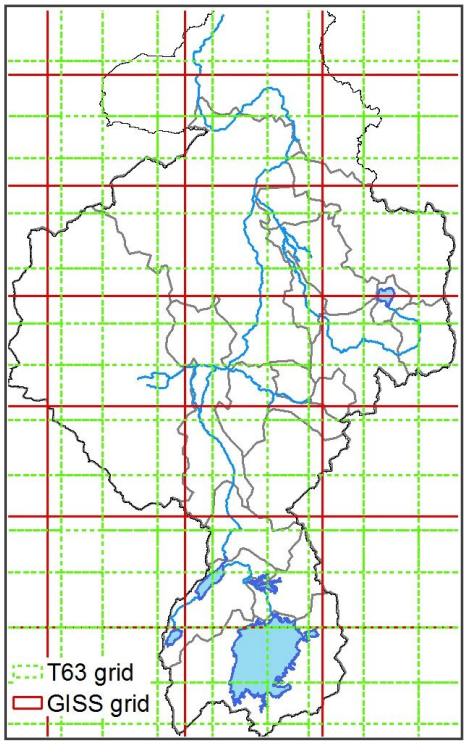

Figure 3.8 - GCM grids

CSIRO-mk3.0

The CSIRO-mk3.0 model is developed at the Australian Commonwealth Scientific Research Organization (CSIRO) and described by (Gordon et al., 2002). The model supplies output for vorticity, divergence, temperature, surface pressure and atmospheric moisture. It uses a T63/L18 grid, which equals a spatial resolution of ±200km and a discrimination of 18 vertical layers (see Figure 3.8). Though, the CSIRO model contains a comprehensive representation of the four major components of the climate system: the atmosphere, biosphere, oceans and ice-sea, developers acknowledge some elements such as a better representation of vegetation types are important improvements for future model version.

The model descriptions show that the used GCMs use different resolutions. Where ECHAM and CSIRO use the finest grid parallel to the earth surface, GISS is on a much coarser resolution. Thereby ECHAM uses the finest discretization in vertical direction. However, in the philosophy of GISS developers, a finer model resolution does not guarantee higher model performance, since it also requires better model parameterization.

3.2.2 Combining GCM data with the NHSM

From raw GCM output, meteorological forcing for the NHSM is to be generated. Since the only output variables provided are rainfall and temperature, the latter is to be converted to evapotranspiration. This is described in the first part of this section. Thereafter, the bias correction applied to correct simulated rainfall and evapotranspiration to the observed mean monthly climatology is discussed. At last, it is described how bias corrected GCM simulations are used as forcing series for the NHSM.

Derivation of reference evapotranspiration

For the conversion of GCM observed temperature to reference evapotranspiration the Blaney-Criddle method, described by Brouwer and Heibloem (1986), is applied (see equation 3.19). Reference evapotranspiration is defined as a function of the mean daily temperature for a month T_{mean}, [C]. The mean daily percentage of annual daytime hours p [-] is retrieved from Brouwer and Heibloem (1986). In essence this parameter indicates the effect of daylight on evapotranspiration. Therefore it changes over season and latitude (begin constant over the entire year at the equator).

$$ET_0 = p\left(0.46T_{mean} + 8\right) \tag{3.19}$$

Where:

ET_0 = Reference evapotranspiration [mm·day^{-1}]
p = Mean daily percentage of annual daytime hours [-]
T_{mean} = Mean daily temperature [C]

Since the Blaney-Criddle method bases reference evapotranspiration solely on one meteorological variable, its value is highly uncertain. The absence of other variables relevant to evaporation, such as cloud cover, wind and vapour pressure makes the method inaccurate compared to the method used in determining observed evapotranspiration. Brouwer and Heibloem (1986) estimate its can be underestimated up to 60% in dry, sunny areas and overestimated up to 40% in calm humid, clouded areas. Therefore, when derived evapotranspiration from GCM results is compared with observed evapotranspiration, uncertainty arises in the simulation of GCMs and the method of estimating reference evapotranspiration from its outputs.

Bias correction of rainfall and reference evapotranspiration

As already described in the introduction of this study, GCMs have great difficulties in representing the Nile climate. Since detailed downscaling of GCM outputs is considered to be beyond the scope of this study, a degree of uncertainty in the spatio-temporal variability of meteorological variables is accepted. However, for simulating realistic future discharges, a bias correction is applied on GCM data to represent the mean monthly climatology given by the observed dataset described in section 3.1.1. Mean monthly observations are divided by mean monthly simulated GCM values at a specific spatial resolution. Regarding the latter, different options exist:

1. Correction on the resolution of NHSM of 10' x 10' (≈20 x 20km).
2. Correction on GCM tiles, with resolutions depending on the type of GCM (see Figure 3.8).
3. Correction to hydrological sub-catchments with varying sizes (see Figure 3.4).

In principle, a bias correction according to one of the first two options is preferred. However, by testing these methods, numerical problems are revealed. With the first option, the scale of correction proved to be too small, with the second option numerical problems emerged in NHSM cells at the boundaries of GCM tiles. Since mean monthly observed cell values are divided by their simulated equivalents, a very high observed value, a very low simulated value or a combination of

the two lead to very high correction factors. When such correction factors are for instance to be applied on daily rainfall, a day with a significant rainfall sum, multiplied with a very high correction factor, results in a very high GMC rainfall estimate for that day after. Bias correction is therefore to be applied on a sufficient spatial scale.

On the scale of sub-catchments, bias correction provided sensible rainfall and evapotranspiration estimates. The method is described for rainfall in equation 3.20, where it is identical to the correction of reference evapotranspiration. In case the 1961-1990 mean monthly rainfall simulated by the respective GCM over the sub-catchment is higher than 1mm (the threshold for wet days), raw GCM rainfall is corrected by dividing mean monthly observed rainfall by the GCM simulated value. In case rainfall observation is less than 1 mm, the sub-catchment is dry according to GCM simulations is and cannot be corrected. To allow for rainfall input in future climates, GCM data is directly imported to the NHSM.

$$P_{GCM}' = P_{GCM} \times \frac{\overline{P}_{obs;sub}}{\overline{P}_{GCM;sub}} \quad \text{if} \quad \overline{P}_{GCM;sub} \geq 1mm$$
$$P_{GCM}' = P_{GCM} \quad \text{if} \quad \overline{P}_{GCM;sub} < 1mm \qquad (3.20)$$

Where:

P_{GCM} = Uncorrected GCM simulated rainfall [mm·day^{-1}]

P_{GCM}' = Corrected GCM simulated rainfall [mm·day^{-1}]

$\overline{P}_{obs;sub}$ = Area average observed rainfall over the sub-catchment [mm·day^{-1}]

$\overline{P}_{GCM;sub}$ = Area average GCM simulated rainfall over the sub-catchment [mm·day^{-1}]

Construction of NSHM forcing for the NHSM

Although GCM data is bias corrected to some extend for producing realistic forcing series for the NHSM, three major sources of GCM uncertainty still exist:

1. Since bias is corrected to meet the observed mean monthly climatology, there will be disagreement between intensity distributions of GCM simulated and observed daily rainfall
2. Mean monthly correction do not guarantee a good representation of interannual variability of monthly rainfall by GCM simulations.
3. An average correction over hydrological sub-catchments suggests spatial differences still exist on the scale of the NHSM.

Based on the three sources of uncertainty mentioned above it is concluded that climates simulated by GCMs give realistic values for both rainfall and potential evapotranspiration, but NHSM-GCM simulations aren't an exact representation of the actual hydro-climate. Differences in the spatio-temporal variability of simulated model forcing lead to different hydrological behavior of the system. In this respect, it is also likely that initial conditions for NSHM simulations with observed forcing (only the states of water bodies in RIBASIM-NILE, since conditions for HBV are arbitrary chosen) are not valid for NHSM-GCM simulations.

Since the GCM data series do not represent a continuous series from the reference period till 2100, initiation problems arise at the beginning of every period. Hence, the climate is likely to change between the periods and so is the state of the NHSM. Problems related to initial conditions are solved by defining s model initialization period before starting the simulation run for a respective period, as shown in Figure 3.9. In example, for a run of ECHAM under the B1 scenario, first the initial condition of the NHSM-ECHAM simulation is determined by running NHSM with forcing derived from

the 1961-1965 ECHAM simulation. Thereafter the reference period of 1961-1990 is simulated. The end state of this simulation plus the model initialization period over 2046-4050 forced by meteorological variables derived from the ECHAM B1 simulation determine the initial state for the 2046-2065 simulation. For the 2081-2100 simulation initial conditions are determined as for the period 2046-2065. Hereby it is assumed that a period of five years is sufficient to mitigate uncertainty due to initial conditions of the NHSM.

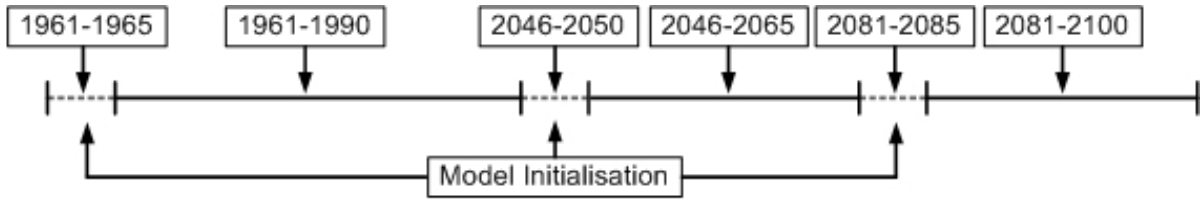

Figure 3.9 - Composition of NHSM-GCM forcing series

According to the systematic shown in Figure 3.9, six model simulations have been commenced, as shown in Table 3.4. As shown, NHSM-GCM simulations for the reference climate have been done twice, for every SRES scenario. However, besides for derivation of discharges, NHSM-GCM simulations for the reference climate are used to define the initial condition of the 2046-2065 period.

Table 3.4 - NHSM model runs with GCM derived forcing

period / *run*	*Reference (1961-1990)*	*climate 2065 (2046-2065)*	*climate 2100 (2081-2100)*
1	NHSM-ECHAM	NHSM-ECHAM B1	NHSM-ECHAM B1
2	NHSM-ECHAM	NHSM-ECHAM A2	NHSM-ECHAM A2
3	NHSM-GISS	NHSM-GISS B1	NHSM-GISS B1
4	NHSM-GISS	NSHM-GISS A2	NSHM-GISS A2
5	NSHM-CSIRO	NHSM-CISRO B1	NHSM-CISRO B1
6	NSHM-CSIRO	NHSM-CSIRO A2	NHSM-CSIRO A2

3.2.3 Assessing NHSM-GCM simulations

Results of NHSM-GCM simulations are assessed for the reference climate, the period 1961-1990, as well as for the 2046-2065 and 2081-2100 periods. The later periods will henceforward be referred to as 2065 and 2100 climates respectively. In this section, methods for assessing NHSM-GCM model performance for the reference and future climates are described.

Representation of current climate

As mentioned in the previous section, NHSM simulations forced by different GCMs for the reference climate most likely produces different hydro-climates. Causes of these differences are biases in the spatio-temporal distribution of simulated meteorological forcing, especially rainfall. Though, the volumes of potential evapotranspiration and rainfall are corrected, differences in the spatial allocation or timing of rainfall have an effect on the actual amount of water which evaporates and evapotranspirates over water bodies and the terrestrial surface:

- Evaporation used as forcing for RIBASIM-NILE (see Figure 3.3) is multiplied by the surface area of water bodies. In case of lakes and reservoirs, these surface areas have a relation with their stages. The stages are related to the reservoir storage, which is related to reservoir inflow. The latter is on its turn related to upstream rainfall. Differences in rainfall timing will therefore have an impact on the amount of water lost to evaporation.

- Potential evapotranspiration is used as forcing for the HBV rainfall-runoff model. The amount of water leaving the system is actual evapotranspiration, which is function of potential evapotranspiration and soil moisture storage (see equation 3.2). Soil moisture is mostly fed by rainfall. Differences in the spatio-temporal distribution of rainfall will therefore affect soil moisture storage and actual evapotranspiration. In case less water is lost to evapotranspiration, more water will be available for runoff.

When it is accepted that simulated hydro-climates differs for every NHSM-GCM simulation, due to remaining bias and will not be identical to a NHSM simulation with observed forcing the agreement of fit between discharge observations and NHGSM-GCM simulations can be used to determine the GCM performance in representing the current climate. For this matter, two types of statistics will be presented:

1. The mean monthly discharges $\overline{Q}(t)$, giving an indication how well the long term average discharge is simulated for the respective month.
2. The interannual variability, giving an indication how well the variability around the average discharge for the respective month is simulated.

To indicate interannual variance, first the standard deviation at a specific month is expressed as in equation 3.21. The statistic used to measure interannual variability is the coefficient of variance *CV,* given by equation 3.22

$$S(t) = \sqrt{\frac{\sum_{i=1}^{n}\left(Q(t)_i - \overline{Q}(t)\right)^2}{n-1}} \tag{3.21}$$

Where:

$S(t)$ = Standard deviation at month *t* [$Mm^3 \cdot month^{-1}$]
$Q(t)_i$ = Discharge at year *i* and month *t* [$Mm^3 \cdot month^{-1}$]
$\overline{Q}(t)$ = Long term mean monthly discharge of month *t* [$Mm^3 \cdot month^{-1}$]
n = Number of years [30]

$$CV(t) = \frac{S(t)}{\overline{Q}(t)} \tag{3.22}$$

Where besides $S(t)$ and $\overline{Q}(t)$ given in eq. 3.21:

$CV(t)$ = Coefficient of variance at month *t* [$Mm^3 \cdot month^{-1}$]

Generation of future climate projections from NHSM-GCM discharges

Climate change is analyzed by comparing GCM simulations for the reference climate with projections for the 2065 and 2100 climates. Climate projections for the Great Lakes areas and Ethiopian Plateau are most relevant, since there the majority of discharge is produced by of rainfall. An average projection over all GCM-scenario combinations gives an indication of change, but comparing the individual combinations reveals uncertainty in predicting climate change for the respective area.

Changes in mean monthly discharges under a NHSM-GCM simulation for a future period under a B1 or A2 SRES scenario can are expressed by 3.23. Here, the average monthly discharge of the simulation is divided by the value after a NHSM-GCM simulation for the reference climate. This change is multiplied by the average monthly observed discharge for the 1990 climate.

$$\overline{Q}'_{GCM(SRES);period}(t) = \frac{\overline{Q}_{GCM(SRES);period}(t)}{\overline{Q}_{GCM;1990}(t)} \times \overline{Q}_{Obs;1990}(t) \quad (3.23)$$

Where:

$\overline{Q}'_{GCM(SRES);period}(t)$ = Mean monthly corrected discharge under the GCM(SRES) simulation for a future period [$Mm^3 \cdot month^{-1}$]

$\overline{Q}_{GCM(SRES);period}(t)$ = Mean monthly NHSM-GCM simulated discharge under the SRES scenario for a future period [$Mm^3 \cdot month^{-1}$]

$\overline{Q}_{GCM;1990}(t)$ = 1961-1990 mean monthly NSHM-GCM simulated discharge at month *t* [$Mm^3 \cdot month^{-1}$]

$\overline{Q}_{Obs;1990}(t)$ = 1961-1990 mean monthly observed discharge at month *t* [$Mm^3 \cdot month^{-1}$]

4. NHSM optimization and performance

Optimization of parameters and the model performance of the NHSM under observed forcing are expounded in this chapter. Paragraph 4.1 and 4.2 describe results after model calibration and validation. In paragraph 0, NHSM calibration and validation results are discussed. Though model performance after calibration and validation are described for all sub-catchments, not all hydrographs are printed in the main report. These hydrographs are found in Annex D.

4.1 Model calibration

Discharge simulations and observations of complete hydrological years between 1961 till 1980 are compared with the combined objective function explained section in 3.1.5. In this paragraph, the optimal parameter set and model performance after calibration are described on sub-catchment scale.

In the optimization of soil moisture parameters, it is noticed that they mainly shift in favor of high soil moisture storages (*FC*) and low limits for evapotranspiration (*LP*) parameter optimization. Clearly, the model parameters are chosen in favor of high soil moisture storage and evapotranspiration, which is supported by the local geography described in paragraph 2.1.

With respect to optimization of response flux parameters, it is noted that equifinality (Beven, 2004) is still present in defining the value of the fast runoff recession coefficient (k_f). Since the parameter is related to floods, having a characteristic temporal scale of hours to days, it is hard to calibrate when only monthly discharge observations are compared. Therefore, for many sub-catchments, sensitivity of model performance to chosen k_f values is low. In exemplification, for the sub-catchment upstream Deim two simulations with extreme k_f values (0.005 and 0.1) are shown in Figure 4.1. Graphs are shown at the scale of calibration (months) and the scale of HBV simulation (days). For a k_f value of 0.005 and 0.1, the COFs at Deim are 0.86 and 0.85, indicating marginal changes in model performance, which is supported by the monthly graphs for both simulations. However, when results on a daily basis are compared, differences in peak behavior are profound. For instance, the discharge peak at the second half of September is ±30% higher with a k_f value of 0.1 relative to a simulation with a k_f value of 0.005.

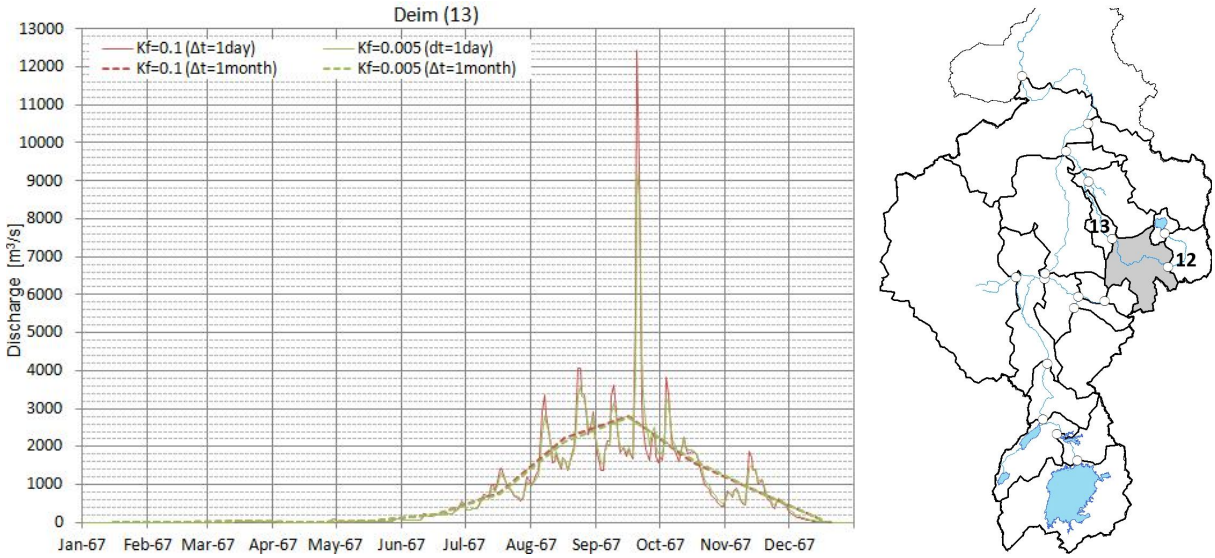

Figure 4.1 – Effect of K_f on mean daily and monthly simulated sub-catchment runoff at the Deim sub-catchment

Table 4.1 – Model parameterization after calibration with 1961-1980 meteorological and discharge observations

River	Basin	#	Soil Moisture Parameters			Response Flux Parameters		
			FC [mm]	*LP* [-]	α [-]	*PERC* [mm·day^{-1}]	k_s [day^{-1}]	k_f [day^{-1}]
White Nile	Jinja	1	800	0.1	6	6[3]	0.0005	0.005
	Kamdini	2	800	0.1	6	2.3	0.0013	0.005
	Packwach	3	800	0.1	6	1	0.0500	0.010
	Mongalla	4	800	0.1	2.5	1.2	0.1500	0.005
	Bahr el Ghazal[1]	5	800	0.1	6	2	0.0250	0.025
	Gambela	6	221	1	1	6[4]	0.0397	0.100
	Baro Mouth	7	500	0.92	2	0.9	0.0402	0.005
	Akobo	8	800	0.1	6	1	0.0500	0.010
	Hillet Doleib	9	800	0.1	6	6	0.0005	0.005
	Malakal[2]	10	800	0.1	1	0	0	0
Blue Nile	Bahir Dahr	11	718	0.9	2	6[3]	0.0255	0.005
	Guder DS	12	800	0.2	2	0.5	0.1500	0.100
	Deim	13	800	0.17	2	1	0.1289	0.009
	Dinder + Rahad	14	800	0.37	2	1	0.0481	0.007
	Khartoum	15	100	0.99	1	4	0.0147	0.093
Main Nile	Atbara	16	800	0.75	2	1.2	0.0422	0.006
	Dongola[2]	17	800	0.1	1	0	0	0

[1] Bahr el Ghazal Catchment is manually calibrated since optimization algorithm compromised (referred to in section 4.1.1.)
[2] Horizontal routing parameters are kept zero, since no lateral river inflow is assumed in these sub-catchments (referred to in sections and 4.1.1 and 4.1.3).
[3] High PERC value. Probably caused by Lake Victoria (Jinja) and Tana (Bahir Dahr) dispersion (referred to in section 4.1.1 and 0).
[4] High PERC value. Probably caused by systematic underestimation of discharge (referred to in sections 4.1.1 and 4.1.3).

Performance of the NHSM after calibration is summed up in Table 4.2. For all seventeen calibration sub-catchments shown in Figure 3.5, performance is expressed in terms of *RVE* and *NS*. |*RVE*| 5-10% and/or *NS* 0.5-0.6 is colored orange, indicating moderate model performance, caused by a high volume error or a low agreement between hydrographs respectively. |*RVE*|>10% and *NS*<0.5 indicate locations for which the model has low to nil predictive value. Model performance in different sub-catchments is described in the coming sections.

Table 4.2 - Model performance for sub-catchments over 1961-1980 data (red/orange = low/moderate predictive value).

River	White Nile										Blue Nile					Main Nile	
Basin	Jinja	Kamdini	Packwach	Mongalla	Bahr el Ghazal	Gambela	Baro Mouth	Akobo	Hillet Doleib	Malakal	Bahir Dahr	Guder DS	Deim	Dinder + Rahad	Khartoum	Atbara	Dongola
#	1	2	3	4	5	6	7	8	9	10	11	12	13	14	15	16	17
RVE [%]	2.44	1.18	1.89	0.56	41.03	-47.96	-0.09	-50.48	-5.87	4.53	1.91	0.24	0.13	-0.84	-0.17	-1.43	5.20
NS [-]	0.85	0.80	0.32	0.57	0.00	0.22	0.89	-1.36	0.66	0.37	0.72	0.66	0.86	0.64	0.84	0.62	0.64
COF [-]	0.83	0.79	0.32	0.57	0.00	0.15	0.89	-0.90	0.63	0.36	0.71	0.66	0.86	0.64	0.84	0.61	0.61

4.1.1 White Nile

Most upstream at Jinja, the outlet of Lake Victoria, discharges are simulated well after NHSM calibration, as shown in Figure 4.2 (*RVE* = 2.44%, *NS* = 0.85). When the hydrographs are examined in more detail, an underrepresentation of discharge variability by the model is shown after 1970. A high *PERC* value in combination with a low value for k_s indicates rainfall is mainly distributed towards the ground water system and the model is optimized towards maximum retention. This observation is supported by the geological characteristics of the sub-catchment (see section 2.1.1). Large reservoirs like Lake Victoria, decrease the identifiability of fast and base flow processes in the upstream catchment, when observation and simulation are compared downstream the lake outlet.

In sub-catchments downstream Jinja, model performance drops. At Kamdini, downstream the outlet of Lake Kyoga, model performance decreases but is still satisfactory. At Packwach, downstream of the Semliki and Victoria Nile confluence, long term discharges volumes are simulated well but performance drops towards a moderate predictive value (*NS* = 0.32), indicating moderate agreement between simulated and observed discharges, as shown in Figure 4.3. Clearly, hydrological processes of the Semliki are not represented well in the NHSM. It is likely, the absence of the upstream lakes, Lake Edward and Lake George, in RIBASIM-NILE results in an underrepresentation of river-lake dynamics in the most upstream part of the Semliki by the NHSM. Downstream effects of this underrepresentation are limited. At Mongalla, model predictive value increases, but remains moderate (*NS* =0.57), since some discharge peaks are not well represented in the simulated hydrograph.

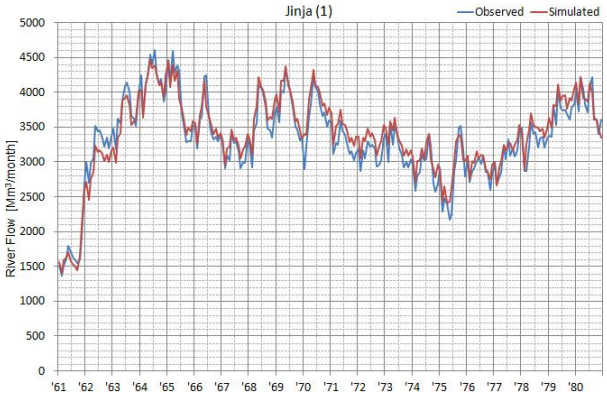

Figure 4.2 – Hydrographs at Jinja downstream the outlet of Lake Victoria after calibration

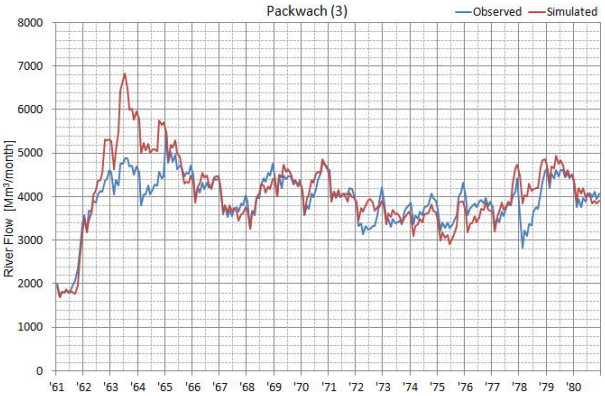

Figure 4.3 – Hydrographs for Packwach downstream the Great Lakes after calibration

In the largest sub-catchment of the White Nile, the Bahr el Ghazal river catchment, fitting the NHSM simulated hydrograph to observations by autocalibration proved to be unsuccessful (see Figure 4.4). A high overestimation of peaks cannot be solved by model calibration. In automatic calibration, the algorithm forces the model to retain water in the upper and lower response reservoirs by decreasing the values of k_f and k_s to their lower domain limits. By this approach a *RVE* and *NS* of 35% and 0.46 are obtained. However, by observing Figure 4.4, it is clear that by autocalibration the simulation of base flow is compromised to reduce simulated peaks. Therefore, the values of k_s and k_f are both manually adjusted after autocalibration to 0.025, resulting in lower *RVE* and *NS,* but a much better optical agreement of the simulated hydrograph versus observations. The clear overestimation of peaks is most likely caused by overestimation of peak rainfall events in the southwest of the sub-catchment. Clearly, model sensitivity in this sub-catchment high to changes in rainfall, or the degree of rainfall overestimation in the sub-catchment is high.

At Gambela, results are compromised by either a structural overestimation of observed discharge or a structural underestimation of observed rainfall volume, as shown in Figure 4.5. Even in runs with zero evapotranspiration, simulated discharge structurally underestimates observed discharge. When a possible bias in discharge observations is ignored, either the catchment area is larger than schematized in NHSM, or observed rainfall intensities over the catchment area are structurally lower. Downstream, at the Baro mouth, model performance is much higher, as shown in Figure 4.6. It is found that the poor calibration at Gambela has a marginal impact on model performance at the Baro mouth. The majority of upstream water flow is diverted to the Machar Swamps according to RIBASIM-NILE and the structural underestimation at Gambela is compensated by sub-catchment runoff between Gambela and the Baro mouth.

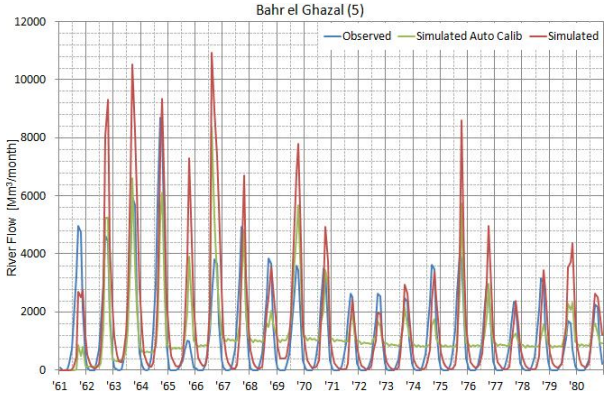

Figure 4.4 – Hydrographs for the Bahr el Ghazal upstream Lake No after calibration

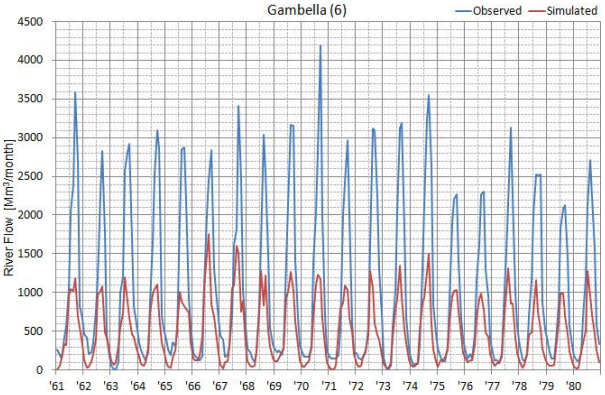

Figure 4.5 - Hydrographs for Gambella on the Baro River after calibration

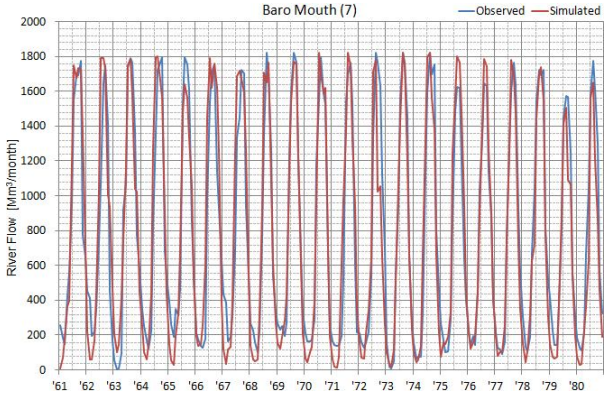

Figure 4.6 – Hydrographs for the Baro mouth after calibration

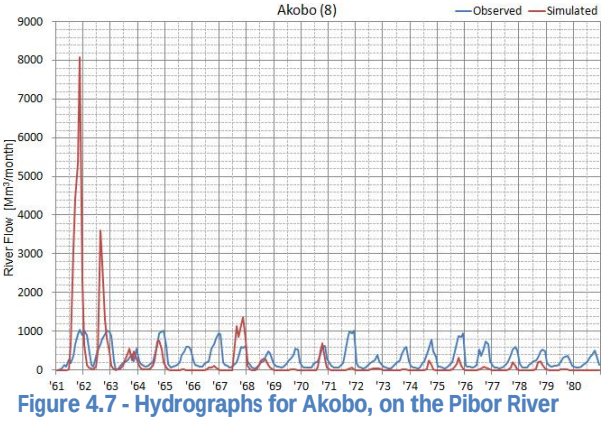

Figure 4.7 - Hydrographs for Akobo, on the Pibor River after calibration

In the Pibor River, flows are observed at Akobo. Here, simulations show a more or less random pattern relative to observations, resulting in nil model predictive value (*RVE* = -50.48%, *NS* = -1.36) as shown in Figure 4.7. Results at Akobo are most likely compromised by similar causes as in the Bahr el Ghazal catchment. The sub-catchment is highly heterogeneous with respect to rainfall, resulting in a high sensitivity to errors in the spatio-temporal representation of rainfall. Downstream the confluence of the Pibor and Baro Rivers, the Sobat receives a small amount of sub-catchment runoff upstream the last recording station at Hillet Doleib near the river mouth (see Figure 4.8). Here, performance is low (*RVE* = -5.78%), since it is the combined flow of well simulated Baro discharge, poor simulated Akobo discharge and a small amount of sub-catchment runoff. Peak flow overestimations at the first two years are therefore coinciding with the peak overestimations at the Pibor, shown in the simulated hydrograph of Akobo in Figure 4.7.

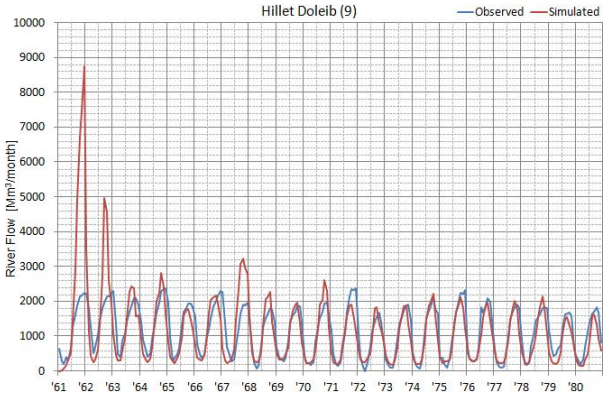

Figure 4.8 – Hydrographs for the Hillet Doleib, upstream the Sobat mouth after calibration

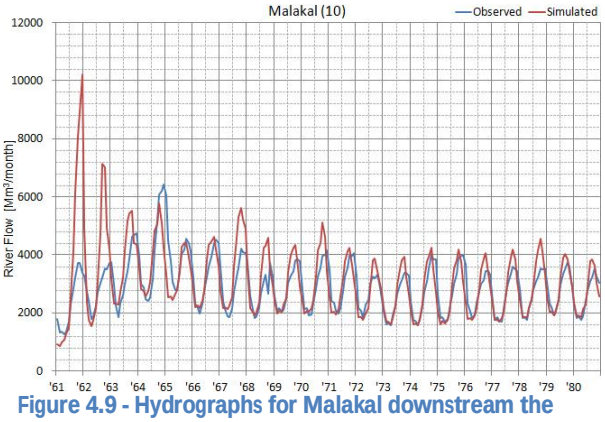

Figure 4.9 - Hydrographs for Malakal downstream the White Nile-Sobat confluence after calibration

Downstream the confluence of the White Nile and the Sobat River at Malakal station, the simulated and observed hydrographs optically show good agreement. This is supported by a *RVE* of 4.53%. Nevertheless, a *NS* coefficient of 0.37 indicates a moderate predictive value. The low value is mainly caused by two highly overestimated discharge peaks at 1961 and 1962 at both the White Nile and Sobat River. Therefore, the model performance at the outlet of the White Nile is considered to be acceptable, but poor in some individual sub-catchments.

4.1.2 Blue Nile

Compared with White Nile responses, discharge regimes at the Blue Nile follow the pattern of the single wet season, with extreme peak flows and almost nil flow in the dry season (see Figure 4.10). Parameters related to soil moisture show a high storing capacity, with high *FC* values and low values for *LP,* increasing the period of where actual evapotranspiration equals potential evapotranspiration. Soil routing, expressed by *β* is lower, than in the White Nile (see Table 3.1), indicating lower storage in the slow runoff reservoir of the model. Response flux parameter *PERC* is optimized towards a quick recharge of the fast runoff reservoir, increasing the contribution of quick runoff to total catchment runoff.

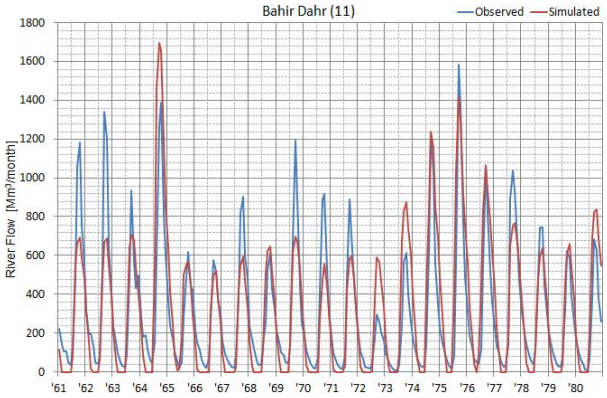

Figure 4.10 – Hydrographs for Bahir Dahr, near the outlet of Lake Tana after calibration

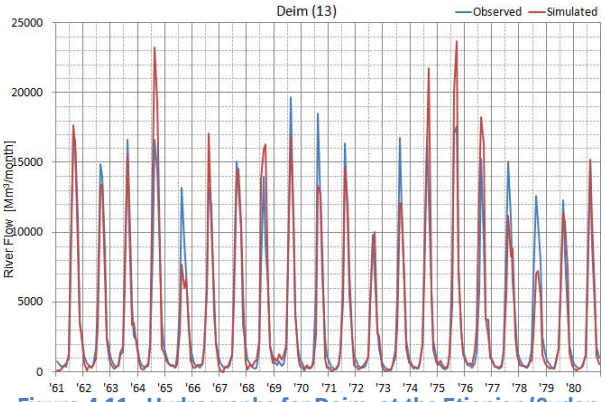

Figure 4.11 - Hydrographs for Deim, at the Etiopian/Sudan Border after calibration

Only for the catchment upstream Lake Tana, the *PERC* value is high, optimizing the catchment towards high retention. The reason for this high parameter value is most likely similar to the high value found for Lake Victoria; retention at the lake makes the identification of upstream fast recharge difficult. As shown in Figure 4.10, base flow is structurally underestimated, which is caused by the stage-flow relation in RIBASIM-NILE. When a certain lake stage is reached, outflow is reduced to zero, where the observed hydrograph shows outflow from the lake the entire year round.

Figure 4.11 shows hydrographs of observed versus simulated discharges at Deim, downstream the Ethiopian Plateau just over the Sudan border. Since base flow is relatively easy to simulate in a monsoon river like the Blue Nile, the simulation follows the observed hydrograph accurately. Peak flows are mostly simulated well, except for some random over and underestimations, most likely related to errors in model forcing.

Downstream the Roseires reservoir, the Dinder and Rahad Rivers join the Blue Nile. Figure 4.12 shows catchment hydrographs after model calibration. There is a distinct overestimation of peak discharge in 1964 for the entire Ethiopian Plateau, which is most distinct at the Dinder & Rahad Rivers. Since the *PERC* value of 1 mm·day^{-1} indicates a lot of water is assigned to the fast runoff reservoir, the recession coefficient k_f is low, slightly reducing the peak of 1964 but also the peaks in other years, which are structurally underestimated.

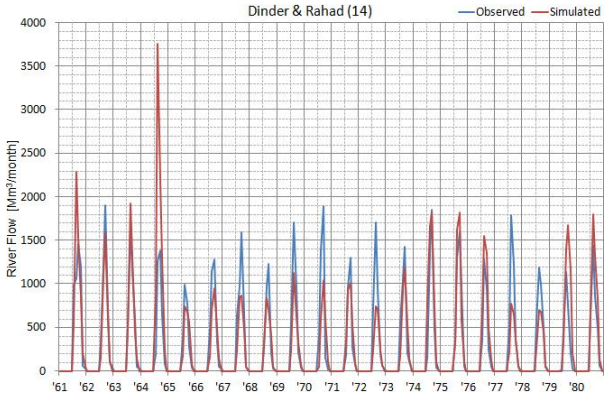

Figure 4.12 – Hydrographs for the Dinder and Rahad) Rivers, downstream Sennar reservoir after calibration

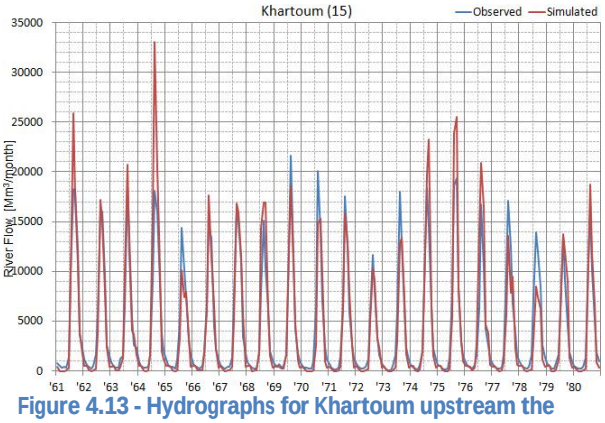

Figure 4.13 - Hydrographs for Khartoum upstream the mouth of the Blue Nile after calibration

The most downstream discharge recording station is found at Khartoum, upstream the Blue and White Nile confluence (see Figure 4.13). Discharge here is an accumulation of the upstream flow at Deim, retained by the Roseires and Sennar reservoirs, Dinder and Rahad inflow and runoff from the sub-catchment between Deim and Khartoum. Despite the distinct overestimation at 1964, to which all accumulated flows contribute, the average flow observation at the most downstream location at the Blue Nile is simulated accurately by the NHSM. A *RVE* of -0.17% shows almost zero long term volume error and the *NS* coefficient of 0.84 indicates a good agreement between simulation and observation. As shown in Figure 4.13, the timing of peaks is accurate.

4.1.3 Main Nile

Discharge of the Main Nile is an aggregation of discharge observed at Malakal, routed through the last part of the White Nile and retained at the Ghabal Aulia Dam, discharge of the Blue Nile observed at Khartoum station and discharge from the Atbara River, the last tributary draining the northern part of the Ethiopian Plateau. Hydrographs observed and simulated near the mouth of the Atbara River are shown in Figure 4.14. The discharge overestimation at 1964, also observed along the Blue Nile has a clear effect on the calibration of the Atbara River. Similar as to the Dinder & Rahad Rivers, the peak is compensated by a structural underestimation of peak discharges in other years.

Hydrographs of the most downstream recording station at Dongola are shown in Figure 4.15. Downstream Atbara mouth, discharge is only routed and no sub-catchment runoff is assumed. The resulting *NS* coefficient of 0.64 indicates a sufficient performance. A *RVE* of 5.2% indicates that long term discharges are slightly overestimated. It must be noted that this long term balance error is

mainly caused by an incidental overestimation of peak flows, partly caused by inaccuracies in rainfall observations. Therefore, the overall conclusion is that the NHSM has sufficient predictive value for discharges at Dongola.

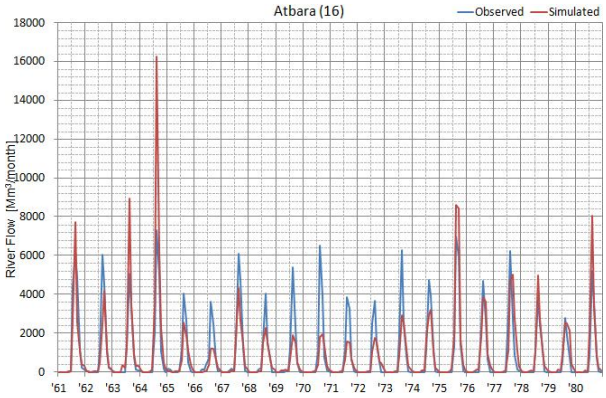

Figure 4.14 – Hydrographs at the Atbara mouth after calibration

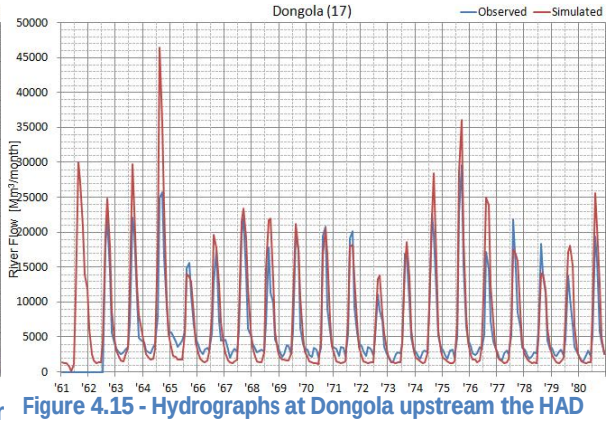

Figure 4.15 - Hydrographs at Dongola upstream the HAD after calibration

4.2 Validation over 1981-2000 data series

To validate the performance of NHSM, a split sample validation is carried out over the period 1981 to 2000. Statistics of Table 4.3 show clearly lower model performance after validation in comparison to calibration. Where, at some sub-catchments performance statistics are supported by overall disagreement between observed and simulated hydrographs, at others *RVE* and *NS* are compromised by incidental peak errors, most likely caused by poor model forcing. In this section, interesting validation results are summarized. Graphs not shown in this chapter are found in Annex D.

Table 4.3 - Model performance for sub-catchment over 1981-2000 data (red/orange = low/moderate predictive value)

River	White Nile										Blue Nile					Main Nile	
Basin	Jinja	Kamdini	Packwach	Mongalla	Bahr el Ghazal	Gambela	Baro Mouth	Akobo	Doleib Hillet	Malakal	Dahr Bahir	Guder DS	Deim	Dinder + Rahad	Khartoum	Atbara	Dongola
#	1	2	3	4	5	6	7	8	9	10	11	12	13	14	15	16	17
RVE [%]	-1.05	-1.73	-2.80	-3.60	30.10	-51.49	-7.53	-54.11	-8.02	-1.24	-9.38	-4.67	-1.66	-8.20	-3.72	-8.93	8.72
NS [-]	0.61	0.57	-0.10	-1.35	-0.29	0.19	0.87	-2.66	0.45	0.25	0.70	0.71	0.86	0.66	0.84	0.51	0.74
COF [-]	0.61	0.56	-0.10	-1.31	-0.22	0.13	0.81	-1.72	0.42	0.24	0.64	0.68	0.84	0.61	0.81	0.47	0.68

4.2.1 White Nile Validation

For Lake Victoria, model calibration showed promising results. However, the poor representation of discharge variability after 1970 is also shown in the validation period (see Figure 4.16). Between 1988 and 1995, the observed hydrograph is structurally underestimated by the NHSM. Clearly at this period either rainfall is underestimated or evapotranspiration is overestimated over the lake and the upstream catchment. From 1995, an agreement between observed and simulated hydrographs improves. Though a long term overestimation of discharge by 1.05% and a *NS* coefficient of 0.61 still suggest an acceptable model performance, it is clearly lower than for the calibration period. At Kamdini and Packwach, performance after validation shows similar trends. However, consistency with the water balance, expressed in low *RVE* suggests the soil moisture balance is simulated well by the model and problems are mostly related to model response.

At Mongalla validation performance statistics are deteriorated by an incidental high peak discharge overestimation in 1988. Obviously, this peak is caused by an extreme overestimation of rainfall. It must be noted that besides this peak, agreement between observed and simulated hydrographs is considerably lower than in model calibration.

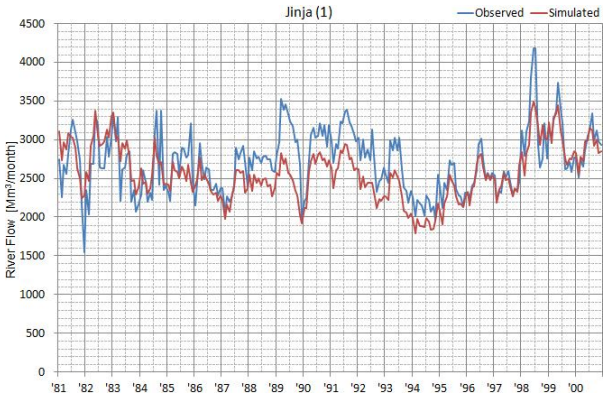

Figure 4.16 – Hydrographs at the Jinja, the outlet of Lake Victoria after validation

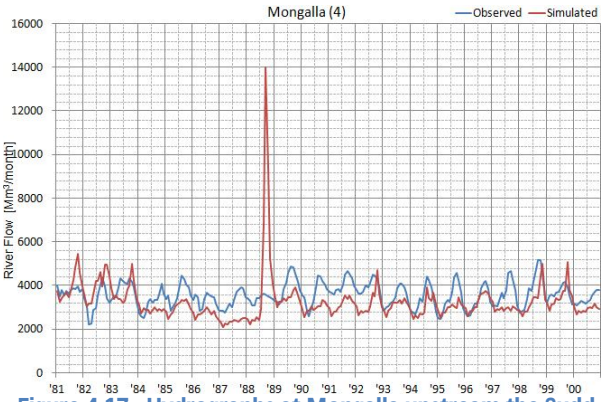

Figure 4.17 - Hydrographs at Mongalla upstream the Sudd swamps after validation

Hydrographs for the Sobat are shown in Figure 4.18. The distinct overestimation at 1988 can be related to a rainfall overestimation at the Pibor catchment upstream Akobo, which has a similar effect on this hydrograph as for the one shown for Mongalla. Observed and simulated hydrographs for the mouth of the Baro River show satisfying results, as in model calibration. The overestimation of discharge at 1988 reduces the *NS* coefficient at Hillet Doleib to 0.45. However, in other years the hydrographs show a good agreement.

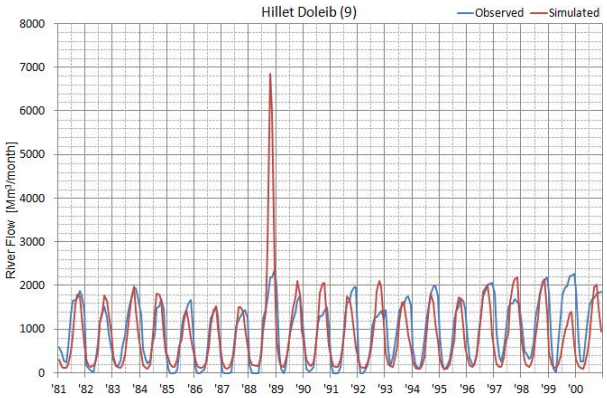

Figure 4.18 – Hydrographs at Hillet Doleib, upstream the Sobat River mouth, after validation

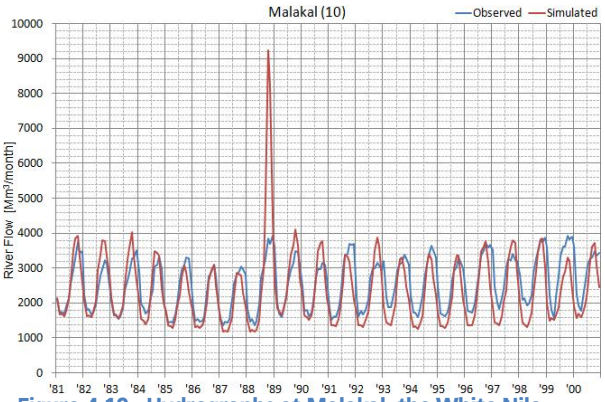

Figure 4.19 - Hydrographs at Malakal, the White Nile downstream Sobat River after validation

For the most downstream gauging station in the White Nile, Malakal, discharge hydrographs are show in Figure 4.19. Clearly, the distinct peak overestimation at 1988 has a dramatic impact on the *NS* coefficient for this station. Though Table 4.3 shows low model performance for Malakal, similar to model calibration, an optical comparison between both hydrographs shows there is a reasonable model predictive value after validation. An omission of the 1988 data increases the *NS* coefficient to 0.55, indicating a much better model validation at the White Nile.

4.2.2 Blue Nile Validation

For the Blue Nile, model validation in general shows satisfying results. The hydrographs at Bahir Dahr (see Figure 4.20) show an underestimation of peak discharges after 1988, resulting in a *RVE* of -9.38%. Also, the construction of the regulation weir at Tis Abay in 1996, not incorporated in the schematization of the NHSM, has a considerable effect on the low flows. Low flow periods are clearly shorter and flows are higher than before the construction of the weir. Since Bahir Dahr contribution to total Nile flow is limited, the propagation of these effects downstream is limited. At the Dinder and Rahad Rivers, the structural underestimation of peak discharges observed during model calibration is also observed during validation, resulting in a *RVE* of 8.20%.

At Khartoum, NHSM performance is still high after validation. Results do not show structural differences between observed and simulated discharges. Therefore, with respect to Blue Nile model simulations are concluded to be sufficiently predictive.

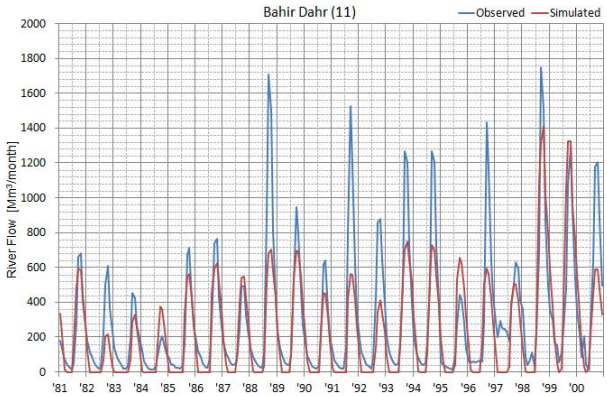

Figure 4.20 – Hydrographs at Bahir Dahr, downstream the outlet of Lake Tana after validation

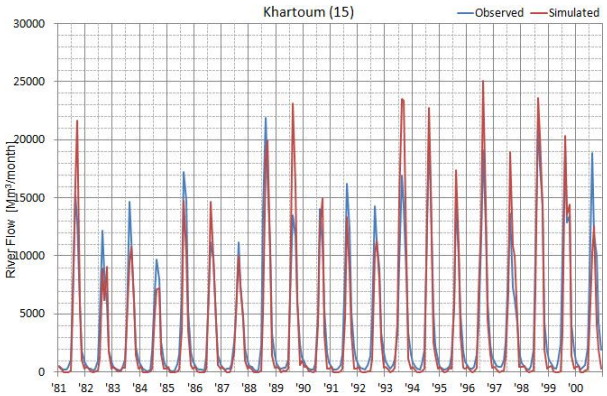

Figure 4.21 - Hydrographs at Khartoum upstream the mouth of the Blue Nile after validation

4.2.3 Main Nile Validation

At Atbara River, the structural underestimations of peak discharges observed during calibration are also shown during validation (see Figure 4.22). However at Dongola, the most downstream location of the Main Nile, results are promising. A *RVE* of 8.72% is still slightly too high, which is caused by overestimations of peak discharges, as in model calibration. Base flow is slightly underestimated for the validation period as well as the calibration period. Less extreme errors in peak flows (most likely related to forcing errors) result in a higher *NS* coefficient after validation compared to calibration.

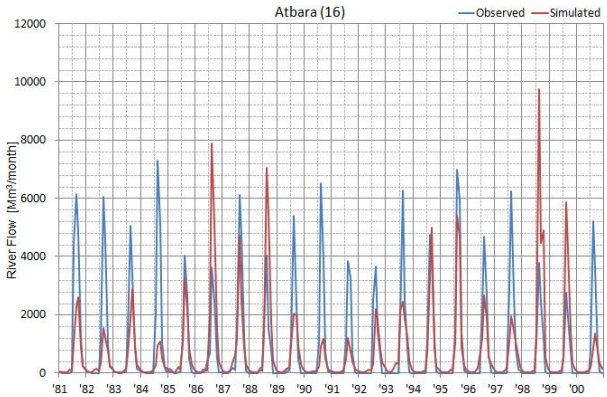

Figure 4.22 – Hydrographs at Atbara mouth after validation

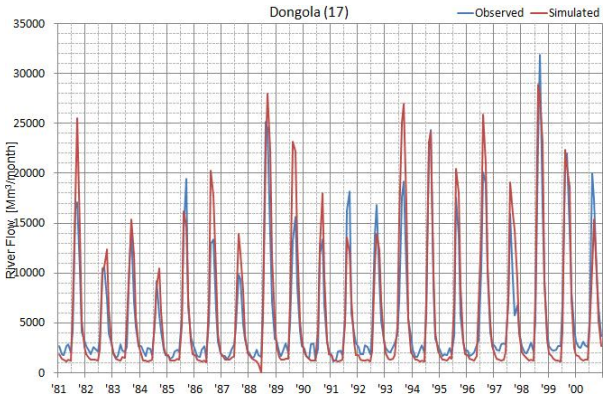

Figure 4.23 - Hydrographs at Dongola upstream the HAD after validation

4.3 Discussion

The general conclusion to be drawn after NHSM calibration and validation is that the model performance with respect to simulation of outflow from main tributaries, the White Nile, Blue Nile and Atbara is acceptable to good. For the entire river basin, observed at Dongola, the model performs well. However, when results on a sub-catchment scale are assessed, performance is not always acceptable. In this paragraph, the main facts of calibration will be discussed, with a focus on the calibration method, model forcing, the HBV rainfall-runoff component and RIBASIM-NILE.

Calibration Method

The automatic calibration method proved to be an efficient way of NSHM optimization. In an objective way, for most sub-catchments an acceptable model performance was achieved with in minimum of model runs. It seems however, that in sub-catchments with very poor data observations, problems emerge in optimization of the runoff routine. Simulations of peak flows are corrected in compensation of base flow. This could be compensated for by using a COF with emphasizing base flow performance in the calibration of the runoff routine.

Forcing Series

At some simulations model performance is clearly compromised by the quality of forcing data, especially rainfall. Clearly, coverage of rainfall stations over the Nile Basin is low, limiting the spatio-temporal representation of rainfall. It is noted that the CRU-TS2.1 dataset seems not to include data from all rainfall stations, when New et al. (2000) is compared with MWRI/Deltares (2009c). This might be related to the omission of stations after quality tests as described by Eischeid et al. (1991). However, it is questionable whether interpolating data from nearby stations in this region yields better results than using the stations' data records.

The interpolation of CRU-TS2.1 data by the ERA40 dataset by Van Beek (2008) is a method which is not extensively validated since it hasn't been published by the date this report is printed. The method is a creative way of deriving rainfall grids, but also experimental. A study to the correlation of the dataset with station observations can give an indication of the quality of the interpolation methods applied.

HBV

Overall, the soil moisture routine seems to work well in simulating actual evapotranspiration. However, in the runoff routine problems emerge in the identification of fast and slow flow routines. It seems that a simpler schematization might produce similar or maybe even better simulation results.

The model seems to be sensitive to errors in the rainfall grids. It is believed, that the application of a semi-distributed application of HBV increases this sensitivity in comparison with the original lumped version. Hence, a semi-distributed requires good rainfall estimations for each grid cell, whereas a lumped version required a good average estimation for each sub-catchment.

RIBASIM-NILE

With respect to RIBASIM-NILE it is noted that river dynamics are underrepresented in the model schematization. Especially in the White Nile, the sub-catchment upstream Lake Albert and the Sudd and Machar Swamps improvements of dynamics would most likely lead to better hydrological model simulations.

5. NHSM-GCM simulations of present and future discharges

This chapter presents the results of NHSM simulations, forced by GCM derived meteorological forcing. For evaluating NHSM sensitivity to changed forcing, results of a sensitivity analysis are given in paragraph 5.1. In paragraph 5.2, NHSM-GCM performance in simulating the reference hydro-climate is expounded. In paragraph 5.3 simulation results for the 2065 and 2100 climates are discussed. This chapter ends with a discussion in paragraph 5.3.2.

5.1 Discharge sensitivity on changed meteorological forcing

To indicate effects of changed climatic conditions to Nile discharges, sensitivity is assessed by changing potential evapotranspiration and rainfall between -20% and +20%. When one meteorological variable is changed, the other is kept constant in order to assess the sensitivity of a single variable to discharges. Results are shown in Table 5.1.

Table 5.1 – Discharge response to a uniform changing climate

ΔIN			Rainfall (Δ*P*)				Potential Evapotranspiration (ΔET_p)			
			-20%	-10%	+10%	+20%	-20%	-10%	+10%	+20%
ΔOUT	Basin	Location								
	White Nile	Mongalla	-52%	-32%	+48%	+111%	+95%	+39%	-24%	-39%
		Malakal	-43%	-26%	+38%	+88%	+71%	+29%	-18%	-29%
	Blue Nile	Deim	-54%	-30%	+34%	+72%	+40%	+17%	-11%	-21%
	Atbara	Mouth	-48%	-28%	+32%	+67%	+27%	+12%	-10%	-18%
	Main Nile	Dongola	-56%	-33%	+41%	+91%	+56%	+23%	-15%	-26%

White Nile

At Mongalla, the inflow to the Sudd swamps, discharge shows high sensitivity to changing rainfall. An increase of 10% in rainfall results in 48% increase of inflow to the Sudd at Mongalla. Sensitivity downstream the Sudd is much lower, either caused by retention in the Swamps, or Sobat inflow, joining the White Nile upstream Malakal. Sensitivity results are comparable with MWRI/Deltares (2009d). Though the NFS shows a lower sensitivity of the White Nile to changing rainfall (ΔOUT= +31% at *ΔP*=+10%), it must be noted that these changes are based on observations at Jinja station and not at Mongalla or Malakal. Discharges are less sensitive to changes in evapotranspiration than to changes in rainfall; +10% evapotranspiration, results in a decrease of discharge by 24%. Also for evapotranspiration, sensitivity is highest upstream the Sudd, observed at Mongalla.

Blue Nile

Sensitivity of the Blue Nile to decreasing rainfall is comparable to the White Nile. A 20% decrease of rainfall results in 54% decrease of discharge at Deim, which is consistent with Gleick(1991), who found a decrease of 50% by the same decrease of rainfall. Blue Nile discharges are less sensitive to changing rainfall than discharges at the White Nile. Most likely, the Blue Nile system has more storage capacity, whereby more extra rainfall is available for evapotranspiration. It is likely that especially in the low flow season all extra rainfall evapotranspirates.

Sensitivity to evaporation changes is considerably lower than for the White Nile. This is supported by the hydrological characteristics of the basin, where less rainfall is stored in soil moisture and water bodies. The rainfall response of the Blue Nile is considerably higher than for the White Nile, which means less water is available for evapotranspiration.

Main Nile

Table 5.1 shows Nile discharges are principally sensitive to changes in rainfall. When rainfall is varied between -20% and +20%, discharge at Dongola varies between -56% and +91%. Similar changes in potential evaporation result in changing discharges from +56% to -26%. The high sensitivity of a changing climate to discharges reconfirms what is already concluded in previous studies (e.g. Conway & Hulme, 1993, 1996; Gleick, 1991; MWRI/Deltares, 2009d). When outcomes of the sensitivity are compared with results of MWRI/Deltares (2009d), it is concluded that they are quite comparable. Only for a 20% increase in rainfall, the NHSM (+91%) simulates significantly more discharge than the NFS (+70%).

5.2 Simulating the reference hydro-climate using NHSM-GCM combinations

In this paragraph the simulation of the Nile hydro-climate using NHSM-GCM combinations is explained. The first section deals with the corrections applied on GCM derived meteorological forcing. In the second section simulations of the reference climate using these meteorological forcing series are discussed.

5.2.1 Bias correction on meteorological forcing

As described in section 3.2.2, GCM temperature and rainfall outputs are transformed to meet the mean monthly climatology of observed data. As shown in Table 5.2, differences in simulated and observed values, defined as the areal average GCM value minus the observed equivalent [Δ%], are high for both rainfall and evapotranspiration. The table shows that e.g. ECHAM underestimates rainfall by 19.8% over the Blue Nile upstream Deim. Correction of these changes for both rainfall and evapotranspiration is described in the coming sections.

Table 5.2 – Bias in annual rainfall and evapotranspiration at different Nile sub-catchments

Basin	Sub-catchment	Rainfall (*P*)				Reference evapotranspiration (ET_0)			
		Observed	ECHAM	GISS	CSIRO	Observed	ECHAM	GISS	CSIRO
		[mm/year]	[Δ%] GCM-Observed			[mm/year]	[Δ%] GCM-Observed		
White Nile	Mongalla US	1256	-4.0	-28.7	13.4	1363	39.5	46.7	46.6
Blue Nile	Deim US	1334	-19.8	32.3	12.3	1344	30.0	29.4	38.0
Atbara		505	8.2	6.5	47.3	1752	14.5	20.4	17.3

Corrected rainfall

Differences between GCM simulated and observed rainfall are high, even at large spatial scales such as the catchments represented in Table 5.2 (with areas ranging from 174,000km^2 to 481,000 km^2). As referred to in section 3.2.2, bias in the spatio-temporal representation of rainfall remains after the application of the correction method.

To give an indication of the remaining temporal bias in meteorological forcing derived from a corrected CSRIO simulation *Pcsiro'* [Mm^3/day] is given in Figure 5.1 for the year 1989 in the sub-catchment upstream of Deim in the Blue Nile basin. The vertical axis shows the average daily rainfall multiplied by the catchment area. The total sum of rainfall simulated by CSIRO is 30% higher for this year than observed. When the bar graph is examined in more detail, it reveals that the CSIRO rainfall distribution of 1989 differs from observed rainfall. In the observed series, 88% of the days are accounted for as wet days with an area average rainfall >0.1mm. In the simulated series 98% of the days are accounted for as wet days. The observed rainfall amount which is exceeded 90% of the time is 0.05 Mm^3 compared with 1 Mm^3 for simulated rainfall. Since this example shows a comparison for one GCM at one location for one year, more detailed studies to the GCM statistics (daily rainfall

distributions, timing of rainfall events, interannual variability in monthly rainfall, etc.) in comparison to observations are required to give the extent of the remaining temporal bias in rainfall simulations.

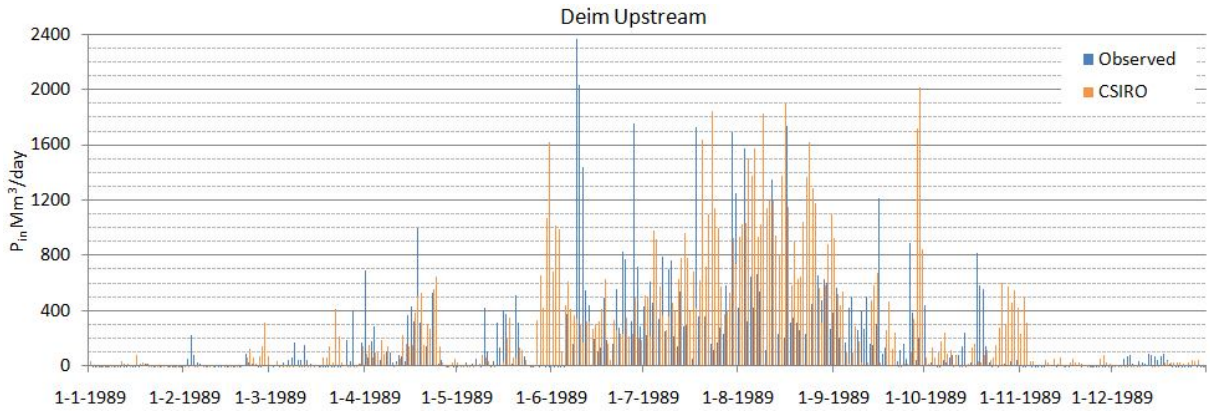

Figure 5.1 – Rainfall input P_{CSIRO}' for the catchment upstream Deim

In Figures E.1 of Annex E biased and corrected simulated annual rainfall maps are given. Though area averaged values at sub-catchment scale equal observed rainfall shown in Figure 2.2, differences on a smaller spatial scale are large. The corrected map of CSIRO annual rainfall shows the best agreement with the observed map. Though ECHAM results also show a reasonable agreement, especially rainfall over catchments surrounding Lake Victoria shows a different spatial distribution compared to the observed grid. A study to spatial representation of simulated rainfall in comparison to observations is necessary to conclude which model shows the best comparison with observations. Issues related to the modeling of hydrology smaller than sub-catchment scale can be solved by either downscaling rainfall and/or upscaling the resolution of the NSHM to lumped sub-catchments.

Corrected evapotranspiration

In Table 5.2 differences in evapotranspiration derived from observed and simulated meteorological forcing are shown. As mentioned in section 3.2.2, these differences are to be related to differences in observed and simulated meteorological variables and the method by which evapotranspiration is derived; the FAO method (Allen et al., 1998) versus the Blaney-Criddle method (Brouwer & Heibloem, 1986). Since all models show equal bias, it is likely that the high overestimations up to 40% are caused by the uncertainty in the Blaney-Criddle method using temperature as the sole meteorological variable from which reference evapotranspiration is derived.

As shown in Figures E.2 of Annex E, the applied correction method shows a much better agreement of annual simulated and observed reference evapotranspiration. The lower spatio-temporal variability of evapotranspiration makes the bias method applied much more applicable for this variable. The high overestimation by raw GCM simulations can de decreased when more meteorological variables are used in the derivation of reverence evapotranspiration.

5.2.2 Reference climate NHSM-GCM simulations

In this section, the reference hydro-climate by HNSHM-GCM simulations is discussed**.** Mean monthly hydrographs are compared with their observed equivalents in order to analyze NHSM-GCM performance for the reference climate. These reference hydrographs are used later in paragraph 5.3.2, for creating projections for the 2065 and 2100 climates based on GCM simulations for these periods. Besides the average climate a second order statistic, the coefficient of variance (given by equation 3.22), is used to examine the representation of interannual variability by NHSM-GCM simulations.

White Nile

For the White Nile, reference hydrographs of mean monthly discharges show that poor spatio-temporal rainfall representations by corrected GCM outputs eventually lead to changes in the water balance (see Figure 5.2). As shown in section 5.1, White Nile flow is sensitive to changes in evapotranspiration. Although potential evapotranspiration is bias corrected, the systems water balance is governed by actual evapotranspiration, being a function of potential evapotranspiration and the state of the NHSM (soil moisture storage, lake storage, etc.). Though the mean monthly volumes are corrected, the remaining spatio-temporal bias in rainfall influences these states, and therefore the amount of water leaving the system by actual evapotranspiration.

For Malakal, a NHSM-GISS simulation for the reference climate shows an extreme overestimation of discharge as shown in Figure 5.4. This peak is caused by a 40% decrease in actual evapotranspiration over the Pibor sub-catchment, solely caused by differences in the soil moisture storage reservoir of the HBV model over its time-space domain. A more detailed explanation of how this poor rainfall coverage leads to a hydrograph as shown in Figure 5.4 is found in Annex F. With respect to the representation of mean monthly flows it seems that NHSM-CSIRO gives the best results under the current climate.

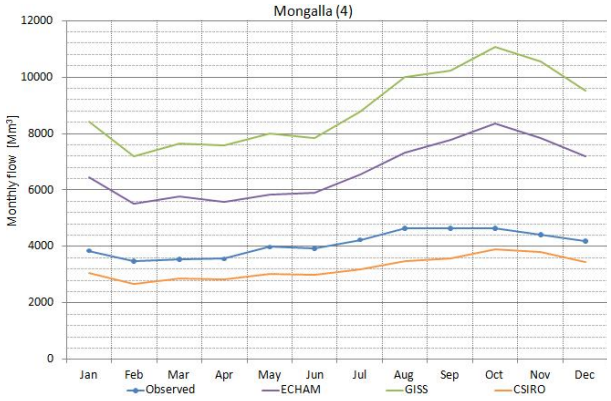

Figure 5.2 - Reference mean monthly discharges at Mongalla

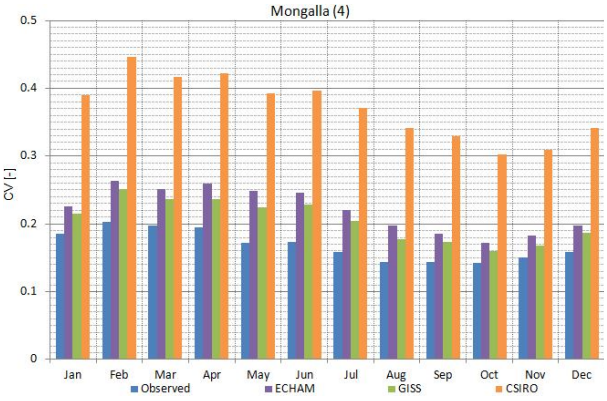

Figure 5.3 - Interannual variability at Mongalla

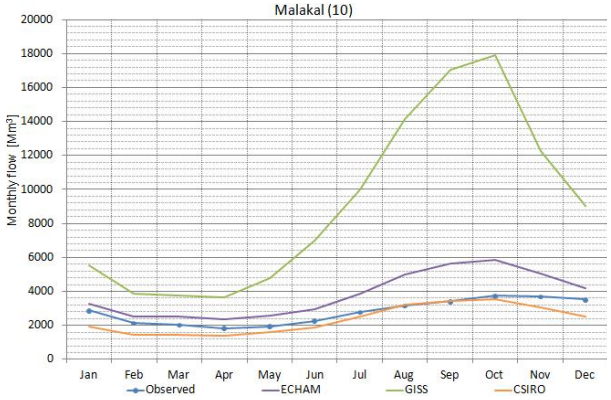

Figure 5.4 - Reference mean monthly discharges at Malakal

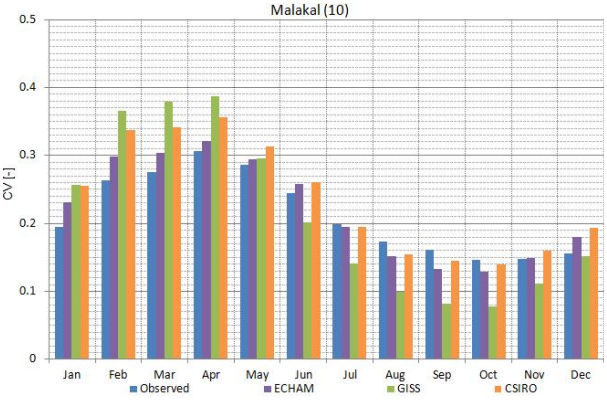

Figure 5.5 - Interannual variability at Malakal

As shown in Figure 5.3 and Figure 5.5, interannual variability is different for all NHSM-GCM combinations in comparison with observed discharge series. Discharges from the Great Lakes region show high overestimations of interannual variability, especially by NHSM-CSIRO simulations. It must be noted that this is relative to its simulated mean monthly flows, which are much smaller than in other NHSM-GCM simulations. With respect to the representation of interannual variability, it seems that NHSM-ECHAM gives the best results for the White Nile under the current climate.

Blue Nile

For the Blue Nile River, NSHM-GCM simulations show much better agreement with observed hydrographs as shown in Figure 5.6. It must be noted that NHSM performance under observed forcing is already higher for this tributary in comparison to the White Nile (see Chapter 4). However, it seems that the recession limb of the hydrograph is not very well simulated by the model. Too much water is retained in the model after the peak of the flooding season. The amount of annual discharge is thereby overestimated by all NHSM-GCM combinations.

With respect to interannual variability, shown for the flood season only in Figure 5.7, all models seem to overestimate interannual variability, especially the NHSM-GISS model combination. Overall, both on mean monthly discharge and interannual variability, the NHSM-ECHAM model combination seems to be the best representation of the current hydro-climate in the Blue Nile.

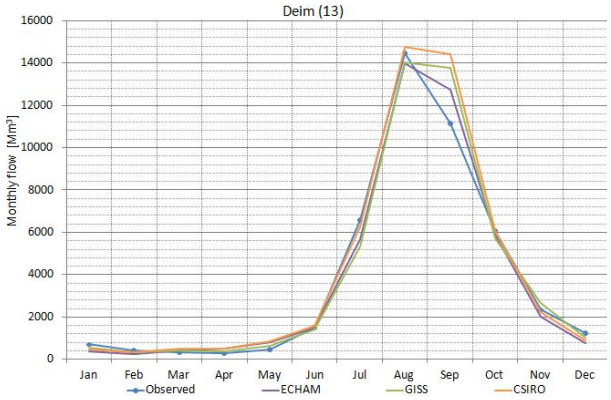

Figure 5.6 - Reference mean monthly discharges at Deim

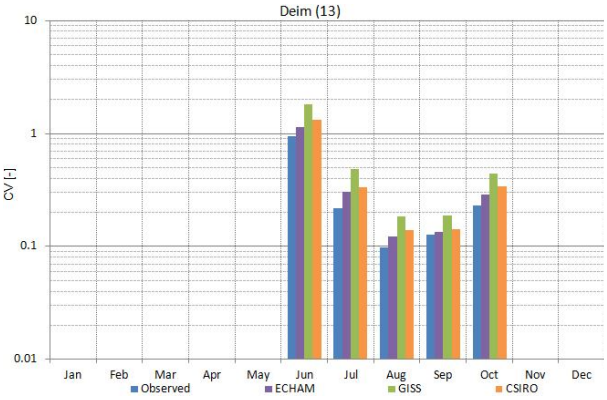

Figure 5.7 - Interannual variability at Deim (y-axis displayed in logarithmic scale)

Atbara River

At the Atbara, combinations of NHSM-ECHAM are underestimating mean annual discharges as shown in Figure 5.8. By interpreting the results is must be taken into account that the NHSM performance for the Atbara River is also low with observed forcing (see chapter 4). However, based on the results shown in the graphs it must be concluded that the NHSM-CSIRO combination provides the best results with respect to mean monthly discharges and interannual variability (see Figure 5.9).

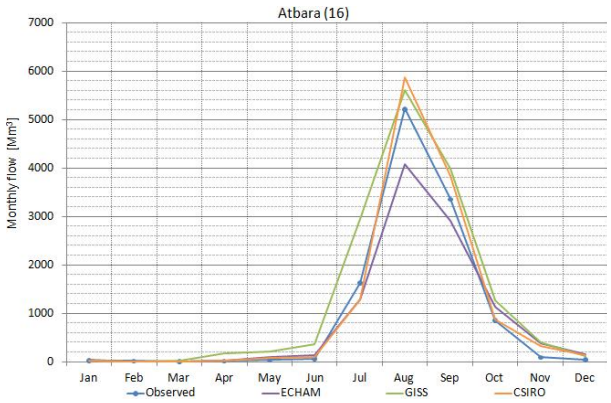

Figure 5.8 - Reference mean monthly discharges for the Atbara River

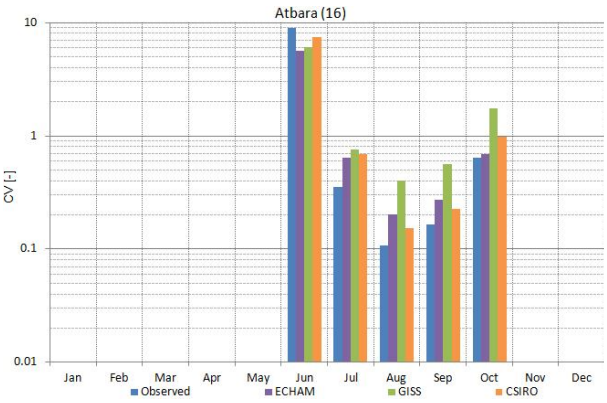

Figure 5.9 - Interannual variability for the Atbara River (y-axis displayed in logarithmic scale)

Main Nile

Reference mean monthly discharges and interannual variability at Dongola are strongly influenced by the results of upstream catchments. Therefore, the overestimation of discharge by the NHSM-GISS model at the White Nile is also visible in the Dongola hydrograph. The other NHSM-GCM

combinations show better representations of mean monthly discharge. However, the interannual variability of the NHSM-CIRO is much higher than for other model combinations. For the Main Nile it is therefore concluded that NHSM-ECHAM gives the best hydrological representation of the current climate.

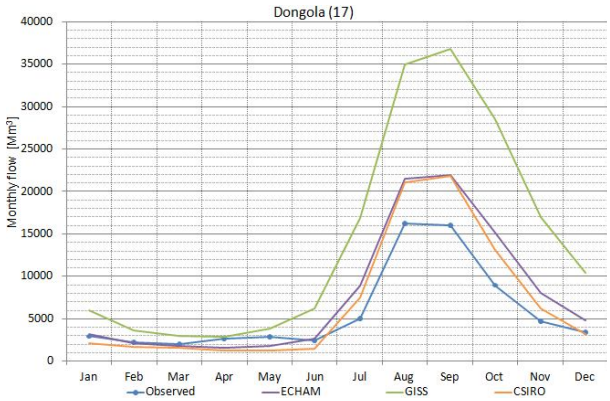

Figure 5.10 - Reference mean monthly discharges at Dongola

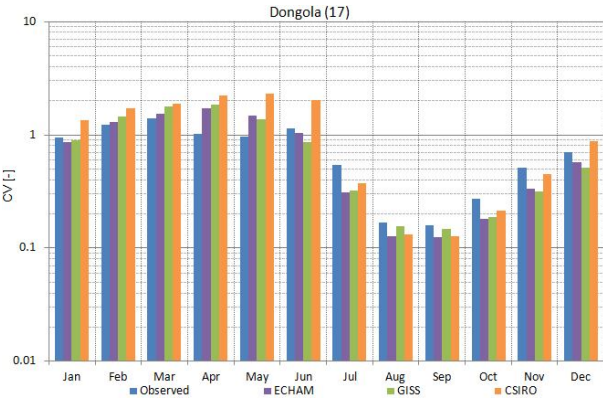

Figure 5.11 - Interannual variability at Dongola (y-axis displayed in logarithmic scale)

5.3 NHSM-GCM simulations for 2065 and 2100 hydro-climates

In this paragraph, results are presented for the 2065 and 2100 hydro-climates. In the first section, meteorological projections of the different simulations for the B1 and A2 SRES GHG emission scenarios (explained in section 3.2.1) are described. In the second section, discharge projections based on these meteorological forcing series are given. In the last section, an overview of the projected Nile River water resources for 2065 and 2100 is discussed.

5.3.1 Meteorological projections

Meteorological projections for rainfall and reference evapotranspiration are given for sub-catchments upstream Mongalla, Deim and the Atbara Mouth. The simulation under two SRES GHG emission scenarios with three GCMs yields six model projections for two climatic periods.

Rainfall

Estimated changes in rainfall for 2065 and 2100 climates are given in Table 5.3 and Table 5.4. On average, a decrease in rainfall by -3.4% and -2.7% is simulated over the Great Lakes district (upstream Mongalla) for the 2065 and 2100 climates For the same periods an increase of +3.7% and +0.3% are projected over the Blue Nile upstream Deim. At the Atbara, differences in projections are the largest, with an increase of +23.7% and +19.6% for the 2065 and 2100c climates respectively.

Surprisingly, different GCM-SRES combinations do not show much agreement in future trends. Where ECHAM simulates increasing rainfall over the White Nile for both scenarios and higher rainfall volumes for 2100 compared with 2065, GISS predicts an opposite trend; less future rainfall with 2100 volumes lower than in 2065. CSIRO agrees with GISS and predicts lower rainfall. However, 2100 rainfall volume is predicted to be more than in 2065. Overall, average GCM-SRES rainfall predictions range from -15.3% to +5.6% and -18.7% to +10.7% for 2065 and 2100 climates respectively. In other basins similar trends are observed; individual projections of simulations show a high degree of randomness. Detailed studies to responses of GCMs under SRES projections for the future climates over the Nile basin are necessary to conclude on the causes of these peculiar results. Where literature confirms a high disagreement in projections (see e.g. Boko et al., 2007; Conway & Hulme, 1996; Hulme et al., 2001), the randomness in trends is not supported.

Table 5.3 - Rainfall projections for the 2065 climate

Basin	Sub-catchment	2065 Rainfall (*P*)							
		Reference	Average	ECHAM B1	ECHAM A2	GISS B1	GISS A2	CSIRO B1	CSIRO A2
		[mm/year]	[Δ%] 2050-1990						
White Nile	Mongalla US	1256	-3.4	5.6	3.8	-6.9	-15.3	-4.7	-2.6
Blue Nile	Deim US	1334	3.7	5.0	9.0	3.8	11.8	0.0	-7.6
Atbara		505	23.7	8.7	17.4	-6.3	21.3	60.0	41.2

Table 5.4 - Rainfall projections for the 2100 climate

Basin	Sub-catchment	2100 Rainfall (*P*)							
		Reference	Average	ECHAM B1	ECHAM A2	GISS B1	GISS A2	CSIRO B1	CSIRO A2
		[mm/year]	[Δ%] 2100-1990						
White Nile	Mongalla US	1256	-2.7	10.1	14.9	-18.7	-18.9	-1.8	-1.7
Blue Nile	Deim US	1334	0.3	-0.2	3.5	4.4	11.7	-4.6	-12.9
Atbara		505	19.6	5.0	11.5	-0.9	10.9	47.4	43.6

Evapotranspiration

Based on the averages of all projections, temperature (and therefore evapotranspiration) is expected to be lower in 2065 than it is now and higher in 2100 than it will be in 2065 for the entire basin, as shown in Table 5.5 and Table 5.6. With this variable, only CSIRO is showing peculiar projections in comparison with the other GCMs and literature (see: Boko et al., 2007; Hulme et al., 2001). CSIRO predicts temperatures would drop in the 2065 climate compared to the reference climate, where after they would rise again in the 2100 climate compared to the 2065 climate. Also, CSIRO is the only model predicting lower temperatures for both periods, which is in disagreement with the other models and literature. An average trend over ECHAM and GISS, whereby CSIRO predictions are neglected, shows an increase of temperatures as expected based on literature.

Table 5.5 - Reference evapotranspiration projections for the 2065 climate

Basin	Sub-catchment	2065 Reference Evapotranspiration (ET_0)							
		Reference	Average	ECHAM B1	ECHAM A2	GISS B1	GISS A2	CSIRO B1	CSIRO A2
		[mm/year]	[Δ%] 2050-1990						
White Nile	Mongalla US	1363	-1.5	1.6	2.5	0.6	2.6	-8.7	-7.3
Blue Nile	Deim US	1344	-0.7	2.5	3.6	1.5	2.9	-8.3	-6.6
Atbara		1752	-0.8	2.9	3.8	2.3	3.1	-9.4	-7.5

Table 5.6 - Reference evapotranspiration projections for the 2100 climate

Basin	Sub-catchment	2100 Reference Evapotranspiration (ET_0)							
		Reference	Average	ECHAM B1	ECHAM A2	GISS B1	GISS A2	CSIRO B1	CSIRO A2
		[mm/year]	[Δ%] 2100-1990						
White Nile	Mongalla US	1363	1.7	4.1	8.6	2.6	6.7	-7.8	-3.8
Blue Nile	Deim US	1344	2.8	5.8	10.6	2.6	7.3	-7.0	-2.6
Atbara		1752	2.7	6.1	11.0	3.2	7.5	-7.9	-3.6

5.3.2 Discharge projections

With the forcing series described in the previous section, discharge projections for the 2065 and 2100 climates are made. In this section, results are shown for the White Nile at Mongalla and Malakal, the Blue Nile at Deim, the Atbara at its Mouth and the Main Nile at Dongola.

White Nile

As a result of changing meteorological forcing, changes in mean monthly discharges are compared to 1990 mean monthly discharges as described by equation 3.27 in section 0. Resulting mean monthly discharge projections for 2065 and 2100 at Mongalla are given in Figure 5.12 and Figure 5.13. Based on these hydrographs, average discharges are expected to increase over the entire year, but a high differentiation with different NHSM-GCM simulations is observed. Overall, agreement in trends between the models is low as is expected based on the disagreement in meteorological trends discussed in the previous section. Where some discharge projections can be explained with the help of the meteorological projections given by Table 5.3 to Table 5.6, other results are rather peculiar. For instance, while the GISS B1 scenario for 2065 shows decreasing rainfall and increasing evapotranspiration for the catchment upstream Mongalla, overall discharged volume at Mongalla increases. Closer examination revealed GISS prognoses an increase of interannual variability of rainfall over the same period in comparison to the simulation for the reference climate, decreasing actual evapotranspiration and increasing rainfall available for runoff.

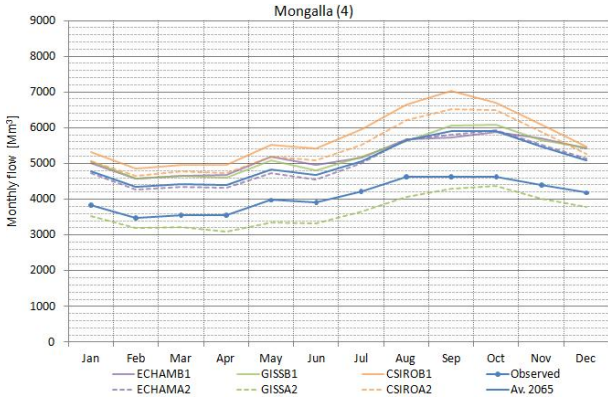

Figure 5.12 - Mongalla discharge projections for 2065

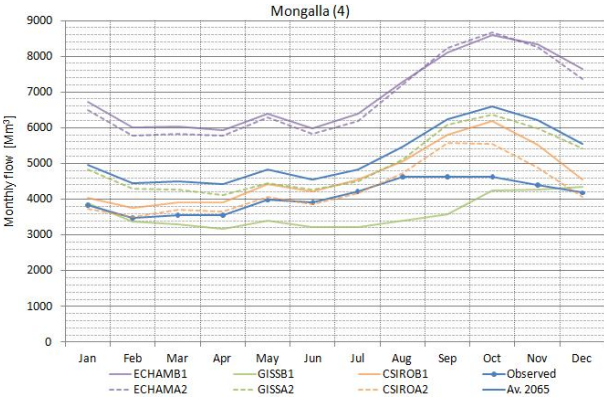

Figure 5.13 - Mongalla discharge projections for 2100

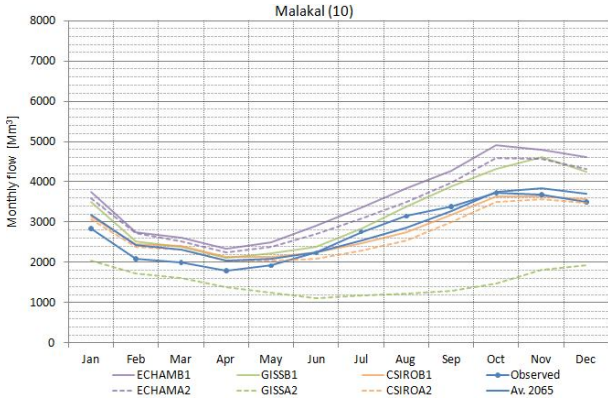

Figure 5.14 - Malakal discharge projections for 2065

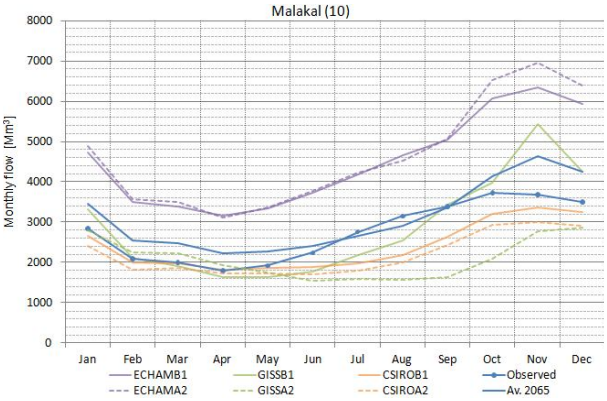

Figure 5.15 - Malakal discharge projections for 2100

For Malakal discharge projections are given in Figure 5.14 and Figure 5.15. Since most discharge from the Great Lakes district is retained by the Sudd Swamps, variations in discharge observed at Malakal are mainly caused by changes in discharge from the Sobat tributary and evaporation over the swamps. Due to the lower sensitivity to changed forcing, shown in paragraph 5.1, a smaller impact of climate change on river discharge at this point is expected. Increasing differences in hydrographs for

2100 in comparison to 2065 hydrographs is expected as uncertainty in model projections increases further in the future. That disagreements between GCMs are much higher than the projected differences for the two SRES scenarios under the same GCM is explained by the variation in climate projections shown in Table 5.3 till Table 5.6.

Blue Nile and Atbara Rivers

Results at Deim and the Atbara mouth are shown in Figure 5.16 till Figure 5.19, for 2065 and 2100 discharge simulations respectively. Hydrographs on average show a decrease of discharge and a shift in the flood period. However, as for the White Nile, results show a high level of disagreement in trends.

Peculiar results are the NHSM-CSIRO simulations showing much lower discharges at the Blue Nile compared with other NHSM-GCM simulations. Annual discharges are decreased by 40% and 60% for the 2065 and 2100 climates respectively. Though model sensitivity is high, as discussed in paragraph 5.1, it seems odd that a -7.6% rainfall with a -6.6% potential evapotranspiration results in -40% discharge as for NHSM-CIRO A2 simulation for the 2065 climate. A decrease in interannual variability for the same simulation in comparison to a NHSM-CSIRO simulation for the reference simulation could explain this high difference.

Another peculiar result is the shift in flood season found in all NHSM-GCM simulations, especially for the Blue Nile. NHSM-GISS B1 simulations for the Blue Nile show an extension of the flood season for the 2065 climate and a second flood peak for the 2100 climate. At the Atbara a similar effect is observed for the 2100 climate.

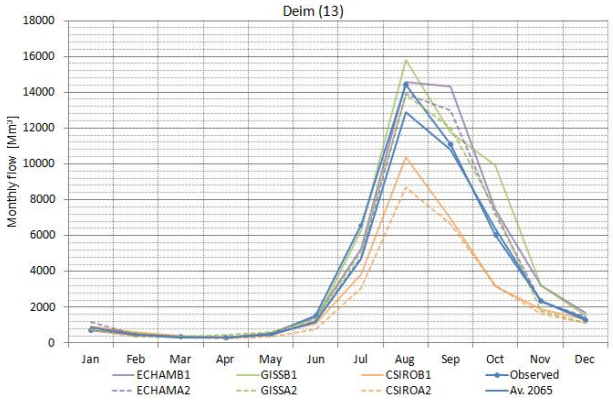

Figure 5.16 - Deim discharge projections for 2065

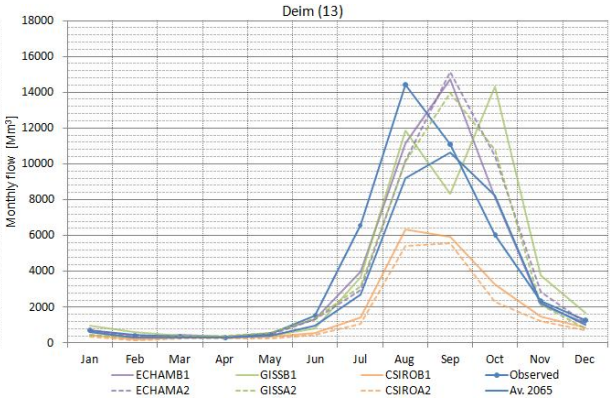

Figure 5.17 - Deim discharge projections for 2100

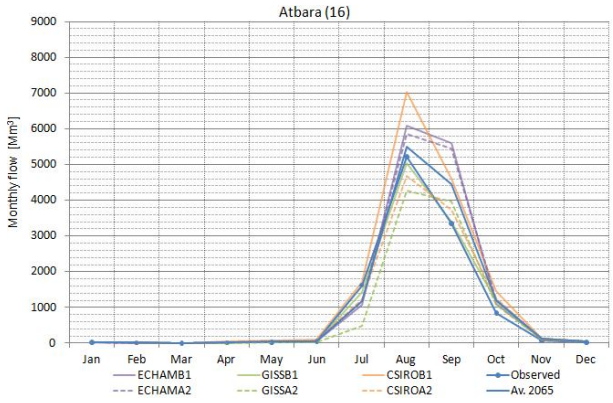

Figure 5.18 - Atbara discharge projections for 2065

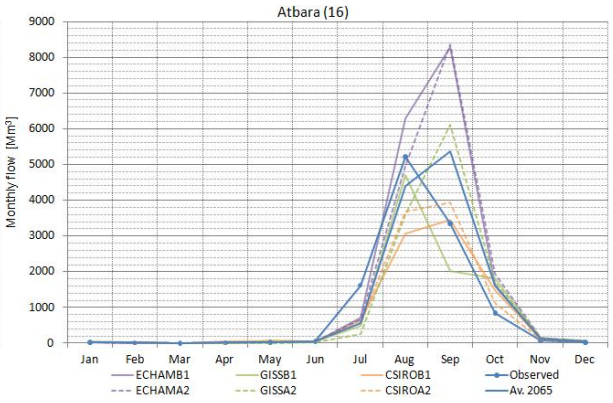

Figure 5.19 - Atbara discharge projections for 2100

Main Nile

Simulation results at Dongola for 2065 and 2100 climates are shown in Figure 5.20 and Figure 5.21. Where for Dongola differences in the flood season are mainly caused by differences in Blue Nile and Atbara flows, during the low flow season, differences are caused by changes in the White Nile regime. For instance, the NHSM-CSIRO B1 simulation shows an increase in low flow discharge, caused by an increase in White Nile discharge. The decrease in peak flow discharge for the same simulation is caused by the lower discharges from the Blue Nile.

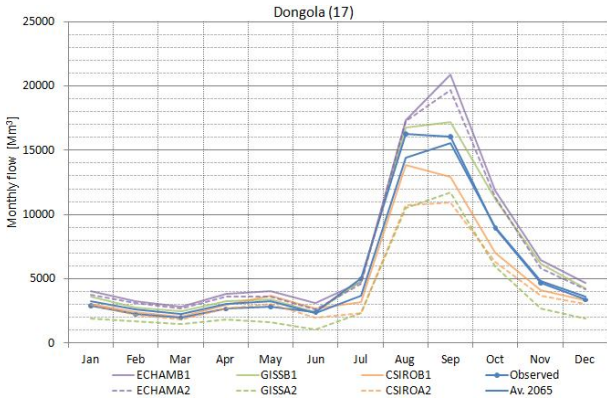

Figure 5.20 - Dongola discharge projections for 2065

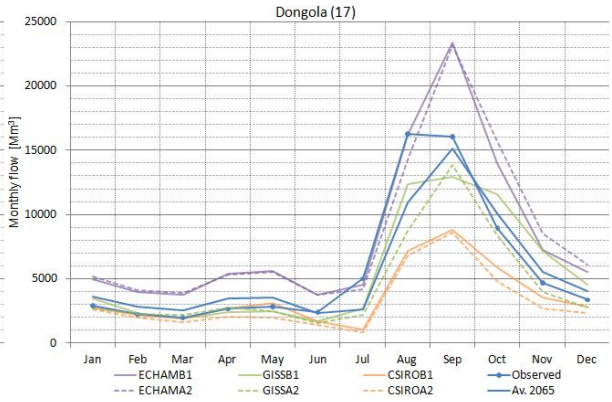

Figure 5.21 - Dongola discharge projections for 2065

5.3.3 Water resources projections

Results of the previous section show a high level of uncertainty in the future hydro-climate of the Nile River. For the purpose of water resources management it is relevant to show the changing hydro-climates together with their uncertainty boundaries, shown in Figure 5.22 and Figure 5.23 for the 2065 and 2100 respectively. Since the simulation sample size is too small to present uncertainty as a confidence interval surrounding the mean projection, an indication is used by taking the maximum and minimum NHSM-GCM SRES simulation of the respective period at a specific location.

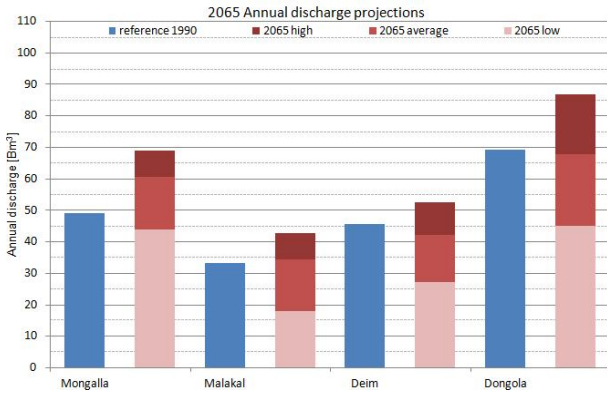

Figure 5.22 - Water resources projection for 2065

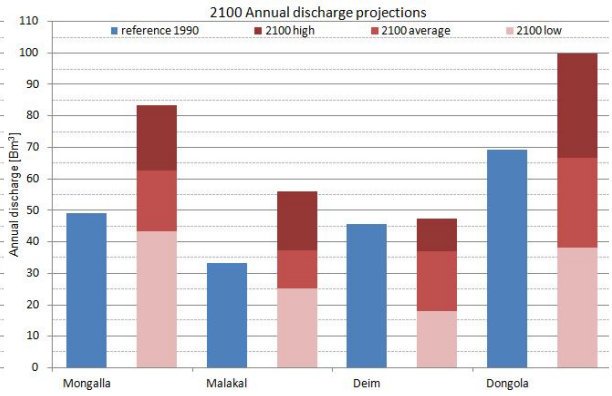

Figure 5.23 - Water resources projection for 2100

As the figures show, uncertainty based on the NSHM-GCM SRES simulations is very high. In exemplification for Dongola, average projections for 2065 and 2100 are -2% (67.7Bm^3) and -4% (66.6 Bm^3) respectively. Taking into account uncertainty, projections are ranging from -35% (45.0Bm^3) to +26% (87.0 Bm^3) and -45% (38.1 Bm^3) to +44% (100 Bm^3) for the same periods. These uncertainties are far too high, in relation to the high water stress at Egypt. A decrease of 45% in water resources would have dramatic consequences on the socio-economic system, far beyond the reach of what could be compensated for by enhanced water resources management.

5.4 Discussion

In the course of this chapter, many peculiar results are shown. These results decrease the confidence with conclusions on climate change impacts to Nile River discharges can be drawn, but also give lots of indications where improvements are to be made for lowering simulation uncertainty. In this paragraph, the results from pervious paragraphs are structured according to the following topics; the NHSM sensitivity to changing climate, NHSM-GCM simulations of the reference and future climates and the applicability of its results in climate change impact assessment.

NHSM sensitivity to changing climates

When a homogeneous change in rainfall and reference evapotranspiration is applied on the NHSM the high sensitivity of the Nile River to a changing climate is revealed. Though sensitivity shows a good comparison with literature, its sensitivity to a change of +20% in rainfall is higher than found in other studies (Conway & Hulme, 1993; MWRI/Deltares, 2009d). This indicates system retention at these high intensities might be underestimated by the NHSM.

NHSM-GCM simulations of the current hydro-climate

Uncorrected GCM simulations show a poor representation of the Nile climate in 1961-1990. Regarding rainfall, the applied bias correction method is insufficient to correct its spatio-temporal variability. A more comprehensive correction of the statistical properties of daily observed rainfall and a spatial downscaling of GCM output could be used to obtain better results. Also the application of a lumped version of HBV would most likely reduce the sensitivity of the NHSM in uncertainty regarding the spatial representation of rainfall within sub-catchments.

Corrected annual reference evapotranspiration shows a good agreement with observations. However, uncorrected maps show a structural overestimation of annual sums, which is most likely related to the used Blaney-Criddle method applied for deriving reference evapotranspiration from temperature. However, the amount of variables simulated by GCMs is insufficient for the application of other methods as proposed by the FAO (Allen et al., 1998).

Simulations for the reference climate by different NHSM-GCM combinations show poor results due to the remaining bias in forcing series as described above. Especially, remaining bias in the spatio-temporal distribution of rainfall has impacts on the state of the NHSM (soil moisture storage, lake levels, etc.) having an impact on the amount of actual evapotranspiration and consequently the discharges along the Nile River.

Regarding the simulation of the current climate by GCMs it is advised to select only models which show a good agreement with observed temporal variability of meteorological variables prior to the bias correction, including the distribution of daily values, timing and interannual variability on sub-catchment scale. A more advanced bias correction method such as used by Ines & Hansen (2006) can result in a higher quality of meteorological forcing. Issues regarding the spatial distribution of meteorological variables, especially rainfall, can be mitigated using downscaling methods. Also, the sensitivity of the NHSM to poor rainfall representations smaller than sub-catchment scale can be reduced by applying a lumped version of the HBV rainfall-runoff model.

NHSM-GCM simulations of 2065 and 2100 hydro-climates

The high degree of randomness in climate and discharge projections for the 2065 and 2100 hydro-climates decreases the confidence in the quality of the datasets. Though literature confirms there is high uncertainty in future climate projections for the Nile Basin, the randomness in trends shown in this chapter is not supported and cannot be explained by logical reasoning. More detailed studies on how GHGs are transferred to meteorological variables by the GCMs are required to give explanations for the peculiar results found.

When it is not possible to achieve a better performance in hydrological simulations of the reference and future climates by meteorological variables directly derived from GCM outputs, an alternative option is to manipulate observed forcing by trends derived from GCM simulations. Changes in statistical properties, such as the average and variability, of GCM simulated meteorological variables between two time periods can be used to manipulate the observed meteorological forcing series to represent a future climate period. Most likely, this will reduce the randomness of projections making them more realistic.

Using NHSM-GCM results in a climate-impact analysis

When all peculiar results are accepted, a water resources projection can be made with an average change and uncertainty boundaries taken from the most extreme NHSM-GCM simulations. By this approach it is revealed that uncertainty is far too high for being useful in defining water resources management strategies mitigating the effects of climate change. It is likely that uncertainty can be reduced by a more precise derivation of meteorological forcing series representing a changing climate.

6. Conclusions and Recommendations

The final conclusions of this study are stated in the first section of this chapter. The second section contains recommendations for further research.

6.1 Conclusions

The conclusions are structured around the research questions formulated in paragraph 1.3 of the introduction chapter. They seek to provide comprehensive answers for meeting the objective of this study: *to simulate present and future discharges at the Nile River upstream Lake Nasser by integrating a rainfall-runoff model in RIBASIM-NILE.*

1. **What is the performance of the NHSM in simulating discharges forced by observed meteorological variables?**

The answer to this first question is given in Chapter 4, where the calibration and performance results of the NHSM under observed forcing are stated. On the scale of main tributaries, the White Nile, Blue Nile and Atbara River, model performance is satisfying after calibration. This is supported by low long term volume errors and a good overall agreement between observed and simulated hydrographs. Performance after validation is comparable, especially after the removal of some outlying peak discharges in simulated series which are most likely caused by errors in model forcing,

For the White Nile model performance on a sub-catchment scale is considerably lower. Poor results range from sub-catchments showing multiple peak overestimations, to sub-catchments where discharge is structural underestimated. Though some of these results are likely caused by errors in model forcing, it is also presumed that a better representation of rainfall-runoff and river distribution processes in NHSM will improve model performance.

2. **How well is the current climate represented by meteorological variables derived from GCM output and what is the performance of the NHSM when it is forced by these variables?**

The answer to this question is given in paragraph 5.2. Bias in the rainfall and reference evapotranspiration derived from GCM simulations is high. The structural overestimation of reference evapotranspiration ranges from +15% in the Atbara basin to +47% in the Great Lakes district. This bias is a product of the methods by which observed and simulated evapotranspiration are derived and the differences between observed and simulated of meteorological variables.

The applied correction method for rainfall and evapotranspiration is insufficient to derive meteorological forcing from GCM simulations which sufficiently reflects the spatio-temporal variability of observations. This is especially the case for rainfall, which has an effect on the actual evapotranspiration simulated by the NHSM. Differences in actual evapotranspiration affect on their turn sub-catchment runoff and subsequently river discharges. For the latter NHSM-GCM simulations show a poor performance in mean monthly values and interannual variability. In general simulations are better for the Blue Nile than the White Nile. Overall the combination of NHSM-ECHAM gives the best representation of the Nile hydro-climate.

3. What is the predictive value of the future climate and discharges, when meteorological projections are derived from GCM output and used as forcing for the NHSM?

The last research question is answered in paragraph 5.3, where bias corrected meteorological forcing is used to give representations of the 2065 and 2100 hydro-climates. Considering the change in climatic conditions predicted by the different GCMs, total randomness in trends is observed over the entire basin. Disagreement in trends regarding the future Nile climate is supported by literature to some extent. Under certain GCM SRES combinations maximum changes are observed in the 2065 rather than the 2100, which contradicts with previous studies. This poor representation of future climate trends is reflected in NHSM-GCM simulations of future discharges.

Based on the NHSM-GCM simulations, uncertainty margins surrounding future projections of water resources along the Nile River would be much higher than the mean projection drawn from all NHSM-GCM simulations. This indicates NHSM-GCM simulations of future discharges have a low predictive value. Considering the high stress in Nile water resources, the predictive value is too low to define sensible water resources strategies in water management.

Having explored the answer to all research questions, a final statement can be made regarding the objective. When observed forcing is used, it can be stated that the performance of NHSM is sufficient to simulate discharges at the scale of main tributaries. For sufficient performance on sub-catchment scale, improvements on NHSM simulations of White Nile basin have to be made. Regarding the simulation of future discharges, an attempt is made to provide representative future meteorological forcing series for the NHSM. Discharges simulated by NHSM-GCM combinations show to much randomness and uncertainty in trends to have sufficient predictive value. The methods by which representative future meteorological forcing is derived are to be improved to increase predictive value within satisfactory limits.

6.2 Recommendations

Recommendations are structured by improvements to the NHSM and the simulation of the future hydro-climate, being in fact an accumulation of comments made during this report. Also a recommendation is made with respect to research beyond the scope of this study

6.2.1 On further development of the NSHM

- The derivation of daily rainfall grids by Van Beek (2008) is a new method and not extensively validated. During the report the question is raised whether the quality of this dataset is sufficient to obtain better NSHM results on a sub catchment scale. Correlation of Van Beek data with daily station observations are necessary to give conclusive answers whether Van Beek (2008) data gives a good representation of daily meteorological observations.
- The semi-distributed version of HBV is presumed to be sensitive to a poor spatial representation of rainfall. It is presumed that on a sub basin scale, better results can be achieved with a lumped HBV version. Besides, it would ease the downscaling of GCM data to the resolution of the NHSM, whereby better results of NHSM-GCM simulations can be achieved.
- Some parts of the Nile River are not represented in RIBASIM-NILE. In other parts, river dynamics are poorly represented. Where possible, the river schematization should be extended as it would improve the representation of water distribution.
- An integrated calibration of HBV and RIBASIM-NILE would improve some parts of the hydrograph. Although not extensively mentioned in the report, a good performance on some aspects of the simulated hydrograph is in some cases limited by RIBASIM-NILE rather than by HBV.

6.2.2 On the simulation of the future hydro-climate

To increase the predictive value of NHSM simulations for the future climate, the method by which future meteorological forcing series are derived has to be improved. This can be done, by (1) improving the used method by which GCM simulations are directly used to derive meteorological forcing or (2) abandoning the direct use of GCM simulations and use trends in climate statistics derived from GCMs to manipulate observed forcing.

When the first option is chosen, it is presumed that better results can be achieved when:

1. only GCMs showing a low bias in representing relevant aspects of the current climate are selected;
2. bias in the temporal representation of simulated rainfall is removed on more aspects than solely the representation of mean monthly values;
3. the spatial representation of simulated rainfall is removed by downscaling GCM simulations to the resolution of the hydrological model.

When the second option is chosen, trends in statistics, such as the mean and variability in simulated meteorological variables can be used to manipulate observed forcing making them representative of only the aspect of the future climate by which forcing is manipulated.

6.2.3 On further research

This research only comprehends a climate change assessment on the natural state of the Nile Basin. Since the NSHM uses RIBASIM-NILE for water distribution, it would be interesting to assess climate change impacts in combinations with other scenarios of socio-economic and river developments. Furthermore RIBASIM-NILE can be used to assess the impacts of climate change in relation to mitigating river basin management strategies.

References

Africa@Home. (2009). AfricanClimate@home. Retrieved 14-07-2009, from http://www.worldcommunitygrid.org/projects_showcase/ach/viewAchMain.do

Akhtar, M., Ahmad, N., & Booij, M. J. (2008). Use of regional climate model simulations as input for hydrological models for the Hindukush-Karakorum-Himalaya region. *Hydrology and Earth System Sciences Discussions, 5*(2), 865-902.

Allen, R. G., Pereira, L. S., Raes, D., & Smith, M. (1998). *Crop evapotranspiration. Guidelines for computing crop water requirements* (Vol. 56): FAO, Rome.

Arnell, N. W. (1999). Climate change and global water resources. *Global Environmental Change, 9*, 31-49.

Bergström, S., & Forsman, A. (1973). Development of a conceptual deterministic rainfall-runoff model. *Nordic hydrology, 4*(3), 147-170.

Beven, K. J. (2004). *Rainfall-runoff modelling: the primer*: John Wiley & Sons Inc.

Boko, m., Niang, A., Nyong, C., Vogel, A., Githeko, M., Medany, B., et al. (2007). *Africa*: Cambridge University Press, Cambridge, United Kingdom.

Booij, M. J. (2002). *Appropriate modelling of climate change impacts on river flooding.* University of Twente, Enschede.

Booij, M. J. (2005). Impact of climate change on river flooding assessed with different spatial model resolutions. *Journal of Hydrology, 303*(1-4), 176-198.

Brouwer, C., & Heibloem, M. (1986). Irrigation Water Management: Training manual no.3. *FAO Irrigation Water needs*.

Christensen, J., Hewitson, B., Busuioc, A., Chen, A., Gao, X., Jones, R., et al. (2007). *Regional Climate Projections.*: Cambridge University Press, Cambridge, United Kingdom.

Conway, D. (1997). A water balance model of the Upper Blue Nile in Ethiopia. *Hydrological Sciences Journal/Journal des Sciences Hydrologiques, 42*(2), 265-285.

Conway, D., & Hulme, M. (1993). Recent fluctuations in precipitation and runoff over the Nile sub-basins and their impact on main Nile discharge. *Climatic Change, 25*(2), 127-151.

Conway, D., & Hulme, M. (1996). The impacts of climate variability and future climate change in the Nile Basin on water resources in Egypt. *International Journal of Water Resources Development, 12*(3), 277-296.

de Kort, I. A. T., & Booij, M. J. (2007). Decision making under uncertainty in a decision support system for the Red River. *Environmental Modelling & Software, 22*(2), 128-136.

Deckers, D. L. E. H. (2006). *Predicting discharge at ungauged catchments: Parameter estimation through the method of regionalisation.* Univeristy of Twente, Enschede.

Deltares. (2004). *RIBASIM Version 6.32*: Deltares, Delft, The Netherlands.

Doorenbos, J., & Pruitt, W. O. (1977). Guidlines for predicting crop water requirements. *FAO Irrigation and Drainage Paper, 24*.

Dumont, H. J. (2009). *The Nile - Origin, environments, limnology and human use* (Vol. 89): Springer.

Eischeid, J. K., Diaz, H. F., Bradley, R. S., & Jones, P. D. (1991). *A comprehensive precipitation data set for global land areas*: US Department of Energy, Washington, DC.

FAO. (2009). Rivers of Africa. Retrieved 06-08-2009, from http://www.fao.org/geonetwork/srv/en/metadata.show?id=12&currTab=summary

Gleick, P. H. (1989). Climate change, hydrology, and water resources. *Reviews of Geophysics, 27*(3), 329-344.

Gleick, P. H. (1991). The vulnerability of runoff in the Nile Basin to climatic changes. *Environmental Professional, 13*(1), 66-73.

Gordon, H. B., Rotstayn, L. D., McGregor, J. L., Dix, M. R., Kowalczyk, E. A., O'Farrell, S. P., et al. (2002). The CSIRO Mk3 climate system model. *Atmospheric Research Technical Paper, 60*.

Green, I. R. A., & Stephenson, D. (1986). Criteria for comparison of single event models. *Hydrological sciences journal, 31*(3), 395-411.

Guo, S., Wang, J., Xiong, L., Ying, A., & Li, D. (2002). A macro-scale and semi-distributed monthly water balance model to predict climate change impacts in China. *Journal of Hydrology, 268*(1-4), 1-15.

Hagemann, S., Arpe, K., & Bengtsson, L. (2005). *Validation of the hydrological cycle of ERA-40*: ECMWF England.

Harlin, J., & Kung, C.-S. (1992). Parameter uncertainty and simulation of design floods in Sweden. *Journal of Hydrology, 137*(1-4), 209-230.

Hulme, M., Doherty, R., Ngara, T., New, M., & Lister, D. (2001). African climate change: 1900-2100. *Climate Research, 17*(2), 145-168.

Ines, A. V. M., & Hansen, J. W. (2006). Bias correction of daily GCM rainfall for crop simulation studies. *Agricultural and Forest Meteorology, 138*(1-4), 44-53.

Kwadijk, J. C. J., Haasnoot, M., Hoogvliet, M. C., Jeuken, A. B. M., van der Krogt, R. A. A., Oostrom, N. G. C., et al. (2008). Klimaatbestendigheid van Nederland als Waterland. *H_20, 23*, 15-20.

Lidén, R., & Harlin, J. (2000). Analysis of conceptual rainfall-runoff modelling performance in different climates. *Journal of Hydrology, 238*(3-4), 231-247.

Lindström, G. (1997). A simple automatic calibration routine for the HBV model. *Nordic hydrology, 28*(3), 153-168.

Lindström, G., Johansson, B., Persson, M., Gardelin, M., & Bergström, S. (1997). Development and test of the distributed HBV-96 hydrological model. *Journal of Hydrology, 201*(1-4), 272-288.

Madsen, H. (2000). Automatic calibration of a conceptual rainfall-runoff model using multiple objectives. *Journal of Hydrology, 235*(3-4), 276-288.

Mohamed, Y. A., Van Den Hurk, B., Savenije, H. H. G., & Bastiaanssen, W. G. M. (2005). Hydroclimatology of the Nile: results from a regional climate model. *Hydrology and Earth System Sciences Discussions, 2*(1), 319-364.

MWRI/Deltares. (2009a). *ANNEX C - Simulation of Lake Nasser inflow (RIBASIM)*: Deltares, Delft, The Netherlandso. Document Number)

MWRI/Deltares. (2009b). *Volume I - Main Report*: Deltares, Delft, The Netherlandso. Document Number)

MWRI/Deltares. (2009c). *Volume III - Nile Forecasting System (NFS)*: Deltares, Delft, The Netherlandso. Document Number)

MWRI/Deltares. (2009d). *Volume VI - Climate Change*: Deltares, Delft, The Netherlandso. Document Number)

MWRI/Deltares. (2009e). *Volume VIII - Hydrology*: Deltares, Delft, The Netherlandso. Document Number)

Nakicenovic, N., & Swart, R. (2000). *Special Report on Emissions Scenarios (SRES)*: Cambridge University Press.

Nash, J. E., & Sutcliffe, J. V. (1970). River flow forecasting through conceptual models - Part I - A discussion of principles. *Journal of Hydrology, 10*(3), 282-290.

New, M., Hulme, M., & Jones, P. (2000). Representing twentieth-century space–time climate variability. Part II: Development of 1901–96 monthly grids of terrestrial surface climate. *Journal of Climate, 13*(13), 2217-2238.

New, M., Lister, D., Hulme, M., & Makin, I. (2002). A high-resolution data set of surface climate over global land areas. *Climate Research, 21*(1), 1-25.

PCMDI. (2009). Multi-Model climate database. Retrieved 10-02-2009, from https://esg.llnl.gov:8443/index.jsp

Randall, D. A., Wood, R. A., Bony, R., Colman, R., Fichefet, T., Fyfe, J., et al. (2007). *Climate models and their evaluation.*: Cambridge University Press, Cambridge, United Kingdom.

Roeckner, E., Bauml, G., Bonaventura, L., Brokopf, R., Esch, M., Giorgetta, M., et al. (2003). The atmospheric general circulation model ECHAM5: part 1: model description. *MPI report 349 (available via MPI, Hamburg, Germany)*, 127.

Schmidt, G. A., Ruedy, R., Hansen, J. E., Aleinov, I., Bell, N., Bauer, M., et al. (2006). Present-day atmospheric simulations using GISS ModelE: Comparison to in situ, satellite, and reanalysis data. *Journal of Climate, 19*(2), 153-192.

SMHI. (1999). *Integrated Hydrological Modelling System (IHMS). Manual version 4.3*: SMHI, Norrköping, Sweden.

Troccoli, A., & Kållberg, P. (2004). *Precipitation correction in the ERA-40 reanalyses*: European Centre for Medium-Range Weather Forecasts (ECMWF), Reading, United Kingdom

Uppala, S. M., Kallberg, P. W., Simmons, A. J., Andrae, U., Bechtold, V. D. C., Fiorino, M., et al. (2005). The ERA-40 re-analysis. *Quarterly Journal of the Royal Meteorological Society, 131*(612).

USGS. (2009a). Global Land Cover Characterization (GLCC2). Retrieved 06-08-2009, from http://edc2.usgs.gov/glcc/

USGS. (2009b). GTOPO30 Digital Elevation Model (DEM). Retrieved 06-08-2009, from http://edc.usgs.gov/products/elevation/gtopo30/gtopo30.html

van Beek, R. (2008). Forcing PRC-GLOB with CRU data. Unpublished Draft Document. Faculty of Geographical Sciences, University of Utrecht, The Netherlands.

Viner, D. (2000). CRU Information Sheet no. 8: Modelling Climate Change. Retrieved 14-11-2008, from http://www.cru.uea.ac.uk/cru/info/modelcc/

Abbreviations

COF	Combined Objective Function
CRU	Climatic Research Unit
CSIRO	Commonwealth Scientific Research Organization
DEM	Digital Elevation Model
ECMWF	European Centre for Medium-Range Weather Forecasts
GCM	Global Circulation Model
GHG	Greenhouse gas
GISS	Goddard Institute for Space Studies
IPCC	Intergovernmental Panel on Climate Change
LDD	Local Drainage Direction (map)
LNFDC/ICC (project)	Lake Nasser Flood and Drought Control / Integration of Climate Change uncertainty and flood risk (project).
MPI	Max Planck Institute for Meteorology
NFC	Nile Forecasting Centre - official body assigned with Nile River forecasting for the MWRI
NFS	Nile Forecasting System - hydrological model described in (MWRI/Deltares, 2009c)
NHSM	Nile Hydrological Simulation Model
NWRI	Egyptian Ministry of Water Resources and Irrigation
PCMDI	Program for Climate Model Diagnosis and Intercomparison
RACMO	Regional Atmospheric Climate Model
RCM	Regional Climate Model
RIBASIM	River Basin Simulation Model
SMHI	Swedish Meteorological and Hydrological Institute
SOF	Single Objective Function
SRES	Special Report on Emission Scenarios (Nakicenovic & Swart, 2000)
USGS	United States Geological Survey

Symbols

α	Non-linearity parameter to fast runoff - parameter in HBV
β	Soil routing parameter in HBV
CF	Capillary flux - flux in HBV
$CFLUX$	Capillary flux parameter in HBV
COF	Combined Objective Function
CV	Coefficient of variance
ET_0	Reference Evapotranspiration
ET_a	Actual Evapotranspiration
ET_p	Potential Evapotranspiration
FC	Maximum soil moisture storage - parameter in HBV
F_r	Discharge release factor - used in the discretization of R_{tot}
H_f	Quick runoff storage - reservoir in HBV
hq	Half of mean annual flood - parameter in HBV
H_s	Slow runoff storage - reservoir in HBV
INT	Spatial variant factor used in the spatial interpolation of observed rainfall and reference evapotranspiration
K_c	Crop Factor
k_f	Recession parameter in fast runoff - parameter in HBV
k_{hq}	Recession parameter to hq - parameter in HBV
k_s	Recession parameter to slow runoff - parameter in HBV
LP	Limit for potential evapotranspiration - parameter in HBV
$MAXBAS$	Parameter in HBV for sub-catchment time of concentration
NS	Nash and Sutcliff Coefficient
P	Precipitation/Rainfall
$\overline{P}_{GCM;sub}$	Area average GCM simulated rainfall over a sub-catchment
$\overline{P}_{obs;sub}$	Area average observed rainfall over a sub-catchment
p	Mean daily percentage of annual daytime hours - parameter used in Blany-Criddle method (Brouwer & Heibloem, 1986)
$PERC$	Percolation parameter in HBV
P_{GCM}	Uncorrected GCM simulated rainfall
P_{GCM}'	Corrected GCM simulated rainfall
Q	Discharge
$\overline{Q}$	Mean monthly discharge
$\overline{Q}_{GCM;1990}$	1961-1990 mean monthly NSHM-GCM simulated discharge
$\overline{Q}'_{GCM(SRES);period}$	Mean monthly corrected discharge under a GCM(SRES) simulation for a climatic period
$\overline{Q}_{GCM(SRES);period}$	Mean monthly uncorrected discharge under a GCM(SRES) simulation for a climatic period

Q_{obs}	Observed Discharge
$\overline{Q}_{obs}$	Mean monthly observed discharge
$\overline{Q}_{Obs;1990}$	1961-1990 mean monthly observed discharge
Q_{sim}	Simulated Discharge
RC	Recharge - Flux in HBV
R_f	Fast runoff - flux in HBV
R_s	Slow runoff - flux in HBV
R_{sub}	Sub-catchment runoff - output flux of HBV and input flux of RIBASIM-NILE
R_{tot}	Total available runoff - flux in HBV
RVE	Relative Volume Error
S	Standard deviation
SM	Soil Moisture storage - Reservoir in HBV
T	Temperature
T_{mean}	Mean daily temperature in over a month

APPENDIX A Derivation of meteorological forcing

In this appendix the equations behind the calculation of used potential evapotranspiration ET_{pot} series (van Beek, 2008) are given. This section only gives a brief summary to the elaborate work completed by the developer of the data series. For an extensive description of data is referred to its developer (van Beek, 2008).

Calculation of Reference Evapotranspiration ET_o

Van Beek uses a slightly different version of the one proposed by FAO guidelines (Allen et al., 1998) as shown in equation A.1. In this equation, e_s and e_a are the saturation and actual vapour pressure [Pa], δ is the slope of the function of saturation pressure versus the air temperature [PA·°C^{-1}], γ is the psychometric constant [PA·°C^{-1}], ρ_a is the density of air [1.205 kg·m^{-3}], c_p is the specific heat capacity of air [1004 J·kg^{-1}·°C^{-1}], R_n is the net incoming radiation and G the ground flux, both in [W·m^{-2}], λ_v is the latent heat of vaporization [J·kg^{-1}], and r_s and r_a are the surface and aerodynamic resistance respectively [s·m^{-1}].

$$ET_o = \frac{\delta\left(R_n - G\right) + \rho_a \times c_p \dfrac{\left(e_s - e_a\right)}{r_a}}{\lambda_v\left(\delta + \gamma\left(1 + \dfrac{r_s}{r_a}\right)\right)} \tag{A.1}$$

From this equation, only the actual vapour pressure e_a can be directly obtained from CRU dataset. The saturation vapour pressure is derived from equation A.2, whereby the average monthly temperature $\overline{T}$ is derived from CRU data. The slope of saturation vapour pressure versus temperature is calculated with equation A.3, using CRU derived air temperature, T. From equation A.4 the psychometric constant can be calculated, using 0.622 for the ratio of the molecular weight of water vapour and dry air ε. Equation A.5 and A.6 to calculate latent heat of vaporization and atmospheric pressure P used in equation A.4. In the calculation of atmospheric pressure, a relation with elevation is derived using elevations from the GTOPO30 digital elevation model (USGS, 2009b). The aerodynamic resistance r_a is derived by equation A.7, whereby the monthly wind speed $\overline{u_z}$ [m·s^{-1}] is derived from the CRU-CL1.0 dataset. The Karman constant, k, is 0.41. Z_m [10m] and z_h [2m] are the assumed elevations at which wind speed and temperature/vapour pressure are measured, z_D is the zero plane displacement height set at 2/3 the vegetation height, z_0 stands for the roughness length set to 0.123 the vegetation height. Z_{0h} is set to 0.1 times Z_{0m}. For each month, the incoming net radiation, R_n, is estimated as in equation A.8, whereby R_s and R_l stand for incoming global shortwave radiation and emitted long-wave radiation respectively. Factor α is the albedo. R_s and R_l are indirectly derived from CRU cloud cover (see (van Beek, 2008)).

$$e_s = 611 \times \exp\left(\frac{17.27 + \overline{T}}{\overline{T} + 237.3}\right) \tag{A.2}$$

$$\delta = \frac{4098 \times e_s}{\left(T + 237.3\right)^2} \tag{A.3}$$

$$\gamma = \frac{c_p \times P}{\varepsilon \times \lambda_v} \tag{A.4}$$

$$\lambda_v = 2.501 \cdot 10^6 - 2370T \tag{A.5}$$

$$P = 101300\left(\frac{293 - 0.0065z}{293}\right)^{5.26} \tag{A.6}$$

$$r_a = \frac{\ln\left(\frac{z_m - z_D}{z_{0m}}\right) \times \ln\left(\frac{z_h - z_D}{z_{0h}}\right)}{k^2 \times \bar{u}_z} \quad \text{(A.7)}$$

$$R_n = (1-\alpha) R_s + R_l \quad \text{(A.8)}$$

Derivation of crop correction factors K_c

To convert reference potential evapotranspiration ET_0 to potential evapotranspiration ET_{pot}, crop factors k_c are required. To calculate these factors three components are distinguished:

1. a 'crop factor' for and the fraction of freshwater (kc_{water} and F_{water});
2. a crop factor for and fraction of short vegetation (kc_{short} and F_{short});
3. a crop factor for and fraction of tall vegetation (kc_{tall} and F_{tall}).

The relations between these fractions are given in equation A.9 and A.10. The calculation of the component *kc* factors is quite extensive and will be only described briefly. For a full description is referred to the developer (van Beek, 2008).

For vegetation surfaces, the development of *kc* values concern the stomatal resistance, active leaf area, as well as vegetated area and surface roughness, as it develops throughout the growing season. The length of the full growing season is determined by the seasonal changes in radiation, temperature and moisture availability as reproduced by the climatology of the CRU-TS2.1 dataset. Other factors, such as fertility are assumed being optimal. Temporal variations in vegetation crop factors correspond with the phenology of vegetation over the growing season, prescribing the different stated of crop or plant development and vigour. Vegetated areas are determined based on the *leaf area index* (*LAI)*, derived from the GLCC2 global landcover dataset (USGS, 2009a).

The 'crop factor' for open water is derived as a result of the difference in albedo, surface roughness and heat storing capacity of deep water influencing heat transfer. GLCC cells containing lake or reservoirs where classified as deep water, cells containing rivers are classified as shallow water.
The three crop values are combined according to equation A.11 and A.12. First a land crop factor is calculated by a weighted summation of short and tall vegetation crop factors by their cell fractions. Thereafter, the total crop factor k_c is calculated by a weighted summation of the land and water crop factors and their cell fractions.

$$F_{land} = 1 - F_{water} \quad \text{(A.9)}$$

$$F_{veg;short} = 1 - F_{veg;tall} \quad \text{(A.10)}$$

$$kc_{land} = kc_{short} \times F_{veg;short} + kc_{tall} \times F_{veg;tall} \quad \text{(A.11)}$$

$$kc = kc_{land} \times F_{land} + kc_{water} \times F_{water} \quad \text{(A.12)}$$

APPENDIX B Issues related to RIBASIM-NILE areal representation

As referred to in the main report, sub-catchments used for the hydrological model and RIBASIM should refer to the same areas. Unfortunately LNFDC/ICC (MWRI/Deltares, 2009e) only provides areas of sub-catchments and no global position. Furthermore, a qualitative description of rainfall-runoff inflow (variable inflow in RIBASIM terms) areas is given (MWRI/Deltares, 2009a). In LNFDC data, two sub-catchment maps where found (See Figure B.1 and Figure B.2), one with 44 and one with 30 sub-catchments. From the areas provided by the LNFDC/ICC and the sub-catchment maps a compilation is made as shown in section 3.1.4 of the main report.

A comparison of Figure B.1 with LNDC/ICC documentation reveals it is used to define the Blue Nile, Sobat and Atbara catchments. Most areas upstream Mongalla correspond with areas given in areas retrieved from the sub-catchment map. Downstream Mongalla, areas are retrieved Figure B.2, leading to a first accuracy; the area of Mongalla presented by LNDC/ICC is overestimated, since part of catchments north retrieved from Figure B.1 are overlapping with the Mongalla catchment retrieved from Figure B.2.

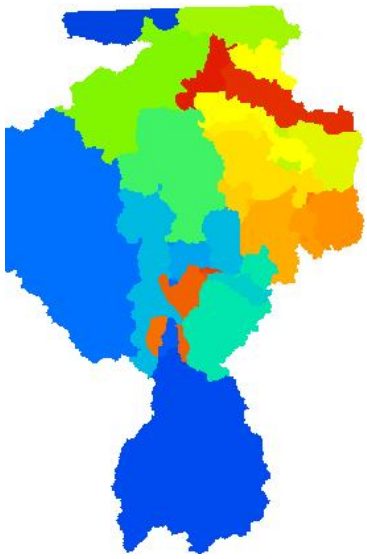

Figure B.1 – Map used for derivation of Blue Nile, Sobat and Atbara Catchments

Especially at the Blue Nile, many inaccuracies are found. Since the flow directions are not forced over a predefined river map, flows follow the path defined by the GTOPO30 DEM (USGS, 2009b). As a result, Lake Tana is shown as a source of the Dinder & Rahad rather than that of the Blue Nile. The catchment Dinder & Rahad also includes a large area of the Blue Nile itself. The most upstream catchments of the Blue Nile could not be related to Figure B.1 matching it with documentation. Therefore, documented outlets where used to derive sub-catchments from a DEM. Using a FAO river map (FAO, 2009) priory rivers are lowered sufficiently to force catchments drainage to these cells.

For the Atbara and Main Nile, composing a sub-catchment map showed similar issues. Two catchments of Figure B.1 are not found in documentation. To prevent areal leaps in the composed sub-catchment map, these areas where assigned to upstream catchments. At the Main Nile, the most distinct inaccuracy is a dischargeing outside its sub-catchment, which does not agree with geophysics.

Figure B.2 – Maps used for derivation of White Nile Catchments

A total number of five inaccuracies found are summed up:

- Catchment downstream Mongalla is smaller than documented. Overlapping areas from both catchment maps have been subtracted.
- At the Blue Nile, Lake Tana catchment is derived from a renewed extraction predefining rivers. This area is subtracted from the Dinder & Rahad catchment defined by Figure B.1.
- Areas of sub-catchments between Deim and the Lake Tana catchment do not comply with documentation, since clear relations with Figure B.1 could not be found.

- Two catchments of the Atbara River, one downstream the Humera Dam and the most downstream sub-catchment, where not accounted for in documentation, resulting in an underestimation of documented Atbara River area.
- The Main Nile between Khartoum and the planned Merowe Dam flows outside its catchment, resulting in an underestimation of the catchment area.

Better model performance would require a redefinition of sub-catchments for increasing geophysical representation. However, such actions require a recalibration of the RIBASIM model, which is beyond the scope of this research. When possible, the following course of action will lead to a better geophysical representation of sub-catchments:

1. Obtain a river map (e.g. FAO (2009)) in the required level of detail.
2. Validate the river streams and define stream orders. A first indication of accuracy can be achieved by simply importing a vector map in Google Maps or comparing the river course with georeferenced mosaics from e.g. Landsat imagery.
3. Manipulate a (high resolution!) DEM by lowering river cells in stream order, whereby main streams are lowered more than tributaries and tributaries more than the most upstream river sections. The river outlet should be lowered the most to force the later generated local drainage direction (LDD) map, from sub-catchment, to stream, to main stream to the outlet point of the river.
4. Define outlet points of sub-catchments. It is important that these points are located on river cells to force the LDD in draining on these outlets.
5. Creating a LDD after filling local depressions. The depth of filling local depressions should be limited by the depth in which the river cells are lowered in step 3.
6. Defining sub-catchments by accumulating the area which drains to the outlet points defined at step 4.
7. For transparency reasons it is suggested to present sub-catchment maps in future reports rather than a table presented in MWRI/Deltares (2009e).

APPENDIX C Golden ratio parameter optimization

In optimization of NHSM using an automatic calibration scheme, calculation time is saved by using Golden Ratio search scheme. Before commencing calibration of a single parameter, the shape of COF(x) (as shown Figure C.1) is unknown. To use the proposed search method the assumption is made that the COF(x) has a global maximum and no local maxima.

The first step is to calculate COF(X) for four locations along the x-axis (the parameter space), the beginning and end of its domain (a^n and b^n, see Figure C.1) and two intermediary locations, x_l^n and x_r^n. The deviations of these locations over the domain [a^n, b^n] is determined by the Golden Ratio, φ, as defined by function D.1. The approximated value of the irrational number φ is given by equation D.2.

$$\varphi = \frac{b^n - a^n}{x_R^n - a^n} = \frac{x_R^n - a^n}{b^n - x_R^n} \tag{D.1}$$

After the first step is taken, the domain is narrowed according to the values of x_l^n and x_r^n. In case COF(x_l^n) is smaller than COF(x_r^n)the optimum can assumed to be on the right hand side of x_l^n narrowing the domain to [x_l^n, b^n], as shown in equation D.3. In case COF(x_l^n) equals or exceeds COF(x_r^n), the domain is narrowed to [a^n, x_r^n] as shown in equation D.4. The procedure of narrowing the parameter domain continues until the domain, [a^n, b^n], is less than 2% of the initial domain [a^1, b^2]. Within this procedure the locations of x_l^n and x_r^n remain the same within the domain.

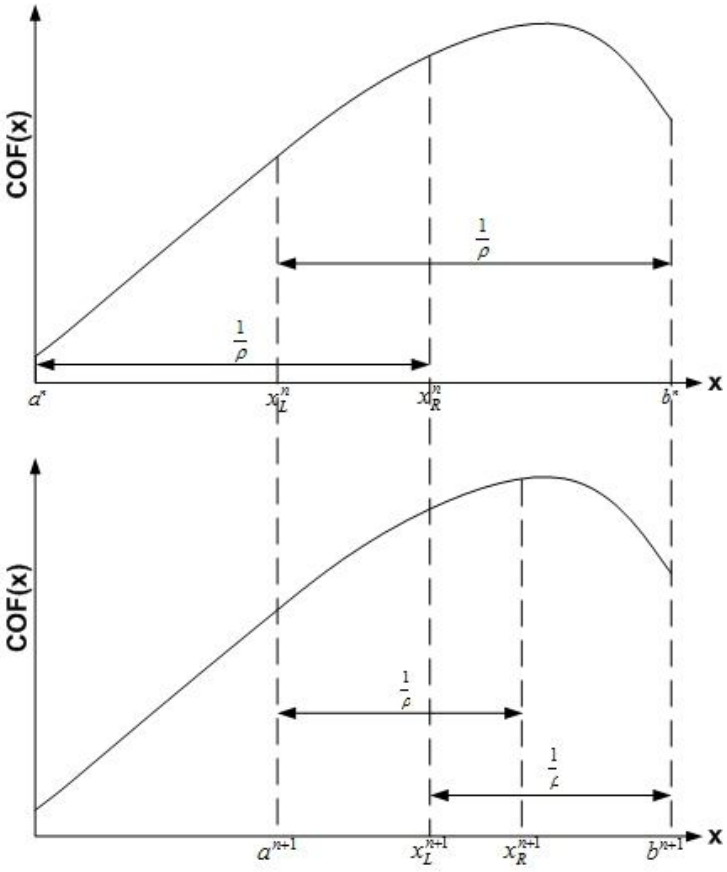

Figure C.1 – Graphical Explication of Golden Ratio Method (Case 1)

$$\frac{1}{\varphi} = \frac{1+\sqrt{5}}{2} \approx 0.618 \tag{D.2}$$

Case 1:

$$COF\left(x_L^n\right) < COF\left(x_R^n\right)$$

$$\text{new domain: } [x_L^n, b^n]$$

$$a^{n+1} = x_L^n$$

$$x_L^{n+1} = x_R^n \tag{D.3}$$

Case 2:

$$COF\left(x_L^n\right) \geq COF\left(x_R^n\right)$$

$$\text{new domain: } [a^n, x_L^n]$$

$$x_R^{n+1} = x_L^n$$

$$b^{n+1} = x_R^n \tag{D.4}$$

APPENDIX D Calibration and validation hydrographs

In this Annex hydrographs not printed in the calibration and validation section of the main report are shown

Calibration Results

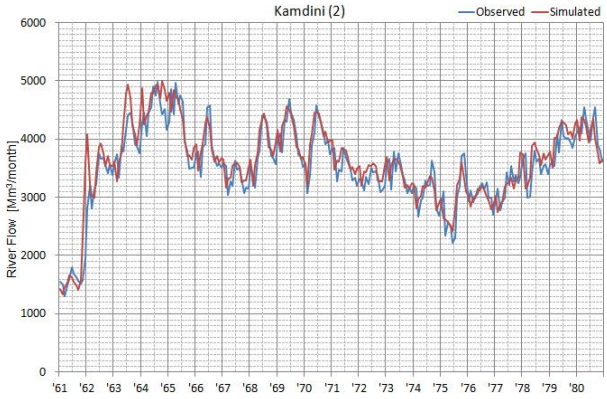

Figure D.1 – Hydrographs for Kamdini, downstream the outlet of Lake Kyoga after calibration

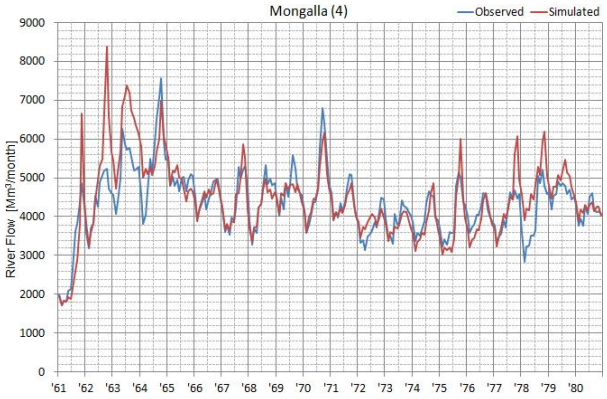

Figure D.2 – Hydrographs for Mongalla, upstream Sudd swamps after calibration

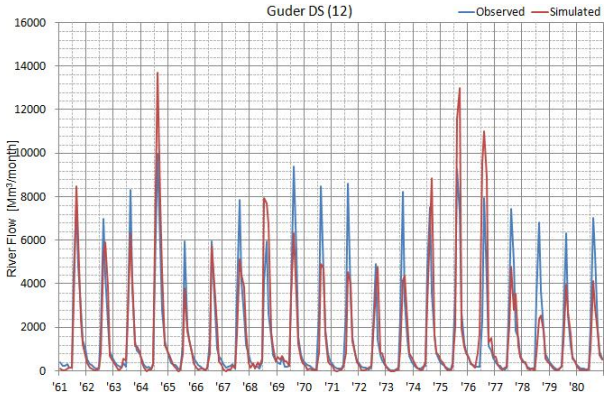

Figure D.3 - - Hydrographs for Guder DS, halfway the Lake Tana – Deim Blue Nile reach after calibration

Validation Results

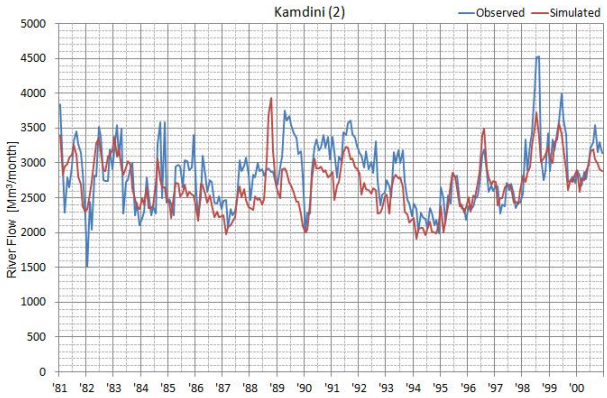

Figure D.4 - Hydrographs for Kamdini, downstream the outlet of Lake Kyoga at validation

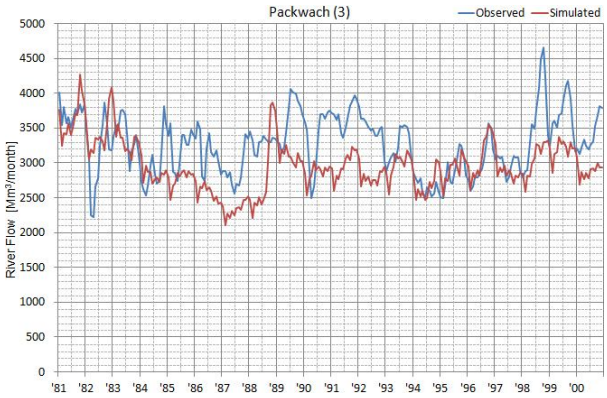

Figure D.5– Hydrographs for Packwach, downstream the Simleki, Victoria Nile confluence at validation

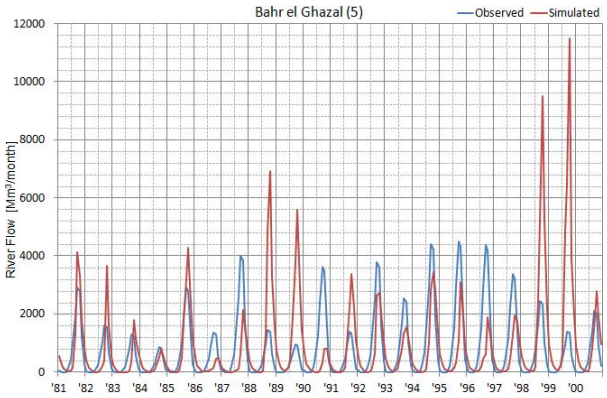

Figure D.6 - Hydrographs of the Bahr el Ghazal, upstream Lake No at validation

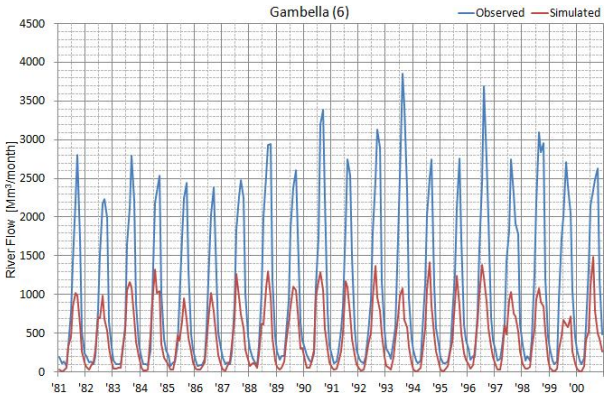

Figure D.7 - Hydrographs at Gambela, at the Baro at validation

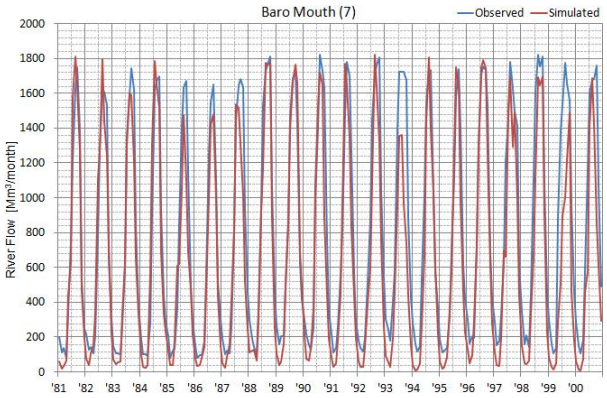

Figure D.8 -- Hydrographs of Baro Mouth after validation

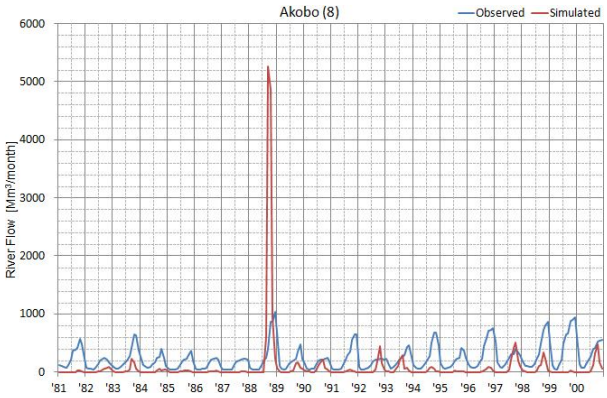

Figure D.9 - - Hydrographs of Akobo at the Pibor River after validation

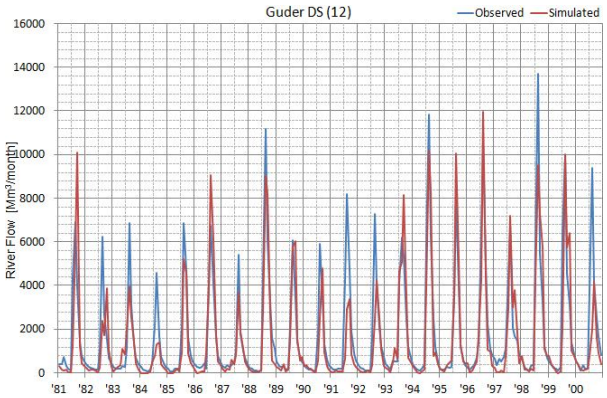

Figure D.10 - - Hydrographs at Guder DS, between Lake Tana and the Sudan Border after validation

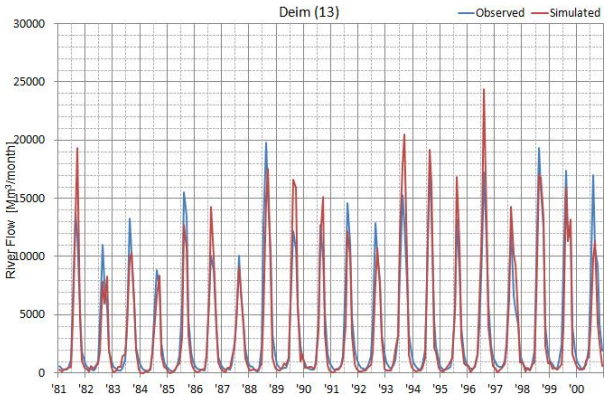

Figure D.11 - Hydrographs at Deim near the Sudan border after validation

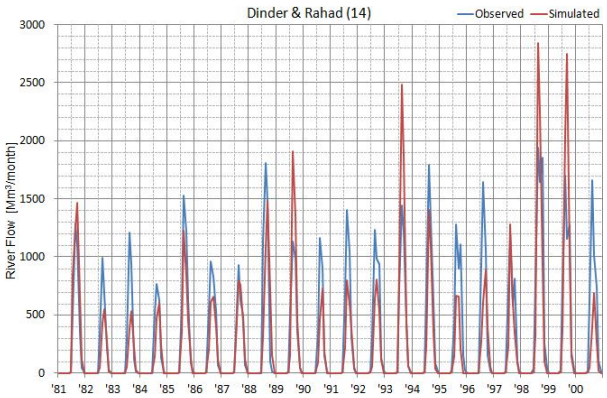

Figure D.12 - Hydrographs of Dinder & Rahad after validation

APPENDIX E Bias correction results

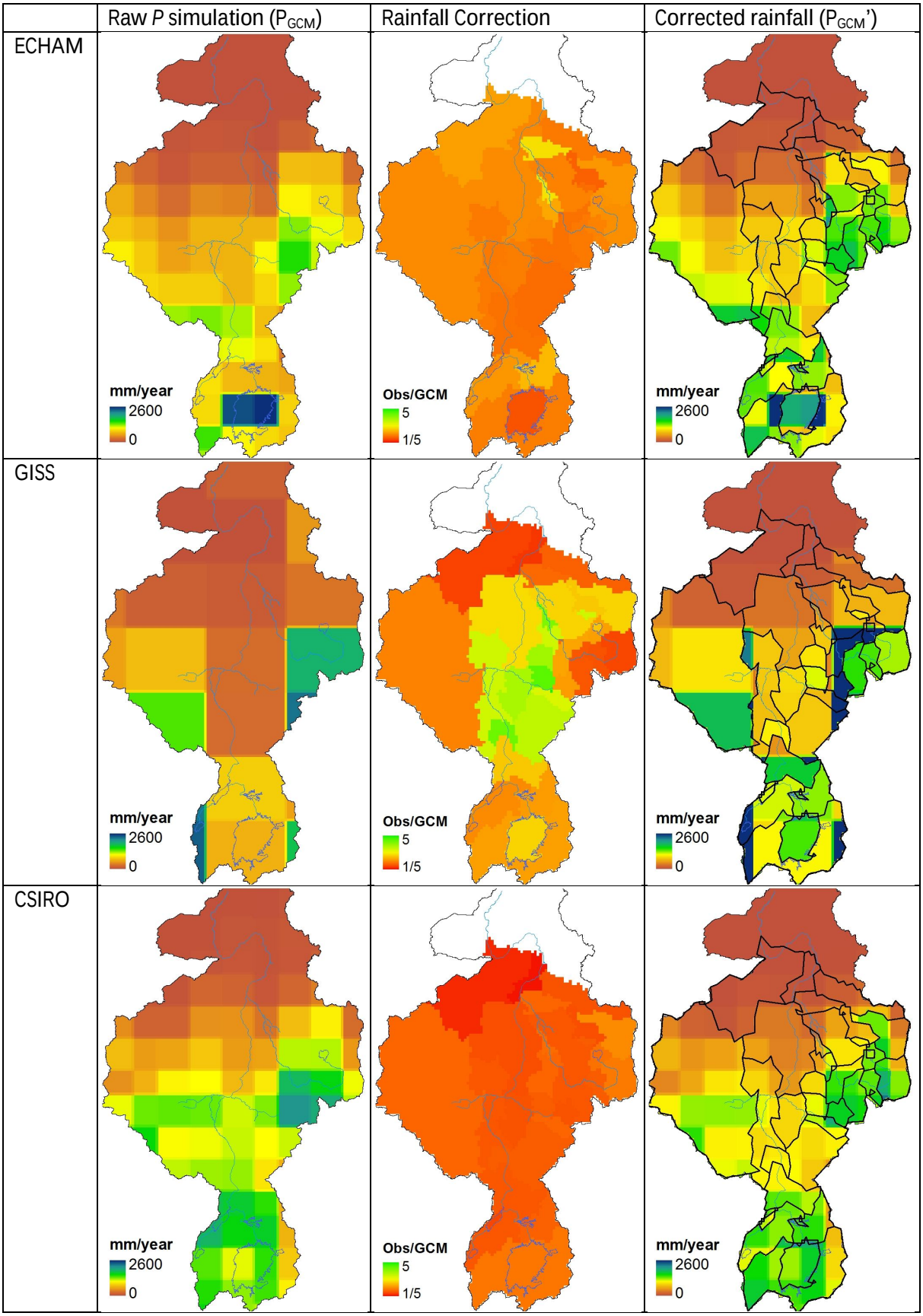

Figures E.1 - Average annual GCM correction applied on Rainfall out (P_{obs}/P_{GCM}). In the most left column hydrological sub-catchments are shown over which area average P is equal for all GCMs.

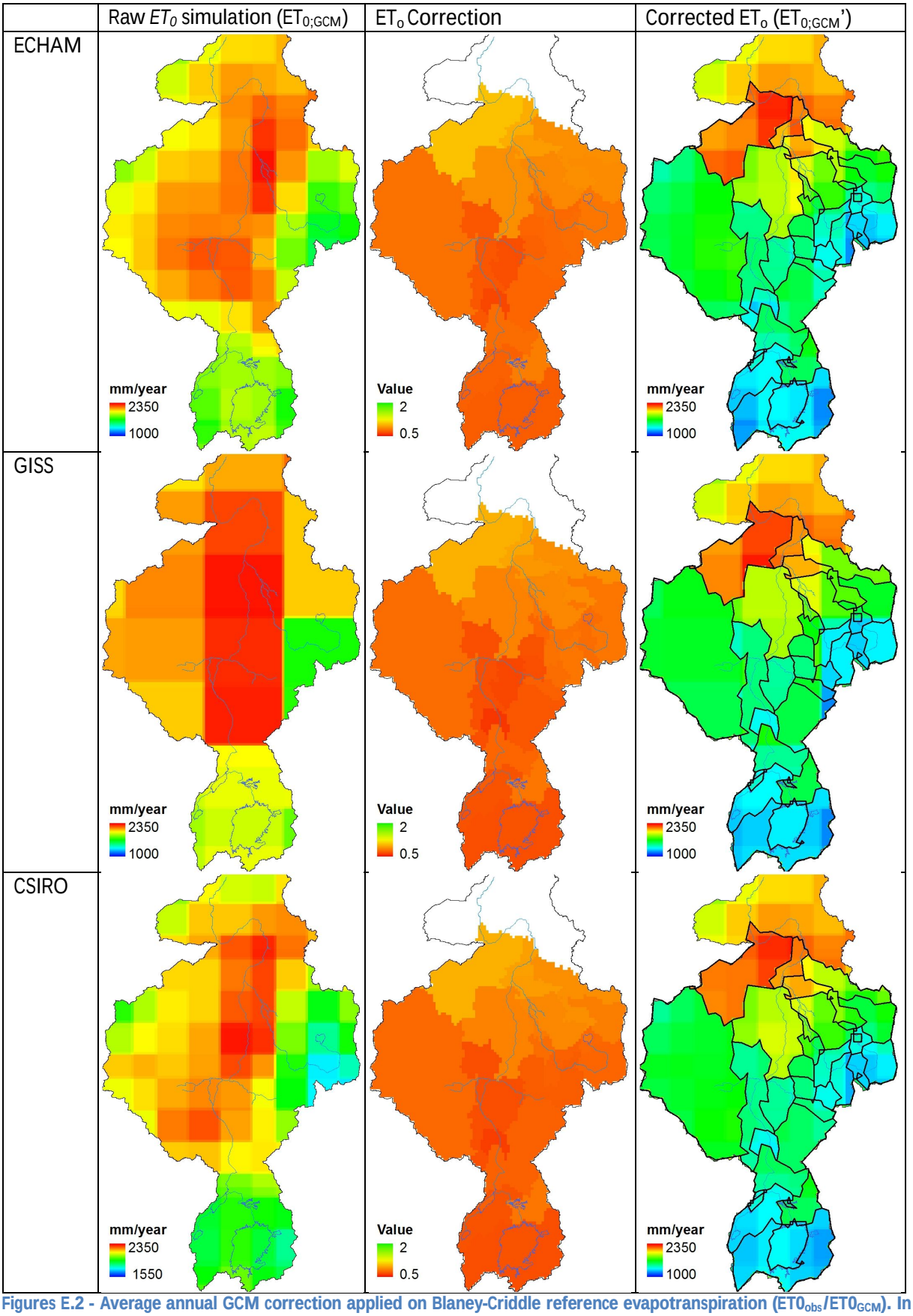

Figures E.2 - Average annual GCM correction applied on Blaney-Criddle reference evapotranspiration ($ET0_{obs}/ET0_{GCM}$). In the most right column, hydrological sub-catchments show over which area average ET0 is equal for all GCMs.

APPENDIX F Bias issues in NHSM-GISS reference hydro-climate

As shown in Figure 5.4, of the main report, the reference mean monthly hydrograph of the NHSM-GISS simulation for Malakal shows a high discrepancy with the observed hydrograph. Since simulated rainfall and reference evapotranspiration are bias corrected on sub basin scale to meet the climatology of mean monthly values (see Figure F.1), the discrepancy can only be a result of differences in actual evapotranspiration. Figure F.2 shows actual evapotranspiration with a NHSM-GISS simulation and a NHSM simulation with observed discharge. The NHSM-GISS simulation accounts for 32% less actual evapotranspiration.

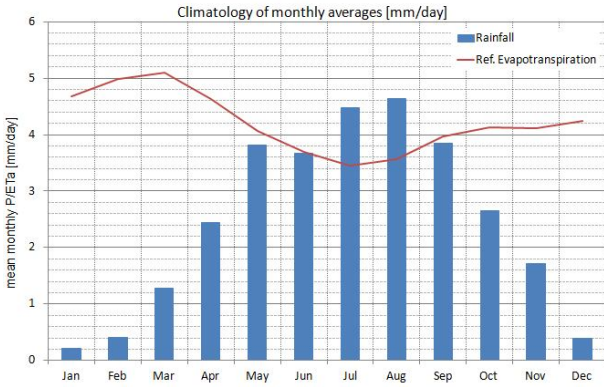

Figure F.1 - Akobo climatology of mean monthly rainfall and reference evapotranspiration

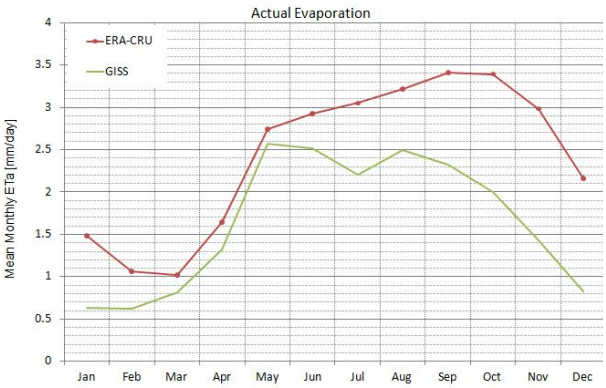

Figure F.2 - Graphs showing simulated mean monthly ETa with ERA-CRU and GISS forcing

As shown in Figure F.3 and Figure F.4, the 32% lower evapotranspiration has enormous consequences on the simulated hydrograph and the water balance of the system. In simulations with GISS forcing annual discharge is 1400% higher than in a simulation with observed forcing.

In the simulation with observed forcing, discharge is only small in comparison with the volumes of rainfall and evapotranspiration. Therefore, the basin is extremely sensitive to changes in meteorological forcing. Since actual evapotranspiration is related to the spatio-temporal variability in rainfall, as referred to in the main report, uncertainty in its variability, has enormous consequences for the river discharge. Better spatio-temporal representation of rainfall is therefore necessary to increase model performance with GISS input. Clearly, for this GCM at this sub-catchment, the used methodology is insufficient.

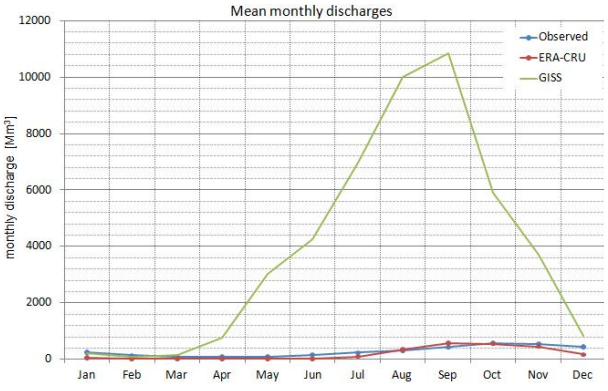

Figure F.3 - Resulting observed, and simulated hydrographs with ERA-CRU and GISS forcing

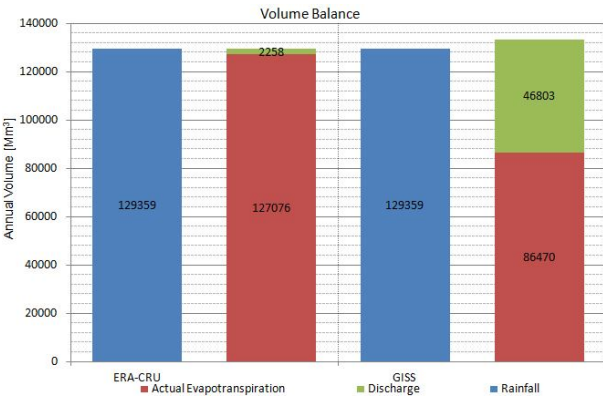

Figure F.4 - Water balances according to simulations with ERA-CRU and GISS forcing